LIDS-TH-1127

AN APPLICATION OF MODERN CONTROL THEORY TO A HIGH BYPASS VARIABLE COMPRESSOR GEOMETRY JET ENGINE

by

Michael S. Idelchik

B.S. Columbia University
(1978)

SUBMITTED IN PARTIAL FULFILLMENT

OF THE REQUIREMENTS FOR THE

DEGREE OF MASTER OF SCIENCE

at the

MASSACHUSETTS INSTITUTE OF TECHNOLOGY

July 1981

Signature of Author.....
Department of Mechanical Engineering, August, 1981

Certified by.....
Thesis Supervisor

Accepted by.....
Chairman, Departmental Committee on Graduate Students

An Application of Modern Control Theory to a High Bypass, Variable Compressor Geometry Jet Engine

ABSTRACT

An application of modern control theory to high bypass, variable compressor geometry jet engine is studied. High bypass, variable compressor geometry turbofans represent a large family of commercial and military subsonic jets, all of which are similar in structure and aerodynamic characteristics. As a specific example, the advanced technology General Electric TF34 turbofan engine is used to generate a linear multivariable dynamic model whose parameters vary with engine operational environment. Based on this model, an adaptive closed loop control system design is developed utilizing the Liner Quadratic Regulator approach and its crossover frequency band is evaluated based on singular value analysis. Using linear TF34 engine dynamic model, the adaptive control performance is compared to that of the current TF34 design.

ACKNOWLEDGEMENTS

I am most grateful to my thesis supervisor, Professor Michael Athans for his help and encouragement. Not only that his technical advice was excellent, but more important was the interest he showed in me as a person.

I would like to thank my G.E. Manager, George Evans and Senior Engineers, Warren Schaefer and Bill Lillydale for their outstanding technical and moral support, and for acting as a sounding board for my ideas as they developed.

I would like to thank Dr. Austin Spang, III, from G.E. Corporate Research and Development Center, Dan Gilmore, G.E. Advance Control Engineer, and Ginny Brown, Systems Analyst for their help in obtaining computer simulations and analysis required for this thesis.

I would like to thank Samir Sayegh, G.E. Lynn Advanced Course supervisor, for arranging my financing, and Kim Hickey, my group secretary, for proof-reading and typing this thesis.

Finally, I would like to thank my wife, Hana, for her support, and for helping me finish on time.

The research was conducted at the M.I.T. Laboratory for Information and Decision Systems, and at the General Electric Company Aircraft Engine Group, Lynn, Massachusetts.

TABLE OF CONTENTS

TABLE OF CONTENTS
(cont.)

LIST OF FIGURES

NOMENCLATURE

A	State Matrix
aij	Elements of A Matrix
Aro	Second Pull Rolloff Matrix
B	Control Matrix
bij	Elements of B Matrix
C	Output Matrix
e(t)	Error Signal
G	Optimal Gain Matrix
GM	Gain Margin
gij	Elements of G Matrix
I	Unity Matrix
J1	Fan Rotor Moment of Inertia ($lbft^2$)
J2	Compressor Rotor Moment of Inertia ($lbft^2$)
J(u)	Quadratic Performance Index
LGR	Linear Guasion Regulator
LOR	Linear Output Regulator
LQR	Linear Quadratic Regulator
L(s)	LQR Loop Transfer Function
m	Number of Inputs
n	Number of States
N1 or NF	Fan Rotor Speed (RPM)
N2 or NG	Compressor Rotor Speed (RPM)
N1COR	Corrected Fan Speed (RPM)
N2COR	Corrected Core Speed (RPM)
p	Number of Outputs
P	Solution of Algebraic Riccati Equation
PM	Phase Margin
Po	Pressure Altitude (feet)
PS3	Compressor Discharge Static Pressure (psi)
PT2	Inlet Total Pressure (psi)
Q	State Weighting Matrix
Q1	Fan Rotor Torque (ft lb)
Q2	Compressor Rotor Torque (ft lb)
R	Control Weighting Matrix
T(s)	L(s) Inverse
TT2	Inlet Total Temperature (°R)
T2C	Compressor Inlet Total Temperature (°R)
T5	Interturbine Gas Temperature (°R)
T5TH	Interturbine Thermocouple Temperature (°R)
u	Control Vector
V1	Fuel Flow Actuator Rate (pph/sec)
V2	Variable Geometry Actuator Rate (°/sec)
VG	Variable Geometry Position (degrees)
WA	Core Airflow (lbs/sec)
WAT	Total Engine Airflow (lbs/sec)
WF	Engine Fuel Flow (pph)
WFCOR	Corrected Fuel Flow (pph)
$\underline{X}$	State Vector
XN1 or XNF	Augmented N1 or NF
XVG	Augmented VG
Xr	Augmented State Vector
y	Output Vector

$\theta_2 = \frac{T_{T2}}{518.7}$	Normalized Inlet Temperature
$\delta_2 = \frac{P_{T2}}{14.67}$	Normalized Inlet Pressure
τ	Interturbine Gas Temperature Time Constant (sec)
τ_1	Compressor Discharge Pressure Time Constant (sec)
$\underline{\theta}$	Ambient Conditions
τ_1' and τ_2'	Second Pole Rolloff Time Constants
$\underline{\sigma}$	Smallest Singular Value
$\bar{\sigma}$	Largest Singular Value
λ	Eigenvalue
$\|\cdot\|$	Matrix Norm
SLS	Sea Level Static
ST. DAY	59°F day

1. INTRODUCTION

1.1 Background

Control of aircraft turbine engine propulsion systems have been the focus of extensive development in recent years. Today's aircraft turbine engines are highly complex dynamic systems with numerous variable goemetry features to allow efficient operation over a wide range of operating conditions. The complexity of jet engine systems is a result of highly nonlinear thermodynamic principles which are governing engine behavior. All these bring about a practical, yet fairly complex control problem for a nonlinear, multivariable system.

Engine control hardware technology is beginning to effectively utilize the capabilities of an on-board digital computer; however, the advances in, and practically unlimited computational capabilities of digital electronics have occured so rapidly that modern control syntheses to realize increased engine performance potentials are scarce. Even fewer are the practical implementations of multivariable control designs for aircraft gas turbines.

Recently, the Air Force Aero-Propulsion Laboratory (AFAPL) and NASA-Lewis Research Center have begun to exploit this area. The F100 multivariable control program sponsored by AFAPL and NASA is, so far, the only single example of the successful demonstration of the multivariable design theory on a current production aircraft turbine engine [1, 2].

1.2 Literature Review

Since 1973 AFAPL and NASA sponsored a number of research projects in application of the multivariable design theory to jet engine propulsion systems. By that time, the basic theory for Linear Quadratic Regulator (LQR), Linear Gausian Regulator (LGR) and Linear Output Regulator (LOR) were formulated and developed.

The first work, which has shown that an adaptive control design by continuous-time linear state regulator can fulfill jet engine control design requirements was done by Michael and Farrar (1973). Also,

Michael and Farrar (1975) were the first to combine least squares identification technique with a dynamic nonlinear filter to identify gas turbine dynamics from stochastic input-output data.

The alternative to full state feedback (LQR), was presented by Levine and Athans (1970), is a Linear Output Regulator formulation (LOR). Application of the Linear Output Regulator to jet engine propulsion systems was studied by Merrill (1975) and (1977). In addition, multivariable control system design methods using a frequency domain viewpoint such as Characteristic Loci and Inverse Nyquist Arrays were developed by McFarlane, et al. (1971) and Rosenbrock (1974). These frequency domain multivariable design methods were applied to jet engine control system designs by Spang (1978), Rosenbrock (1978) and McFarlane (1978).

Systems Control Inc. was probably the most significant contributor in the area of multivariable control synthesis for the gas turbine engine [1, 2, 6]. Of course, there were many other contributors who helped to bring about a better understanding and practical potentials of multivariable syntheses [3, 4, 5, 7, 9, 10, 11, 12, 13].

1.3 Contributions of the Research

The control system design for General Electric TF34 advanced technology turbofan engine presented in this thesis has three major differences in control system design philosophy as compared to the currently used philisophy in jet engine control system design.

First is an introduction of the compressor variable geometry position, VG, as a control variable. On the majority of today's jet engines, compressor variable geometry is scheduled as a function of the instantaneous corrected core (compressor) speed for steady state as well as transient engine operation. The compressor variable geometry position schedule represents the most efficient compressor operation along the engine steady state operating line, and consequently the lowest specific fuel consumption at steady state. The approach taken in this thesis is to use the compressor variable geometry position as a scheduled system output and a state variable. By doing this, we assure convergence on the steady state schedule while

allowing optimal trajectory during engine transients. The optimal variable geometry trajectory for engine transients was formulated based on Linear Quadratic Regulator control system design methodology and the compressor stall margin constraints.

Second is the optimal control gains scheduling as a function of corrected engine dynamic variables; fan speed, core speed, and fuel flow. The optimal control gains were calculated based on the perturbation along the engine steady state operating line using the Linear Quadratic Regulator design methodology, and define transient characteristics within the perturbation, subject to the engine constraints.

Third is the development of the target value estimator and trajectory control. The target value estimator will provide a feed-forward input, and trajectory control will assure that large transient trajectories are within the engine constraints.

The variable geometry transient trajectory combined with optimal control gain scheduling, target estimator, and trajectory control represent a new control system design approach for high bypass, variable geometry turbofan engines. Linear engine simulations with the proposed control system show significant improvement in acceleration time as compared to current TF34 nonlinear transient deck predictions.

1.4 Report Overview

The main body of the report is divided into the four chapters.

In Chapter 2, the general approach is developed for jet engine linear model identification and it's generation in state space form is presented. In particular the TF34 linear engine model is formulated and compared to engine nonlinear deck simulation.

In Chapter 3, the systematic way for local control system design based on LQR methodology is presented. In addition transient response at a number of points along the engine operating line are presented and compared to current TF34 transient responses. Finally, frequency

domain analysis such as singular values, and Inverse Nyquist Arrays are presented and discussed.

In Chapter 4, the approach to the global control system design is developed. To demonstrate this design step response stability, crossover frequency band and Inverse Nyquist Arrays at 36,000 ft. altitude and .4 Mn are evaluated.

2. MODELING THE TF34 ENGINE

2.1 Introduction

In this chapter we discuss the generic turbofan engine structure, and its mechanical and thermodynamic constraints. Special attention is given to compressor stall boundary definition and the importance of variable geometry schedule is discussed. Also, a general approach to jet engine linear model identification, and engine linear model generation in state space form is developed. The comparison of linear and nonlinear models is discussed, and applicable step responses are presented. Finally, general constraints for local and global control system designs are formulated and discussed.

2.2 Engine Description

The engine considered in this study is the TF34-100, advanced technology General Electric High Bypass turbofan engine shown in Fig. 2.1.

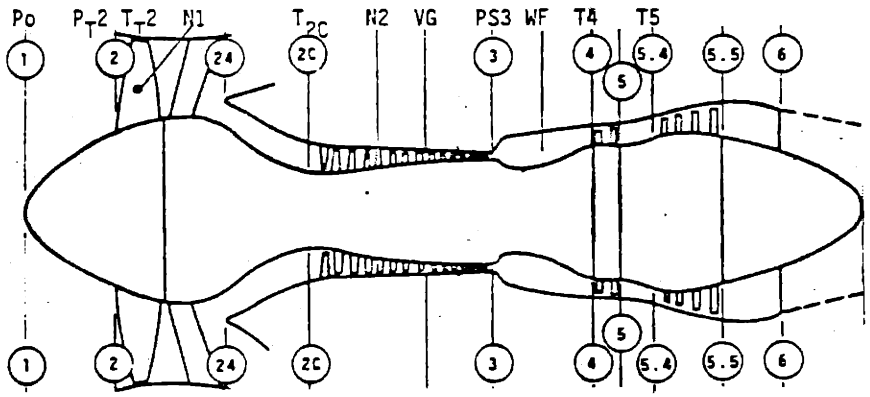

Fig. 2.1 TF34 Engine Stations

2.2.1 General Characteristics

The TF34 is a twin-spool turbofan engine. The compressor and high pressure turbine form the core assembly. The compressor variable geometry, VG, is scheduled to match compressor and high pressure turbine mass flow rate characteristics. The VG schedule is implemented as a function of the corrected core speed, N2K2, and provides maximum efficiency and stall free operation of the compressor. The low pressure turbine drives a one-stage fan. Total engine airflow is divided between cold and hot streams. Cold stream is defined as a total engine airflow minus core air flow, which is defined as a hot stream. The thrust division between cold and hot streams is

approximately 6:1 at max power, and 3:1 at idle. This explains why a high bypass turbofan engine scheduling of corrected fan speed (N1K2), practically, can be viewed as a scheduling of the thrust.

High bypass, variable compressor geometry turbofans are the most fuel efficient jet engine configurations and represent a large family of commercial and military subsonic jets, all of which are similar in structure and aero-dynamic characteristics.

2.2.2 Engine Constraints

A summary of the engine constraints is presented in Table 2.1

Table 2.1

Parameter	Limits
T5 Absolute Value	2000°R
PS3 Absolute Value	330 psi
N2 Absolute Value	18,200 RPM
N2K2 Absolute Value	16,900 RPM
N1 Absolute Value	7,300 RPM
N1K2 Absolute Value	None
Compressor Stall Margin	See Figs. 2.2, 2.3 and 2.4

The compressor stall margin characteristics represent a complicated issue which deserves special attention. Figs. 2.3 and 2.4 show compressor characteristics for nominal VG schedule (Fig. 2.2). The VG nominal schedule along the steady state operating line represents the best efficiency match between compressor and a high pressure turbine.

In some cases, allowing VG to be only 10° more open than nominal at the steady state may result in a compressor stall. However, transient stall characteristics are not necessary the same as steady state ones, and more freedom on VG position as possible. As we see from Fig. 2.3 there is a region where having VG more open will not result in substantial stall margin reduction. In addition, opening VG will result in an increase of the compressor discharge pressure, due to increased core airflow. This in turn will increase the allowable fuel flow step during the acceleration (Fig. 2.4).

The location of the stall boundary is determined based on steady state compressor characteristics and it is influenced by a number of conditions such as; Mach number, compressor deterioration, inlet distortion and off-nominal VG position. Most of these effects can be defined only empirically.

In this report stall margin constraints were verified based on Fig. 2.2, 2.3, and 2.4. The Mach number, deterioration and inlet distortion effects were assumed to be second order effects and hence neglected.

2.3 Engine Linear Model Identification

One goal of this study is to identify a usable linear dynamic model of the high bypass turbofan engine, and to limit the number of state variables in order to make the final design implementable by an on-board digital computer.

The dynamic characteristics of the engine can be obtained from analysis or tests. Both approaches are advisable to use; however, it is usually not possible to obtain engine test data until late in the engine development program. The analysis approach has historically consisted of the solving the engine cycle for unbalanced torque characteristics from which the linear engine characteristics can be obtained. Usually this task is performed with the help of the engine steady state computer simulation. Obtaining engine characteristics suitable for dynamic analysis is a very involved task, which is understandable when one considers that the engine cycle may have as many as five independant inputs and that a cycle calculation is an interactive process. [4, 9, 11]

When engine dynamic characteristics are defined, the next step is to construct a linear operating point model using only inputs and outputs available on an actual engine. This model will be used in the applications of Linear Quadratic Regulator theory (LQR) to high bypass turbofan engine control design.

The LQR application to complex nonlinear systems like the turbofan engine makes the choice of state space variables and design points an important consideration from the design and implementation point of view. There are numerous states in the turbofan engine. In addition, many of the states are not measureable or directly observable, which makes it difficult to use them without extensive computations. So, the number of states must be reduced to get a reasonable control law. However, if the chosen state vector does not include all pertinent states, then the fit of the outputs for the linear operating point model will be poor, because an insufficient set of state variable cannot describe the outputs completely. Thus, a poor fit of the outputs would indicate that further states should be included in the engine model. On the other hand, the inclusion of undesired states would make the linear operating point model overdetermined, which causes model order identification problems.

Furthermore, the engine consists of mechanical components, such as rotors, which responed relatively slow as compared to the thermodynamic components, such as pressure and temperature. Time constant for rotors are typically on the order of a second. On the other hand, characteristic time for pressure propogation is usually on the order of milli-seconds. The same is true for gas temperature of combustion dynamics, which is also on the order of milli-seconds.

In this study, the dynamic model of the engine consists of two slow variables, fan and compressor rotors speeds, and two fast variables, compressor discharge pressure and gas temperature between high and low pressure turbines. It was considered necessary to include fast variables in the dynamic model because these variables will define the tradeoff between controls and states weighting matrices in the LQR design.

The next problem is the choice of the linearization point around which the Linear Quadratic Regulator is designed. If the engine was always near a steady state operating line, then at every flight condition (altitude and Mach number) there is only one independant parameter which specifies the linear engine model dynamics. This parameter could

be fan or compressor rotor speed, or engine fuel flow. An engine can be linearized along the steady state operating line for the entire range of variation of the chosen independant parameter. However, in fast transients, particularly quick accelerations from a low to a high power setting, deviations from the steady state operating line is likely to occur. Changes in engine dynamics during the quick transients are very difficult to determine because of their time dependance. In this study, only steady state operating line dynamics are used in the Linear Quadratic Regulator design. The basic idea in selection of the design points in the flight envelope is to select fewer points in those regions where there are small changes in the linear models and to increase the density of design points in those regions where linearized models are changing rapidly. It should be noticed that near idle, due to unchocked engine nozzle and low pressure turbine, the nonlinear behavior of two rotors becomes slower and uncoupled. This uncoupled behavior causes rapid changes in engine dynamics along the operating line. As a result it was necessary to have three design points in the region from idle to intermediate power settings. On the other hand, from the intermediate to max power region one design point was considered to be sufficient.

The linear engine model block diagram is shown in Fig. 2.5. The gas temperature dynamics time constant τ is shown, as a function of engine fuel flow, in Fig. 2.6. The characteristic time for pressure propogation τ_1 was assumed to be a constant of .01 sec.

2.4 Engine Linear Model Generation

The following equation can be written about nominal operating points:

$$\underline{f}(\underline{x}, \underline{u}, \underline{\theta}) = 0 \qquad (2.1)$$

where $\underline{f}(\underline{x}, \underline{u}, \underline{\theta})$ - is a full nonlinear equation governing system operation. The states, $\underline{x}$, are a group of independant dynamic variables (N1, N2, T5, PS3). The controls, $\underline{u}$, are the inputs into the system (WF, VG). The ambient conditions, $\underline{\theta}$, determine the operating line (TT2, PT2, Po).

Linearization of eg (2.1) yeilds the following:

$$\Delta \dot{\underline{X}} = A \Delta \underline{X} + B \Delta u + \mathcal{F}(\Delta \underline{X} + \Delta \underline{u}) \qquad (2.2)$$

Where: $\Delta \underline{X}$ are the states perturbed about the nominal operating point. $\Delta \dot{\underline{X}}$ are the perturbation states rates, $\mathcal{F}$ represents a second order

effects of the perturbation, and A and B are the constant matrices.

For selected controls and ambient inputs, the operating point is defined based on non-linear engine deck. The next step is to perturb one dynamic variable (state or control) at a time, while holding the rest of states and controls constant. The resulted states derivatives can the be calculated, and elements of A and B matrices are defined as follows:

$$(a_x)_{ij} = \left(\partial \dot{x}_i / \partial x_j\right)\Big|_{\Delta x_K = 0} \qquad i;j;K = 1....n,\ K \neq j$$

$$(b_u)_{il} = \left(\partial \dot{x}_i / \partial u_l\right)\Big|_{\Delta x_j = 0} \qquad l = 1....m \tag{2.3}$$

To improve the low frequency accuracy of the model [6], the so called steady state forced match technique is used. The forced match technique has the advantage of producing an exact reproduction of control gains at steady state. This technique is based on unforced system dynamics and the nominal engine operating line. The calcualtion of the control matrix $\underline{B}$ by using forced match technique can be written as follows:

$$(b_u)_{il} = \left(\sum_{j=i}^{u} [(a_x)_{ij} \cdot \Delta x_j]\right) / \Delta u_l \qquad i = 1....n,\ j = 1....n,\ l = 1....m \tag{2.4}$$

The detailed demonstration of engine model generation for the TF34 engine is give in Appendix A. The state equation then becomes of the form $\Delta \dot{\underline{x}} = A \Delta \underline{x} + B \Delta \underline{u}$, more precisely:

$$\begin{bmatrix} \Delta \dot{N}_1 \\ \Delta \dot{N}_2 \\ \Delta \dot{T}_5 \\ \Delta \dot{P}_{S3} \end{bmatrix} = \begin{bmatrix} a_{11} & a_{12} & a_{13} & a_{14} \\ a_{21} & a_{22} & a_{23} & a_{24} \\ a_{31} & a_{32} & a_{33} & a_{34} \\ a_{41} & a_{42} & a_{43} & a_{44} \end{bmatrix} \cdot \begin{bmatrix} \Delta N_1 \\ \Delta N_2 \\ \Delta T_5 \\ \Delta P_{S3} \end{bmatrix} + \begin{bmatrix} b_{11} & b_{12} \\ b_{21} & b_{22} \\ b_{31} & b_{32} \\ b_{41} & b_{42} \end{bmatrix} \begin{bmatrix} \Delta W_F \\ \Delta VG \end{bmatrix} \tag{2.5}$$

The A and B matrices of the engine linear model are given in Appendix B. Note that all the variables are given in non-dimensional form and the numerical values of the A and B matrices reflect this. Table 2.2 shows non-dimensional variables and provides reasons for selecting the basis for non-dimensional form.

Table 2.2

Variable	Non-dimensional Form	Base Selection
Fan speed N1	N1/70%	7000 RPM is a 100% fan speed at SLS St. Day
Core speed N2	N2/15683%	15683 RM is a 100% air dynamic core speed
Interturbine Temp T5	T5/2000°R	2000°R max allowable temp at station 4.5
Compressor Discharge Static Pressure PS3	PS3/330 psia	330 psia max allowable pressure at station 3
Engine Fuel Flow WF	WF/4000 pph	4000 pph max level of fuel flow
Compressor Variable Geometry VG	VG/41°	41° full VG travel from open to closed position

2.5 Comparison of Linear and Nonlinear Models

The linear engine model at every design point was simulated for step change in each control input (WF and VG) separately and results were compared to the response of the TF34 nonlinear transient deck. The size of the step input was defined to assure validity of the linear model within the resulted perturbation. Fuel flow step of 10-20% of the steady state value and variable geometry step of 4-5° were found to be satisfactory. The figures which show the comparison of linear and nonlinear models are give in Appendix C.

In general the linear and nonlinear models step responses are very close. The linear model is transiently faster by 30-40 milli-seconds than the nonlinear one at TAKEOFF power and up to .4 seconds at idle; however, this applies only to the certain regions of transients. The convergence time on the steady state is practically the same for both linear and nonlinear models. In addition within 10-20% of the final value, linear and nonlinear models behave almost identical. The

differences in the transient response between the linear and non-linear models can be contributed to heat sink and second order non-linear effects which can amount to 30-40 milli-seconds at TAKEOFF power and up to .1 sec. at Idle, and cannot be modeled based on unbalance torque analysis. The relatively large (.4 sec.) difference at Idle can be contributed to the limited knowledge of engine dynamics at this region. As a result, unbalanced torque calcuations were somewhat off. However, the linear model is found to be satisfactory even at Idle region based on good convergence on steady state value, excellent prediction of T5 overshoot, and relatively loose constraints on rotors speed overshoot at low power region.

2.6 Sensor and Actuator Dynamics

The dynamics of sensors measuring control variables are usually incorporated into the linear model. However, sensor dynamics can be neglected if they are 3 to 4 times faster than crossover frequency, or can be confidently predicted and compensated for. Rotor speed measurements are obtained from frequency conversion of an alternator output (core speed) and magnetic pick up (for speed). Time delays of these signals vary from 2 ms at TAKEOFF to 25 ms at low power. This is due to counter delays at the low speed. Actuators, fuel flow and variable geometry, position signals are provided by linear variable transducers (LVDT) which measure stroke on the servo position. These instruments measure phase shift between excitation and return signals passing through the variable inductance device. The phase converters are free running, and measured values are asynchronously loaded into the control system processor. There is practically no time delay, and the error sources are due primarily to load deflection on the linkages and hardware deterioration.

Pressure measurements are accomplished by vibrating crystal transducers. These devices produce high response signals with 1-2 ms time delay. The interturbine temperature measured by thermocouple provides an accurate linear temperature/resistance relationship. This device has an airflow dependant time constant which can exceed three (3) seconds at high altitude, low power settings. The compensation for thermocouple time delay can be accurately provided based on fuel flow and altitude measurements.

One of the design objectives is to make crossover frequency less than ten (10) rad/sec. By imposing this constraint on the design we can neglect sensors dynamics, and assume that all the variables can be measured instantaneously.

The control actuator dynamics are modeled as pure integrators and LQR design will define how fast they have to be to satisfy transient performance objectives. The saturation limits are taken to be the same as for the currently used control system.

The control design is limited by actuator saturation limits and one of the constraints on LQR design is to avoid saturation of actuators at any operating condition.

2.7 General Constraints

Engine linear models are generated at four points along the engine operating line at sea level static, standard day conditions as shown in Fig. 2.7.

The local control system design is done by perturbations around each design point. The size of perturbations is limited to assure validity of the linear model within the design interval. The transient system response within each perturbation has to be performed in a minimum amount of time and has to satisfy engine constraints, summarized in Table 2.1.

In addition there are performance and hot section life constraints which can be stated as follows:

- o No fan speed (N1) overshoot
- o Max allowable T5 temperature level of 2080°R with .4 sec. time limit at that temperature.

The engine dynamics and operating lines vary with operating conditions, such as: altitude, ambient air temperature, mach number, and bleed/power extractions. The qualitative illustration is given in Figs. 2.8, 2.9, 2.10. The engine flight envelope is given in Fig. 2.11

It is obvious, at this point, that optimal control gains have to be adapted to the changing plant dynamics in order to assure equally good transient performance throughout the engine flight envelope (Fig. 2.13) To accomplish this an optimal control gains scheduling will be developed as a part of the global control design. The global design will incorporate targe estimator, optimal control gains scheduling, and trajectory control. The trajectory control will assure engine operation within its constraints during large engine transients. The global design will be developed based on the engine dynamics corrected for altitude and ambient air temperature. The Mach number effects can be neglected for subsonic jets, and will not enter into the global design. The bleed/power extraction effects on the engine operating line is assumed to be handled by a separate T5 limiting function or N1 reference bias in order to prevent T5 overtemperature.

To avoid modeling of high order sensors and control hardware dynamics and assure high attenuation in the region of unmodeled uncertainties; hydraulic and mechanical resonances and thermo time delays, the cross-over frequency in both loops will be limited to 10 rad/sec.

2.8 Conclusions

The variable geometry position can be off schedule, either open or closed, in certain regions during the engine transient operation. By positioning VG more open than nominal, where it is possible from stall margin considerations, will decrease engine acceleration time.

Based on engine unbalanced torque equations a fairly accurate engine linear model can be developed. Engine corrected dynamics are required for global design to assure good transient characteristics throughout the flight envelope.

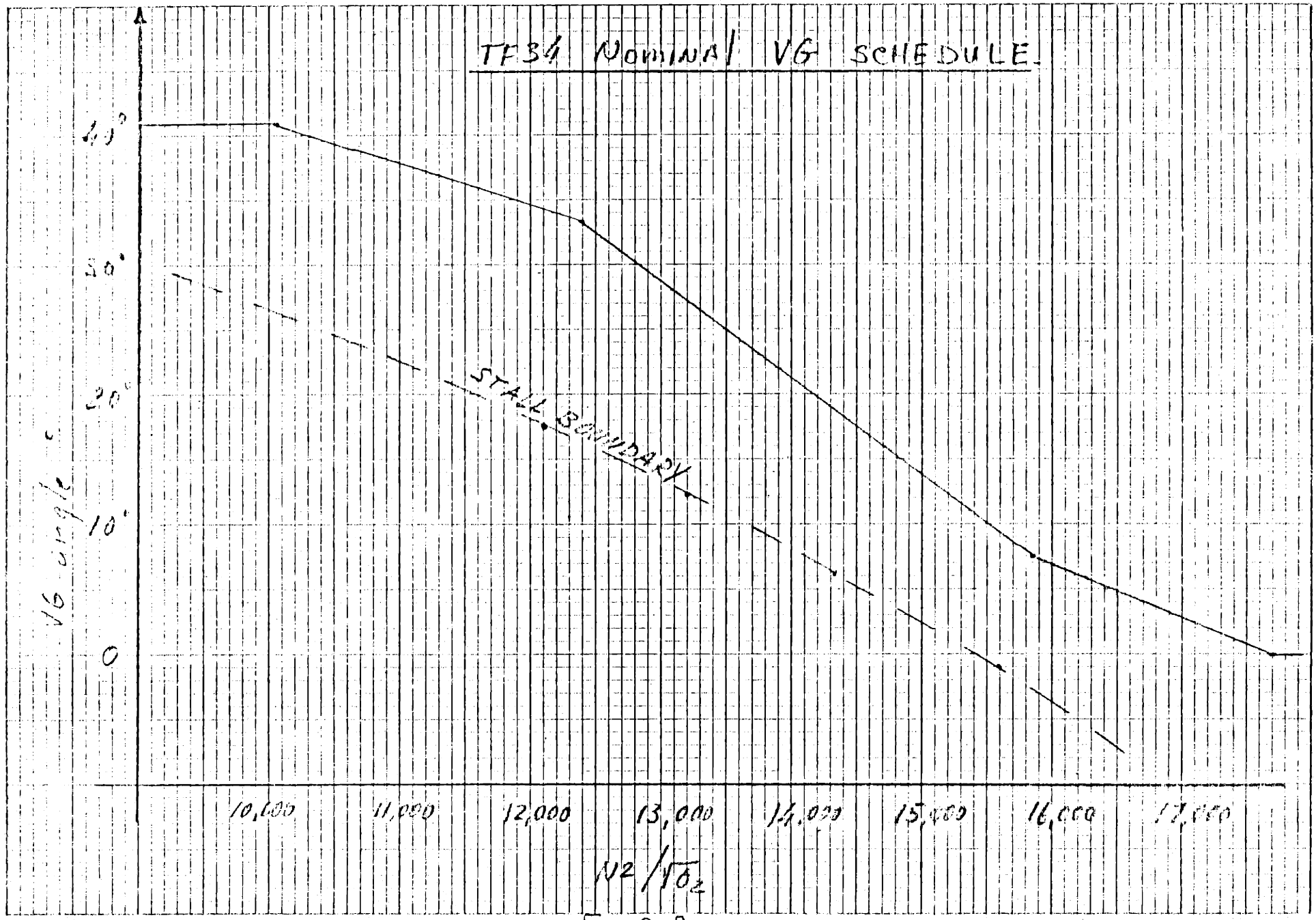
TF34 NOMINAL VG SCHEDULE
40°
30°
20°
10°
0
VG angle
10,000
11,000
12,000
13,000
14,000
15,000
16,000
17,000
N2/√θ2
STALL BOUNDARY

Fig 2.2

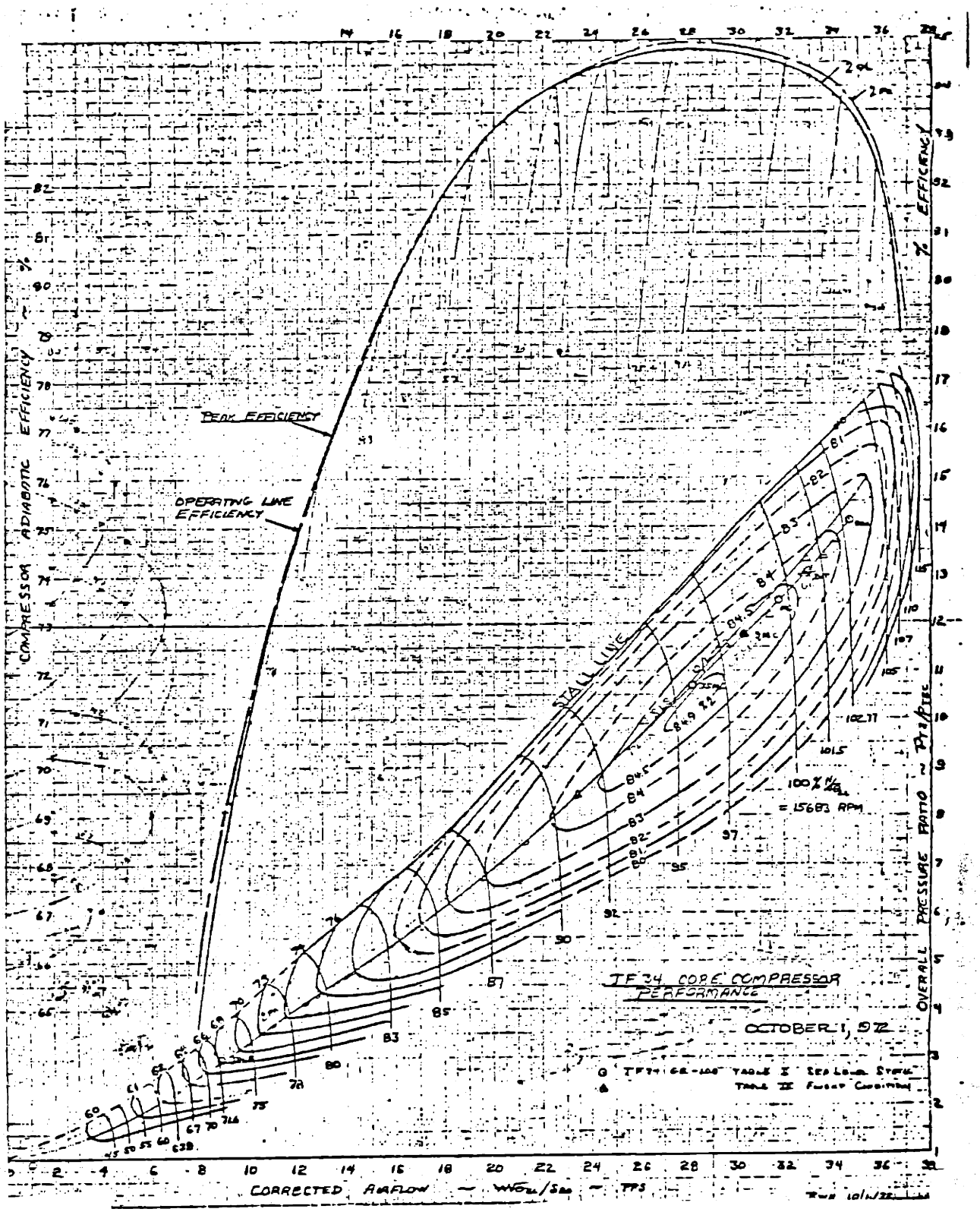

TF34 CORE COMPRESSOR
PERFORMANCE
FIG 2.3

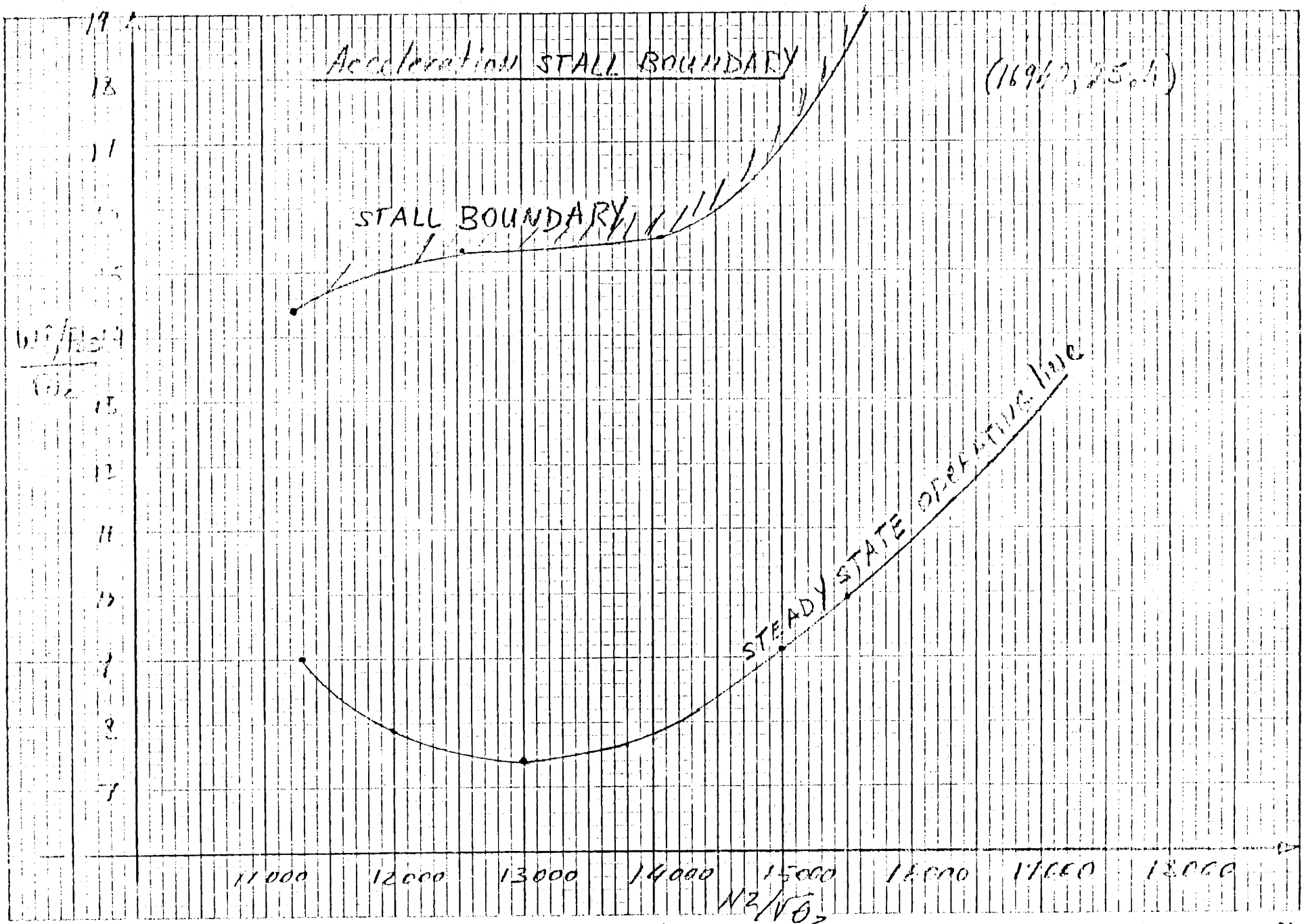
Acceleration STALL BOUNDARY
(169½, 25.4)
STALL BOUNDARY
STEADY STATE OPERATING LINE
19
18
17
16
15
14
13
12
11
10
9
8
7
11000
12000
13000
14000
15000
16000
17000
18000
N2/√θ2

Fig 2.4

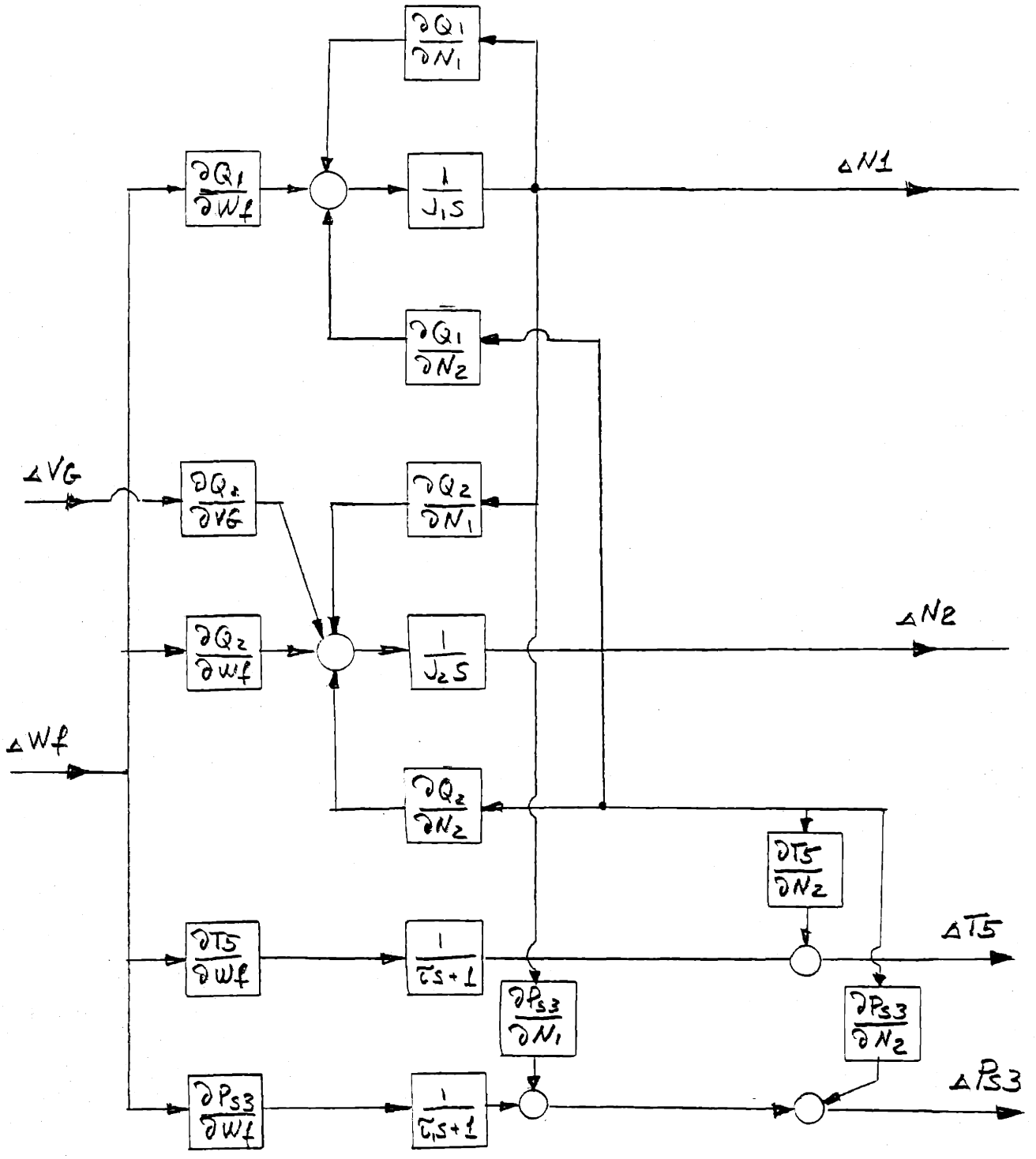

J1 = 158 lb ft^2 = 35.97 ft lb/% N1/sec
J2 = 38 lb ft^2 = 19.38 ft lb/% N2/sec

Fig. 2.5

TF34 Linear Model
Block Diagram

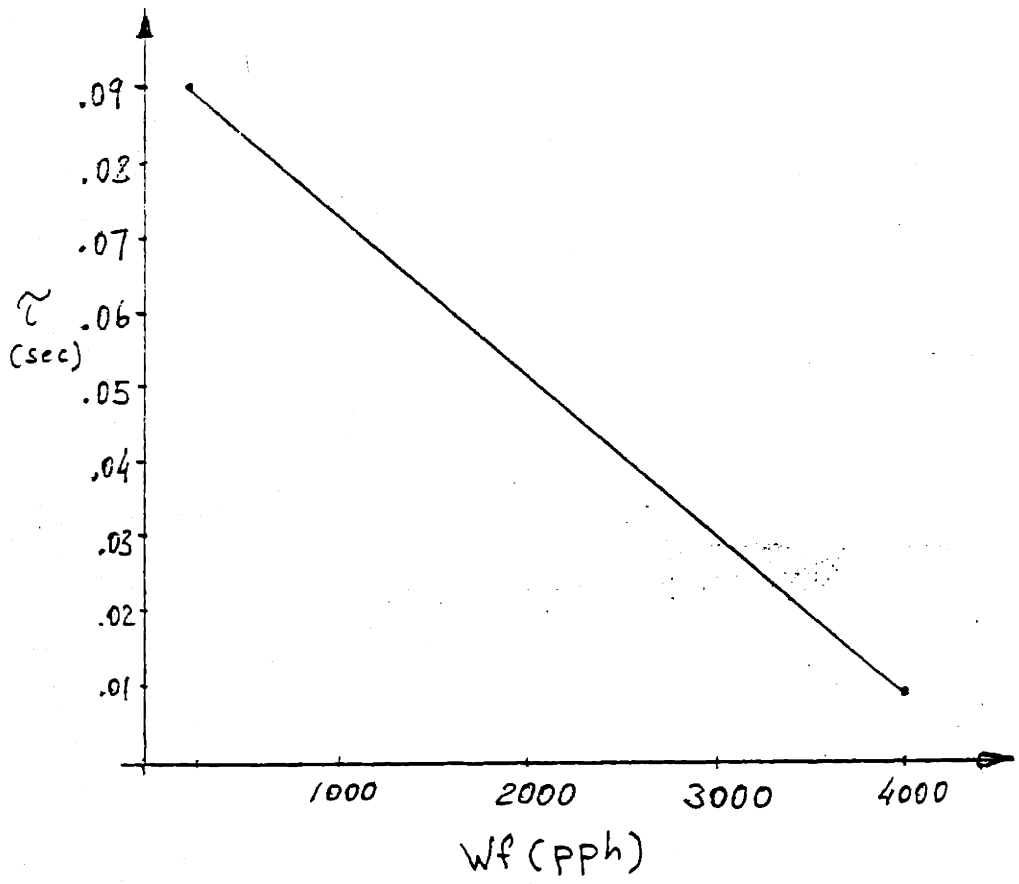

INTERTURBINE GAS TEMPERATURE TIME CONSTANT

FIG 2.6

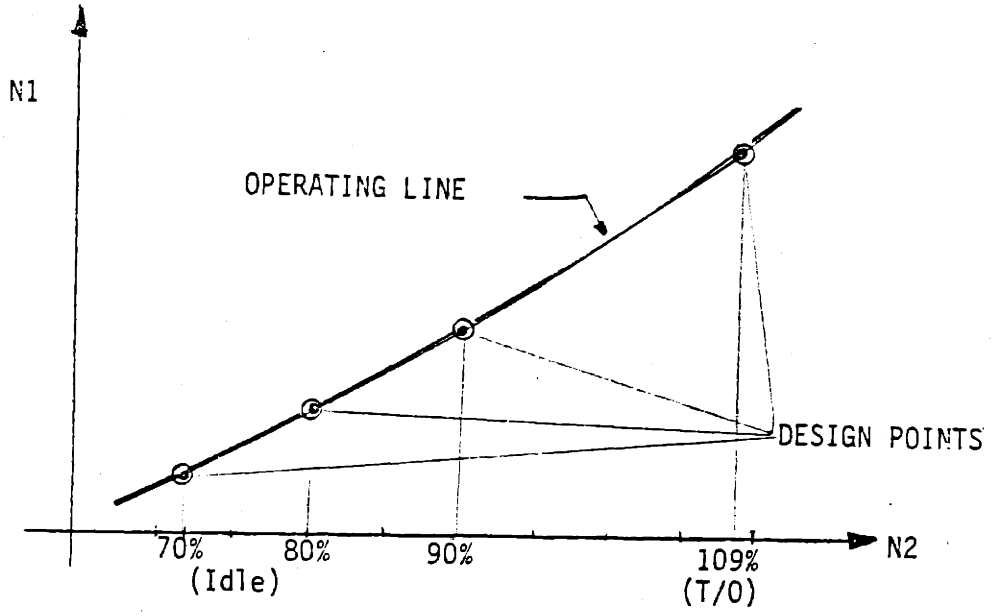

LQR DESIGN POINTS

FIG 2.7

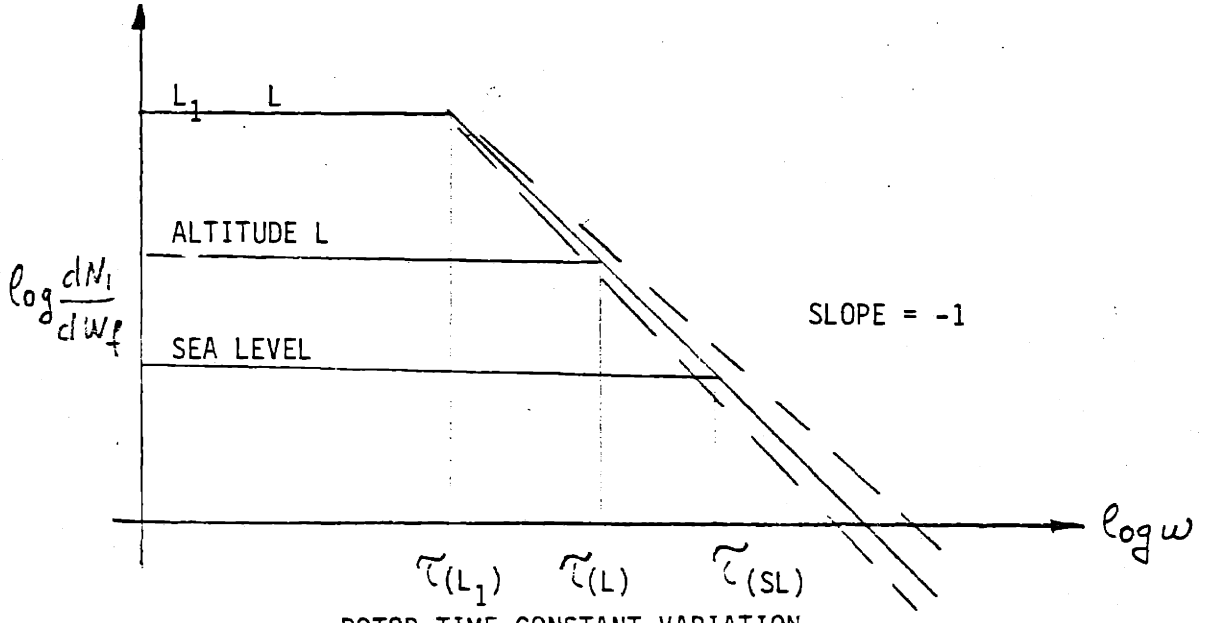

ROTOR TIME CONSTANT VARIATION
AT CONSTANT ROTOR SPEED
AS A FUNCTION OF ALTITUDE

FIG 2.8

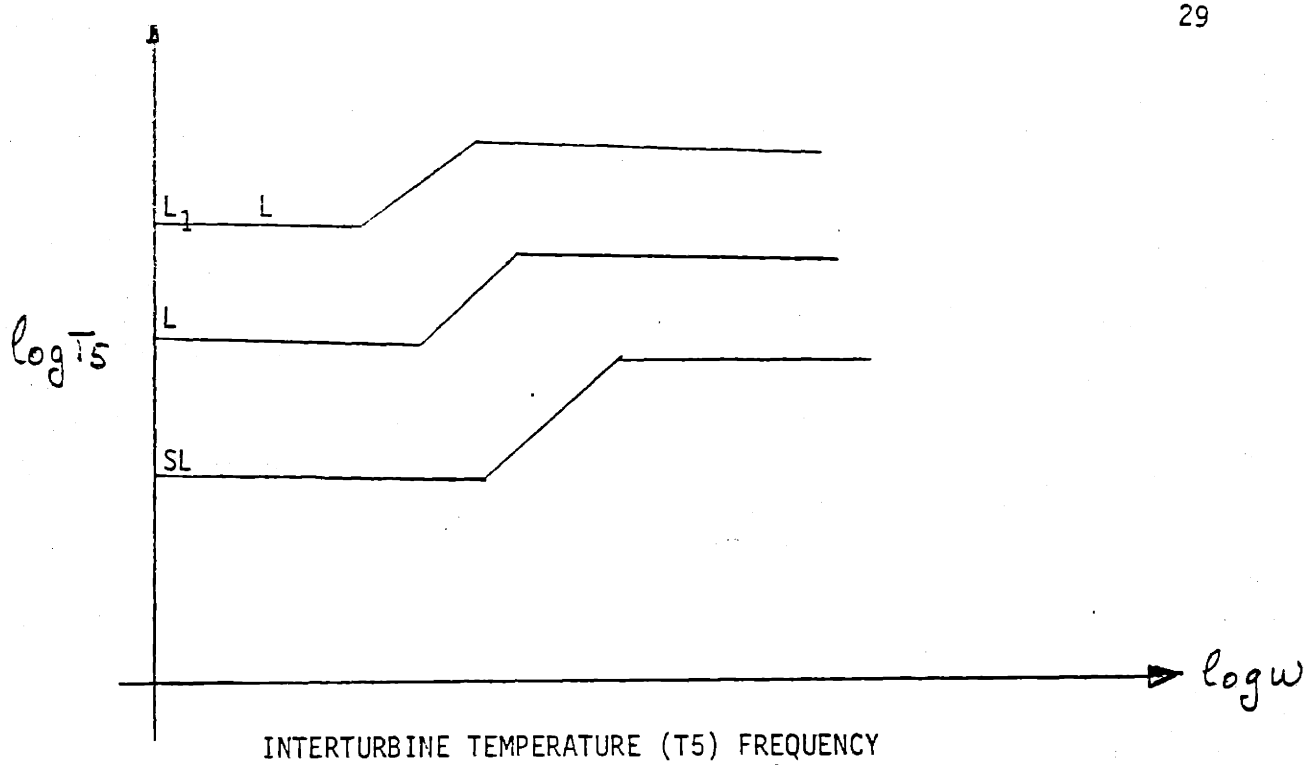

INTERTURBINE TEMPERATURE (T5) FREQUENCY
RESPONSE AT CONSTANT T5 AS
A FUNCTION OF ALTITUDE

FIG 2.9

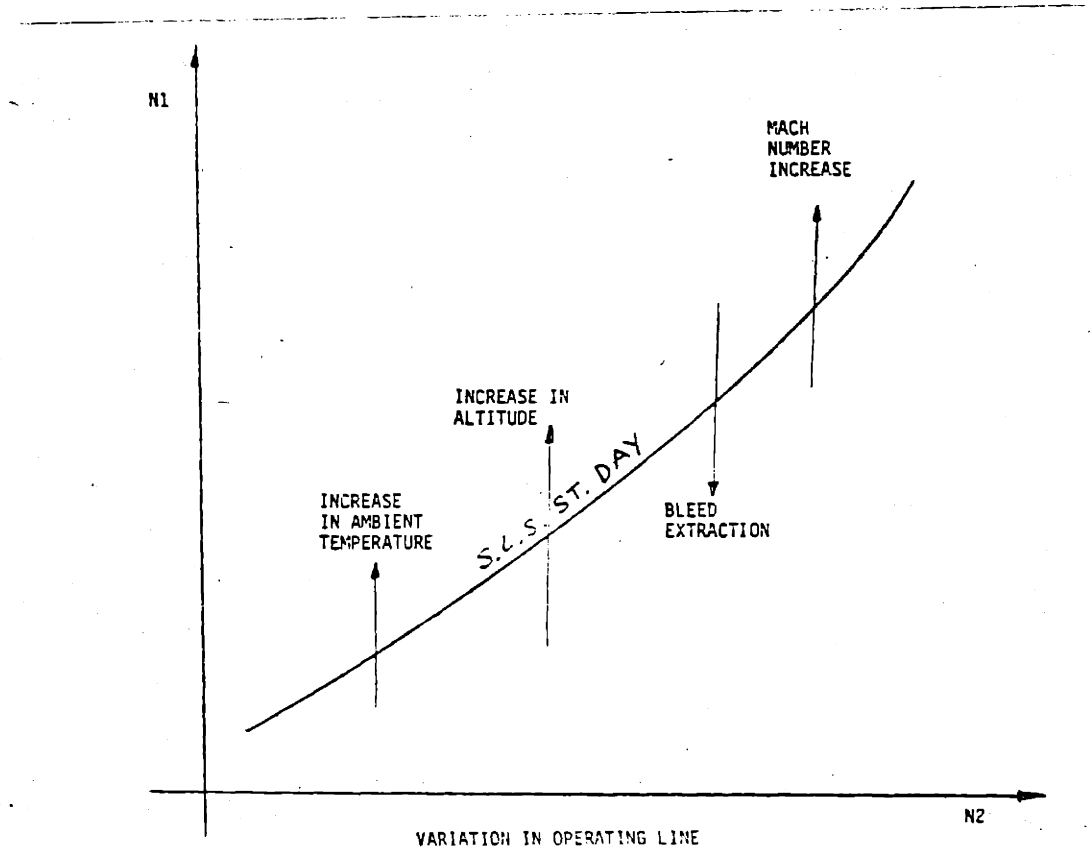

VARIATION IN OPERATING LINE
WITH OPERATING CONDITIONS

FIG 2.10

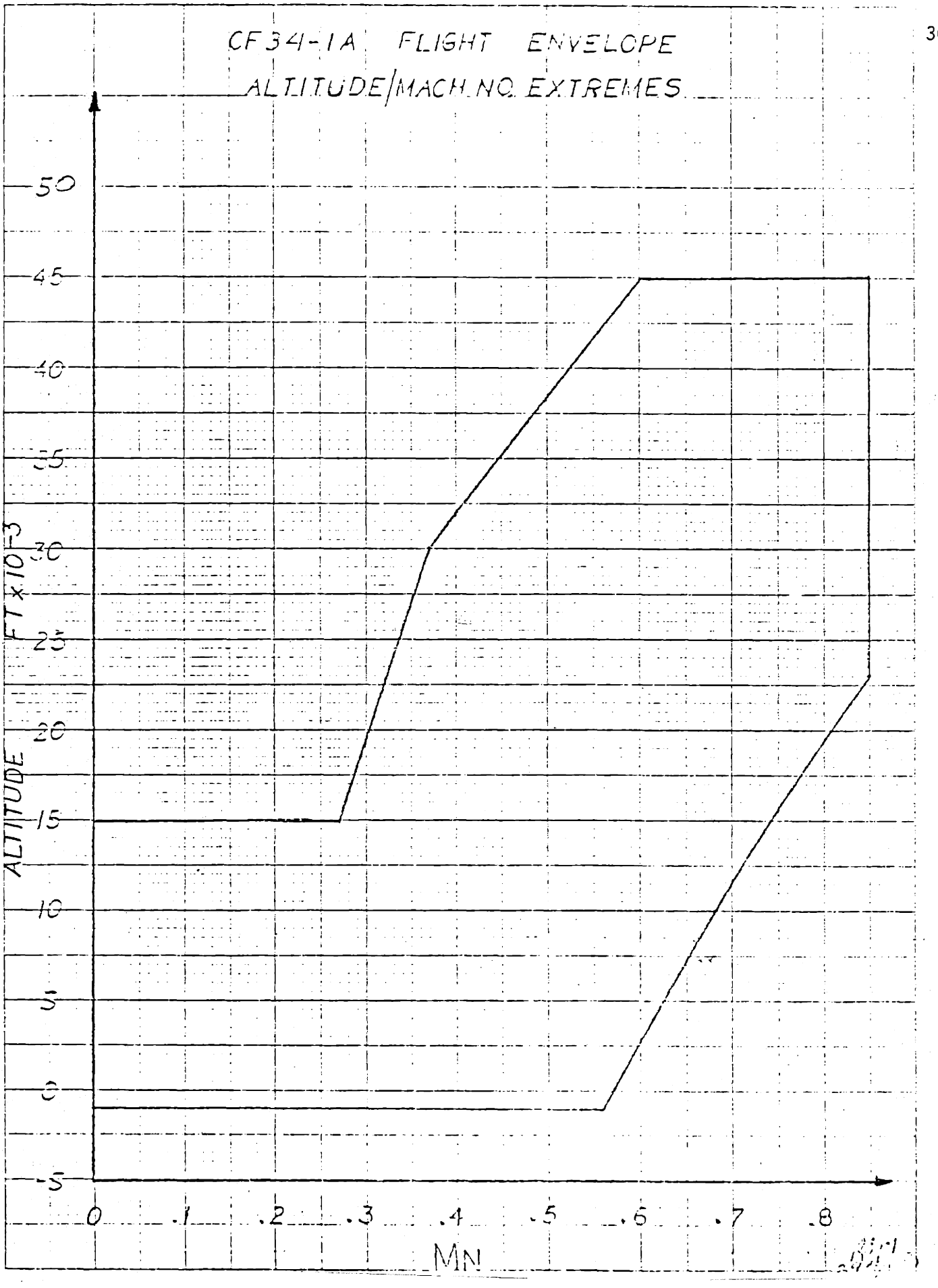

Fig 2.11

3. LOCAL CONTROL SYSTEM DESIGN

3.1 Introduction

The modern multivariable jet engine control syntheses rely upon the methodology of the linear optimal control theory, in particular, the Linear Quadratic Regulator (LQR) [7, 12, 13]. The LQR method is based on Linearization of the jet engine nonlinear dynamics about a nominal operating point, and then selection of the appropriate state variable and control gains to generate a linear feedback control system. In this chapter a rational way to use LQR methodology for local control system design is outlined.

3.2 Control System Design Based on Linear Quadratic Regulator Methodology

Basic Linear Quadratic Regulator (LQR) methodology can be stated as follows:

[7]

For a given linear system with the state space representation:

$$\dot{X} = AX + BU \tag{3.1}$$

Where $X \in R^n$, $u \in R^m$

and $\left.\begin{array}{l}(A,B) \text{ - stabilizable} \\ (AQ^{\frac{1}{2}}) \text{ - detectible}\end{array}\right\}$ (3.2)

The optimal linear control law which minimizes the quadratic performance index: $J(u) = \int_0^\infty (x^T Q x + \rho u^T R u)\, dT$

$$\text{where} \quad Q = Q^T \geq 0 \quad \text{and} \quad R = R^T > 0 \tag{3.3}$$

is given as $u^* = -G\underline{x}$ (3.4)

where $G = R^{-1} B^T P$ (3.5)

and $P = P^T > 0$ is the unique positive definite solution of Algebraic Riccati Equation:

$PA + A^T P + Q - PBR^{-1}B^T P = 0$

The linear closed loop system is guaranteed to be stable and has <u>at least</u> gain margin $GM = (\frac{1}{2}, \infty)$ and

Phase margin $PM = \pm 60°$, [8] as long as R is diagonal.

It is important to emphasize that actual gain and phase margins can be substantially wider.

There is, however, one deficiency in LQR type controller, namely, in classical sense it has "proportional plus derivative" structure. As a

result, there will be some finite steady state error when constant disturbances act upon the system. This becomes specifically important for the control of a nonlinear system such as jet engine, where conversion on the schedule value of the outputs is very important.

This problem can be handled by introducing integral control structure into the system.

3.2.1 Integral Loop Shaping

Rewrite eq (1A) by introducing constant disturbance vector $\underline{d} \in R^n$

$\dot{\underline{X}} = A\underline{X} + \underline{B} + \underline{d}$

The controlled outputs eq:

$y = c\underline{x}$

where $x \in R^n$, $Y \in R^p$, $u \in R^m$ and $p \leq m$

The open loop model is:

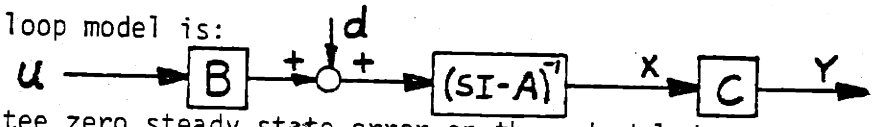

To guarantee zero steady state error on the scheduled ouput Y we'll introduce augmented states $\dot{X}r = Y = Cx$, then the augmented open loop model becomes

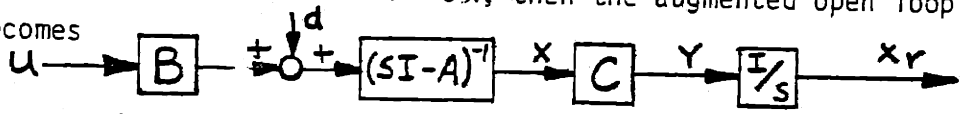

The state equation becomes:

$$\begin{bmatrix} \dot{x} \\ \dot{x}_r \end{bmatrix} = \begin{bmatrix} A & B \\ C & 0 \end{bmatrix} \cdot \begin{bmatrix} x \\ x_r \end{bmatrix} + \begin{bmatrix} B \\ 0 \end{bmatrix} \cdot u + \begin{bmatrix} d \\ 0 \end{bmatrix} \quad \text{or} \quad \dot{\underline{x}} = \tilde{A}x + \tilde{B}u \qquad (3.6)$$

The augmented plant is controllable if the original plant is controllable and has no transmission zeros at the origin. For definition of transmission zeros see Appendix D.

Conditions for augmented plant controllability is satisfied for the jet engine, which can be easily seen by inspection.

In the TF34 control system design we will use two augmented states to guarantee unique steady state point. N1 and VG will be scheduled outputs, and so they are the ones which will be augmented:

$$X_r = \begin{bmatrix} XNF \\ XVG \end{bmatrix} \quad \text{where} \quad \begin{aligned} \dot{XNF} &= NF \\ \dot{XVG} &= VG \end{aligned}$$

Two inputs into the system fuel flow (WF) and variable geometry (VG) are the actuators outputs. Model of these actuators will be included into engine model. The actuators will be modeled as simple integrators.

3.2.2 Addition of the Input Dynamics to the Open Loop Model

Let the fuel flow actuator input be V1, and variable geometry actuator input be V2, then

$$\dot{\underline{u}} = \underline{V} = \begin{bmatrix} V_1 \\ V_2 \end{bmatrix}$$,and system state equations:

$$\dot{\underline{\tilde{x}}} = \underline{\tilde{A}}\,\underline{\tilde{x}} + \underline{\tilde{B}}\,\underline{V}$$

$$\begin{bmatrix} \dot{\underline{x}} \\ \dot{\underline{u}} \end{bmatrix} = \begin{bmatrix} \underline{\tilde{A}} & \underline{\tilde{B}} \\ 0 & 0 \end{bmatrix} \begin{bmatrix} \underline{x} \\ \underline{u} \end{bmatrix} + \begin{bmatrix} 0 \\ I \end{bmatrix} \underline{V} \qquad (3.7)$$

It can be easily show that if the original system satisfies conditions (3.2), system with added input dynamics does also.

3.2.3 High Frequency Rolloff (Attenuations)

The standard Linear Quadratic Regulator loop transfer function has a single pole rolloff. It was shown [14] that physical system has at least two poll rolloff. This implies that single pole rolloff is inadequate when frequency range of uncertanties (neglected time delays, mechanical resonances, and unmodeled high frequency dynamics) is close to crossover frequency. In this study, introduction of second pole rolloff will be discussed, but dynamics associated with them will not be considered in LQR design and simulations. This approach can be supported by the fact that second pole rolloff dynamics will be on the order of milli-seconds and will not effect the system transient characteristics. In addition, by not weighting states associated with second pole rolloff dynamics in the performance index we will assure no change in feedback gain matrix.

The basic idea in obtaining two pole rolloff using linear quadratic control theory is to cascade dynamic compensator with a plant input as shown:

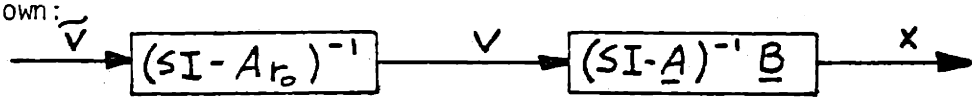

The equation for dynamic compensator: $\dot{\underline{V}} = A_{ro} + \tilde{\underline{V}}$; (3.8)

$$A_{ro} = \begin{bmatrix} 1/\tau_1' & 0 \\ 0 & 1/\tau_2' \end{bmatrix} \qquad (3.9)$$

and $\dot{V}_1 = -\frac{1}{\tau_1'} V_1 + \tilde{V}_1 \; ; \quad \dot{V}_2 = -\frac{1}{\tau_2'} + \tilde{V}_2 \; ;$

or $V_1 = \left(s + \frac{1}{\tau_1'}\right)^{-1} \tilde{V}_1 \; ; \quad V_2 = \left(s + \frac{1}{\tau_2'}\right)^{-1} \tilde{V}_2 \; ;$

τ_1' and τ_2' can be sized to provide a second pole rolloff in the frequency range where it is needed.

Thus the state equations are:

$$\begin{bmatrix} \dot{\underline{x}} \\ \dot{\underline{v}} \end{bmatrix} = \begin{bmatrix} \underline{A} & \underline{B} \\ 0 & A_{ro} \end{bmatrix} \cdot \begin{bmatrix} \underline{x} \\ \underline{v} \end{bmatrix} + \begin{bmatrix} 0 \\ I \end{bmatrix} \underline{\tilde{V}} \qquad (3.10)$$

The new system is clearly controllable if the original system is controllable to start with.

It is important to notice that for the open loop system (3.10) LQR design will guarantee phase and gain margin at the inputs into the dynamic compensator ($\underline{\tilde{V}}$) but not at the inputs into the actuators ($\underline{V}$). However, by selecting τ_1' and τ_2' such that second poles rolloff are placed 1.5 - 2 times the original plant crossover frequency, we will assure practically the same stability margins at the inputs into the dynamic compensator ($\underline{\tilde{V}}$).

Note that jet engine lowest frequency uncertainties are at 30-40 r/sec. Therefore, by forcing crossover frequency to be below 10 r/sec. we have sufficient range to select τ_1' and τ_2', so they will not effect system characteristics.

3.2.4 Final Set of Linear Dynamics

The final set of linear dynamic equations, based on which LQR design is implemented, consists of six engine states; N1, N2, T5, PS3, Wf,

VG, two augmented states; XN1 and XVG and two inputs; V1 and V2, which are fuel flow and variable geometry actuators positions respectively.

$$\begin{bmatrix} \Delta\dot{N}_1 \\ \Delta\dot{N}_2 \\ \Delta\dot{T}_5 \\ \Delta\dot{P}_{S3} \\ \Delta\dot{W}F \\ \Delta\dot{V}G \\ \dot{XN}_1 \\ \dot{XVG} \end{bmatrix} = \left[\begin{array}{cc:cc:cc} \multicolumn{2}{c:}{\multirow{4}{*}{A}} & \multicolumn{2}{c:}{\multirow{4}{*}{B}} & 0 & 0 \\ & & & & 0 & 0 \\ & & & & 0 & 0 \\ & & & & 0 & 0 \\ 0 & 0 & 0 & 0 & 0 & 0 \\ 0 & 0 & 0 & 0 & 0 & 0 \\ 1 & 0 & 0 & 0 & 0 & 0 \\ 0 & 0 & 0 & 0 & 1 & 0 \end{array}\right] \begin{bmatrix} \Delta N_1 \\ \Delta N_2 \\ \Delta T_5 \\ \Delta P_{S3} \\ \Delta WF \\ \Delta VG \\ \Delta XN_1 \\ \Delta XVG \end{bmatrix} + \begin{bmatrix} 0 & 0 \\ 0 & 0 \\ 0 & 0 \\ 0 & 0 \\ 1 & 0 \\ 0 & 1 \\ 0 & 0 \\ 0 & 0 \end{bmatrix} \begin{bmatrix} V1 \\ V2 \end{bmatrix} \qquad (3.11)$$

For A and B matrices see Appendix B.

3.3 LQR Weighting Matrices

3.3.1 Control Weight Matrix R

The R matrix was chosen to be diagonal R = diag (r11, r22). The r11 to r22 ratio will define relationship between weightings on the control inputs V1 and V2.

This ratio was determined based on steady state operating lines characteristics Fig. 3.1 and 3.2.

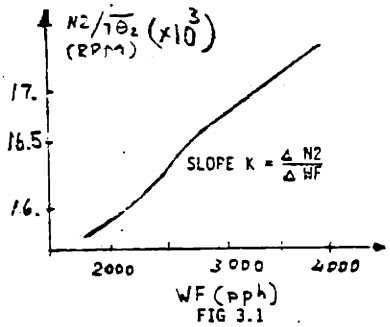

FIG 3.1

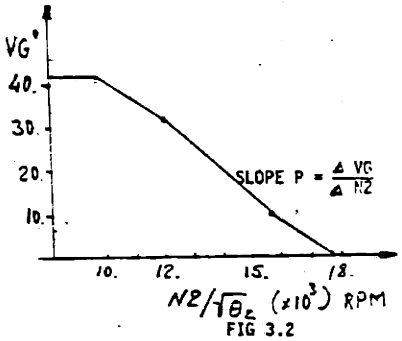

FIG 3.2

For any equilibrium point along the operating line the following equations can be written:

$$\frac{\Delta VG}{\Delta N_2/\sqrt{\theta_2}} = \frac{\Delta VG}{\Delta WF} \cdot \frac{\Delta WF}{\Delta N_2/\sqrt{\theta_2}} = P \qquad (3.12)$$

or $$\frac{\Delta VG}{\Delta WF} = K \cdot P \rightarrow \Delta VG = KP\,\Delta WF \qquad (3.13)$$

Hence, performance index is expressed as a quadratic criterion we can use an absolute value of (k·p). Taking derivative of both sides of eq (3.12)

$$\Delta \dot{V}G = |K \cdot P|\,\Delta \dot{W}f \qquad (3.14)$$

OR $V_2 = |kp|\,V_1 \longrightarrow$ from this equation relationship between r11 and r22 is

$$\frac{r_{11}}{r_{22}} = \frac{V_1}{V_2} = \frac{1}{|K \cdot P|} \; ; \qquad (3.15)$$

3.3.2 States Weighting Matrix Q

All the states were normalized (see Table 1) and the matrix Q was chosen to be a diagonal Q = diag (q11, q22, q33, q44, q55, q66, q77, q88).

The relationship between the diagonal elements of the Q Matrix in performance index determines the penalty assigned for overshoot of one state variable relative to the others. In addition, these diagonal elements define relative relationship between the driving frequencies and the natural frequencies (or time constants) for the state variable.

The closed loop eigenvalues were limited to the following location in the S-plane:

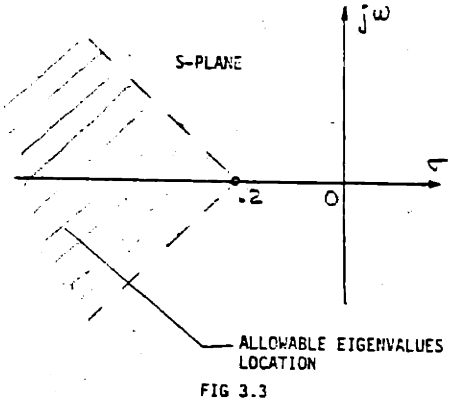

FIG 3.3

The diagonal elements for Q Matrix were determined by analyzing physical significance of weightings on the states, and by demanding certain closed loop eigenvalues locations. The numerical

weighting matrices, R and Q are given in Appendix E.

3.4 Structure of LQR Design

The LQR design was performed at every design point along the engine operating line based on the final set of linear dynamics (eq 3.10). The set of calculated linear gains was simulated with a linear engine model to assure minimum time and within the constraints acceleration. The numerical value of the optimal control gains, and open and closed loop system eigenvalues are given in Appendix F.

The resulted structure of LQR design is presented in Fig. 3.4.

It is interesting to note that open loop eigenvalues of fast thermodynamic variables (T5 and PS3) remain practically at the same location for the closed loop system. This means that solution for optimal control based on LQR methodology automatically defines open loop eigenvalues which have to be moved to satisfy performance criterion (eq 3.3). Another important result is that magnitudes of the feedback gains from T5 and PS3 are much smaller than the rest of the gains. Based on that observation, state weighting matrix Q can be modified to have zero weights on T5 and PS3. This kind of the Q matrix in performance index produce zero gains from T5 and PS3, but at the same time has, practically no effect on the rest of the gains or closed loop eigenvalues position. The fact that no feedback gains required from T5 and PS3 is simplifies significantly LQR design implementation. However, this does not mean that fast variables can be neglected in LQR design. In fact, only these variables define how fast the LQR loop can be made.

3.5 Crossover Frequency for Multivariable System

The singular value analysis are used to define range of crossover frequency variation for LQR design. The singular value of multi-input, multi-output system loop transfer function has the same meaning as a loop transfer function magnitude for single input, single output case.

The crossover frequency of the multivariable system is bounded between smallest, $\underline{\sigma}$, and largest, $\bar{\sigma}$, singular values of its loop transfer function when both, smallest and largest, singular values

are equal to unity. The singular values of the loop transfer function are functions of frequency and smallest and largest of them is defined through the use of the matrix norms:

$$\underline{\sigma} = \min \|Ax\|_{(\|x\|_2 = 1)} = \sqrt{\lambda_{min}(A^H A)}$$

$$\bar{\sigma} = \max \|Ax\|_{(\|x\|_2 = 1)} = \sqrt{\lambda_{max}(A^H A)} \qquad (3.16)$$

where $\|\cdot\|$ is the Euclidian norm

$\lambda(\cdot)$ denotes eigenvalue

A^H - is the harmition transpose of A

$\underline{\sigma}$ and $\bar{\sigma}$ are called minimum and maximum singular values of A respectively.

The singular values can be calculated with available linear system software, for example EISPACK. More information on singular values and their properties can be found in any advanced linear algebra book, for example "Linear Algebra and it's Applications" by Gilbert Strang.

The loop transfer function smallest and largest singular values are plotted as a function of frequency. Figs. 3.5, 3.6, 3.7, 3.8, for all the design points. The crossover frequency is smaller than 10 rad/sec for all the design points. The crossover frequencies ranges are presented in Table 3.1.

Table 3.1

Design Point	Crossover Frequency Range
TAKEOFF	4.6 - 6.2 r/s
90% N2	2.2 - 8.1 r/s
80% N2	1.2 - 4.2 r/s
Idle	.8 - 2.9 r/s

3.6 Inverse Nyquist Arrays

The Inverse Nyquist Arrays is a magnitude plot of the separate entrances of the inverse of the loop transfer function as a function of frequency. For our 2 x 2 loop transfer function we have four (4) separate plots for each design point, as shown in Figs.

The expression for the LQR loop transfer function is:

$$L(s) = G(sI - A)^{-1}B$$

The inverse of the L(s) is: $T(s) = L^{-1}(s) = \begin{bmatrix} T_{11}(s) & T_{12}(s) \\ T_{21}(s) & T_{22}(s) \end{bmatrix}$ (3.17) (3.18)

For diagonally dominant systems the magnitudes of T11(s) and T22(s) must be much larger than magnitudes of T12(s) and T21(s). Figures 3.9, 3.10, 3.11, 3.12 show that for TAKEOFF power LQR transfer function represents a diagonally dominant system; however, at lower power settings diagonal dominance becomes weaker, and at Idle diagonal dominance does not exist. This result was quite unexpected. It is not known at this point in time, and it is outside of the scope of this thesis to try to define set of conditions, which have to be satisfied by the plant open loop model in order to guarantee diagonal dominance by the LQR loop transfer function. More research in the area of LQR methodology is needed to answer this question.

3.7 Transient Responses of LQR Design vs. Current TF34 Control System

Transient response of LQR design is consistantly faster than current TF34 control system transient response. At simulated acceleration from part power to TAKEOFF. LQR design was twice as fast as current TF34 design. In addition, T5 overshoot is only 20°F vs. 91°F. This type of acceleration is very common in real life applications and reduction of acceleration time from 4 to 2 sec represents a significant improvement in engine performance.

The summary of the fan speed and T5 transient characteristics is given in Table 3.1 in addition to comparison between transient responses for LQR design and current TF34 is presented in Appendix G. It is worth mentioning that for PLA transients from 29.8 to 46.8 degrees, and from 23.5 to 29.8 degrees the acceleration time for LQR design is twice and one and a half times faster respectively than for the current TF34; however, there is a penalty of approximately 200°F higher overshoot on gas temperature T5 as compared to the current TF34 design. The gas temperature overshoot during these transients has a ramp type of the profile with a pick value reached at approximately .4 to .5 sec. This type of the transient gas temperature overshoot does not cause any temperature overshoot of the high pressure turbine blades and concluded to be acceptable. To support this conclusion, we note that based on the TF34 engine experience, the tip of the leading edge of the high pressure turbine blades has, practically, the same thermal time constant as the thermocouple probe at station 5. The thermocouple time constant is defined based on physical core aiflow as follows:

$$\tau_{TH} = 2.8 \left(\frac{3.98}{WA}\right)^{.35} \quad (3.19)$$

As an example, consider PLA transient from 29.8 to 46.8 degrees. The core airflow averaged over the first .5 sec equal to 14.97 lb/sec, and thermocouple time constant evaluated from eq 3.19 is 1.76 sec. The Fig.3.13 shows gas temperature and resulted thermocouple temperature for this transient. The gas temperature at station 4 is proportional to the gas temperature at station 5 for a chocked high pressure turbine. As a result, the gas temperature at station 4 will have the same transient profile as the gas temperature at station 5.

The similarity in thermal time constants and transient gas temperature profiles between station 5 thermocouple and leading edge of the high pressure turbine blades (station 4) implies that during the transient the temperature of the leading edge of the blades does not overshoot.

Table 3.1

PLA TRANS	TIME TO REACH SCHEDULED FAN SPEED		GAS TEMPERATURE T5 OVERSHOOT OVER FINAL SS VALUE		TIME TO PICK GAS TEMPERATURE T5	
	LQR	CURRENT TF34	LQR	CURRENT TF34	LQR	CURRENT TF34
46.8 - 85.4 Part Power to Takeoff	2.0	4.0	20	70	.8	2.0
29.8 - 46.8	2.0	4.0	380	185	.4	.8
23.5 - 29.6	2.0	3.0	755	515	.5	.7
18.5 - 23.5	3.0	4.0	300	585	.7	.7

3.8 Conclusions

The rational procedure for applying LQR methodology for the linearized engine model is developed. Based on linear simulations, LQR design is 2 to 1.5 time faster and more accurate in providing thrust transients than current TF34 design. There were no fan speed overshoots in LQR simulated transients, which for high-bypass engine means no thrust droop or overshoot.

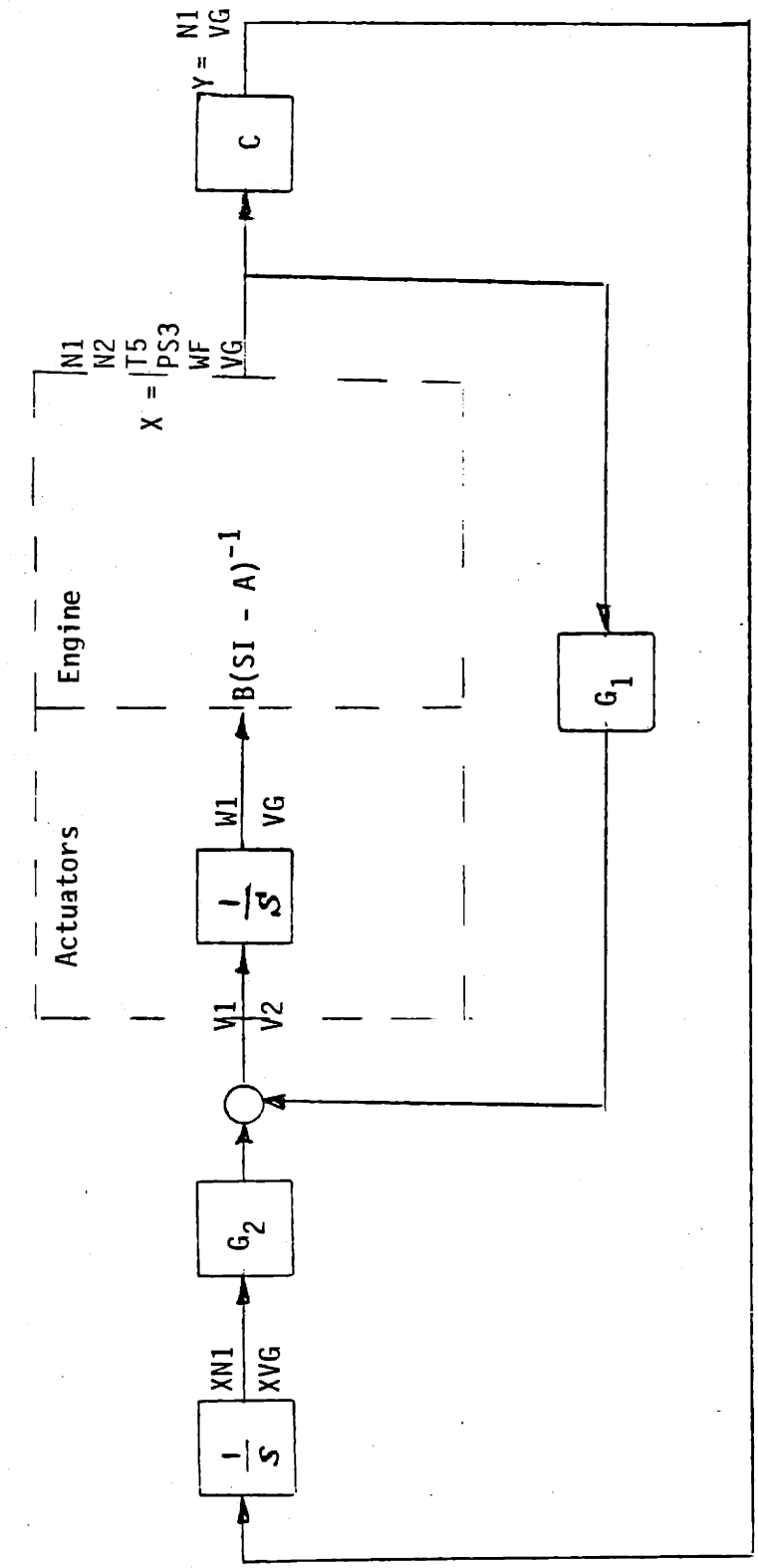

$G = [G_1 \cdot G_2]$ $\quad Y = CX$

STRUCTURE OF LQR DESIGN

FIG 3.4

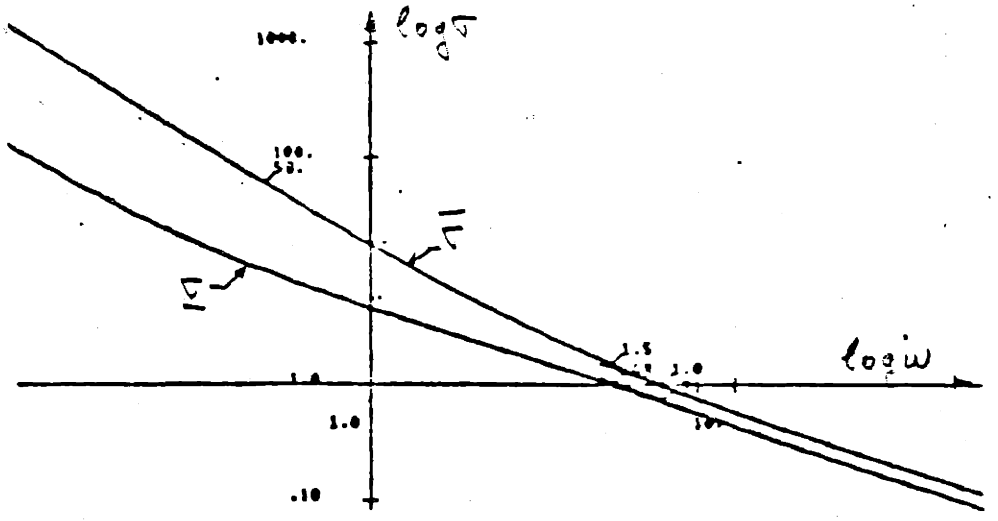

CROSSOVER FREQUENCY BAND
AT TAKEOFF

FIG 3.5

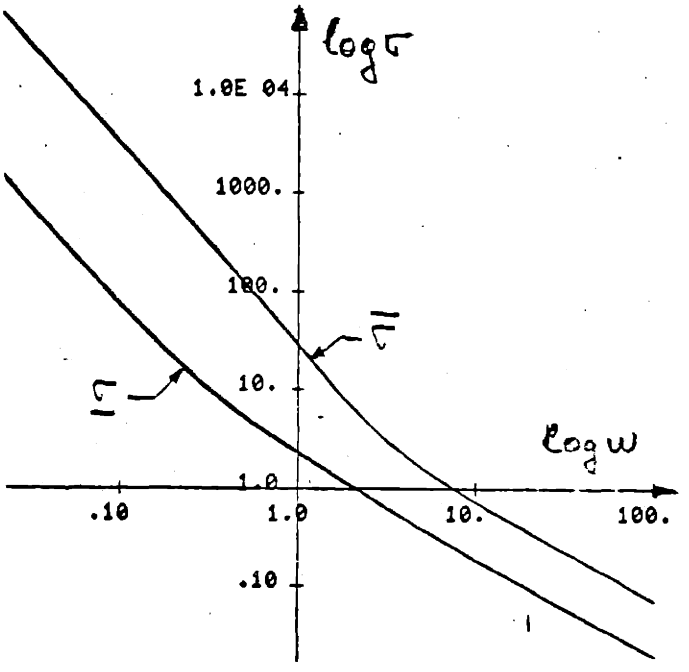

CROSSOVER FREQUENCY BAND
AT 90% N2

FIG 3.6

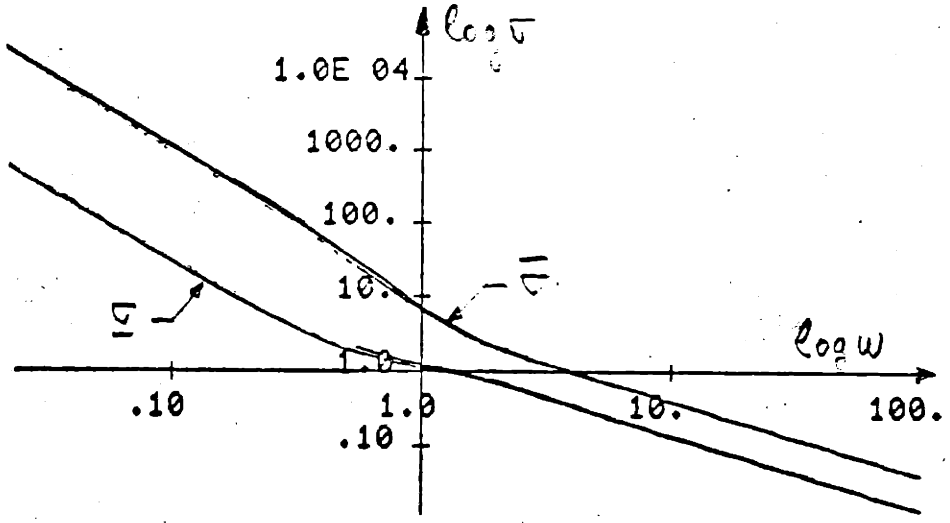

CROSSOVER FREQUENCY BAND
AT 80% N2

FIG 3.7

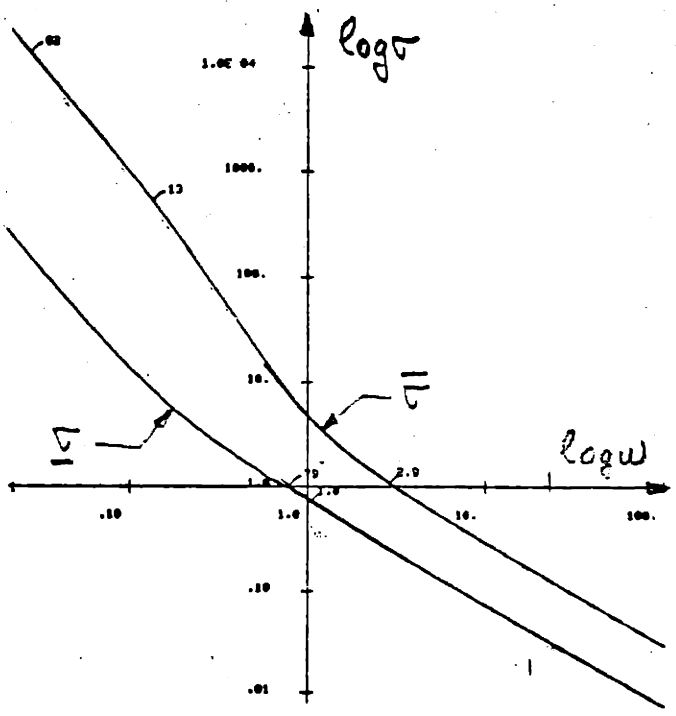

CROSSOVER FREQUENCY BAND
AT IDLE

FIG 3.8

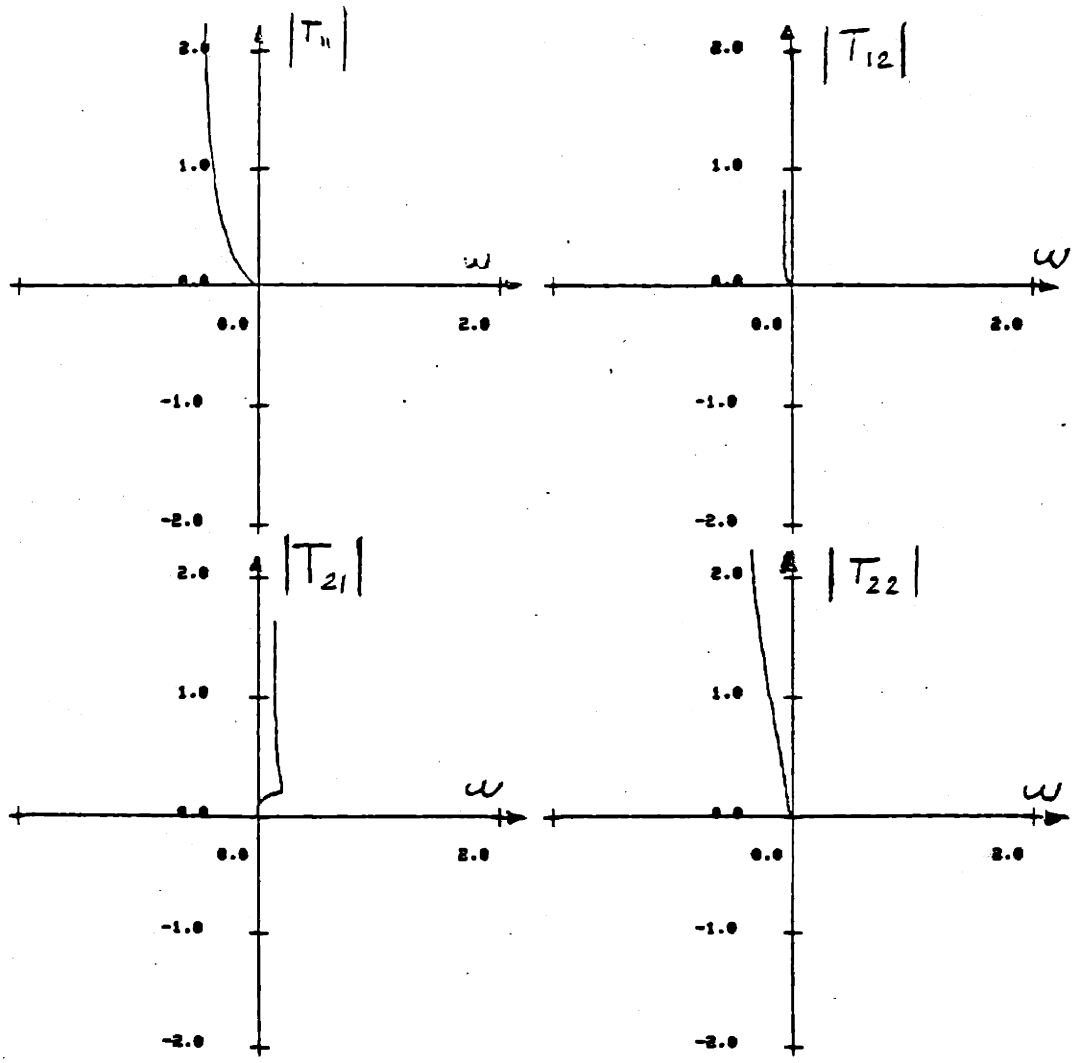

INVERSE NYQUIST ARRAYS FOR THE LQR
LOOP TRANSFER FUNCTION
AT TAKEOFF

FIG 3.9

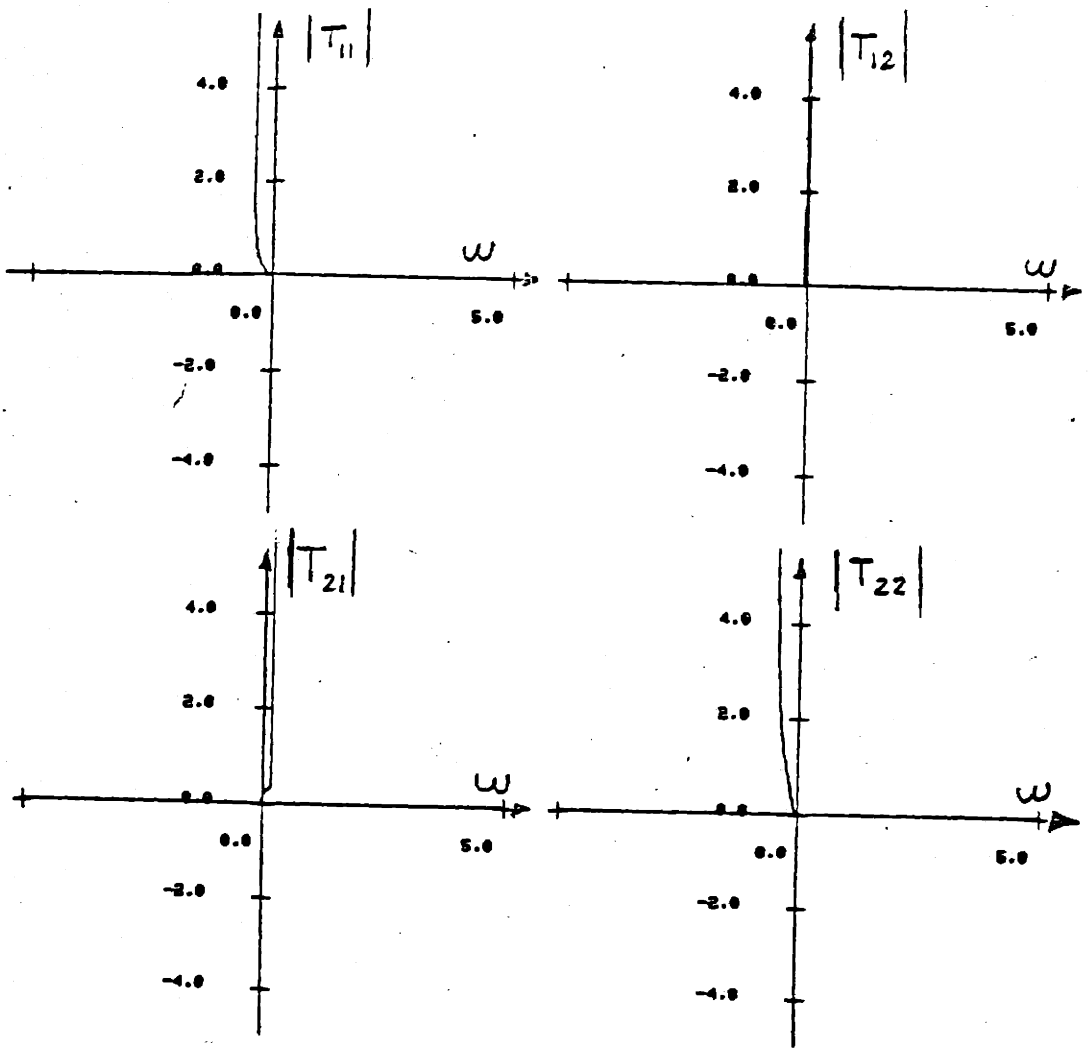

INVERSE NYQUIST ARRAYS FOR THE LQR
LOOP TRANSFER FUNCTION
AT 90% N2

FIG 3.10

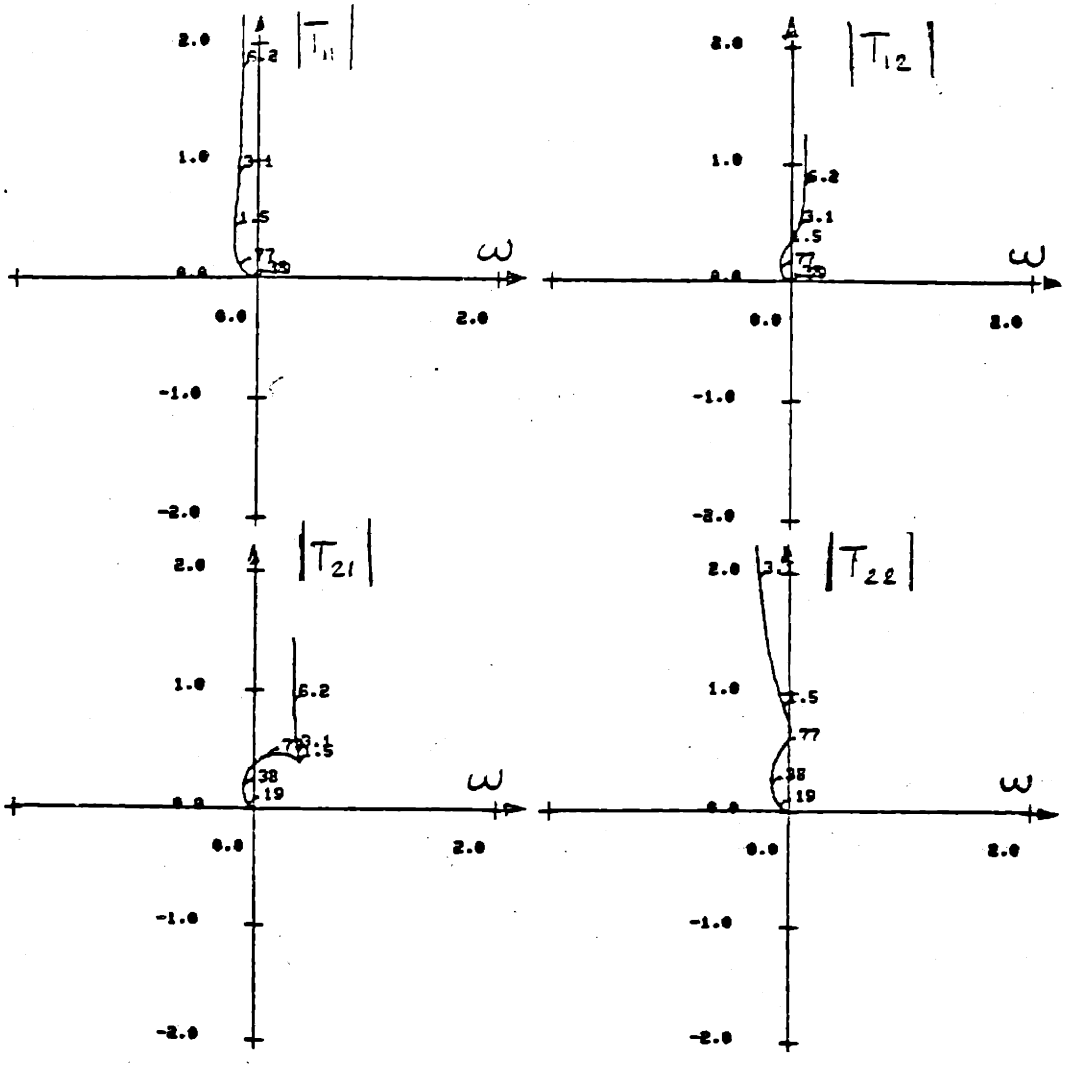

INVERSE NYQUIST ARRAYS FOR THE LQR
LOOP TRANSFER FUNCTION
AT 80% N2

FIG 3.11

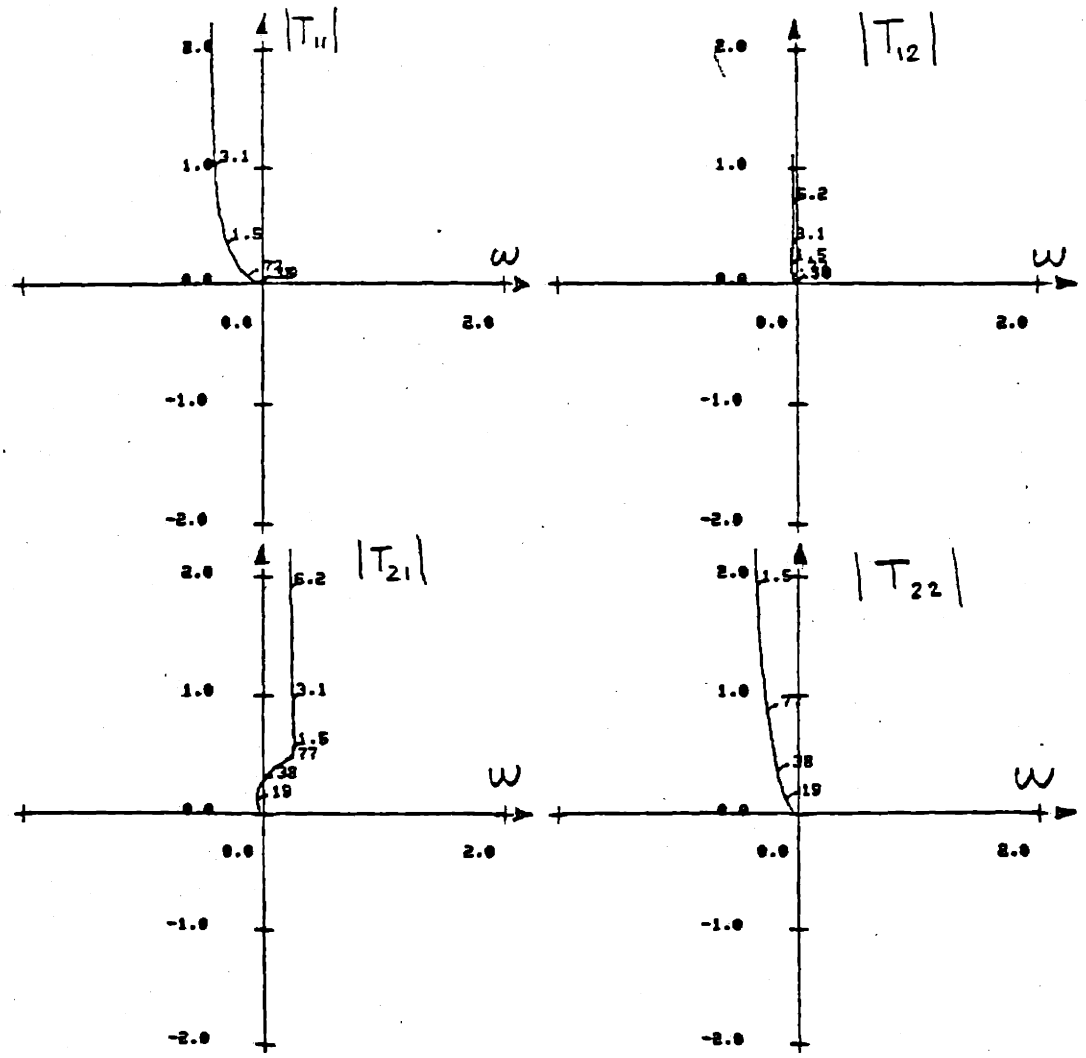

INVERSE NYQUIST ARRAYS FOR THE LQR
LOOP TRANSFER FUNCTION
AT IDLE

FIG 3.12

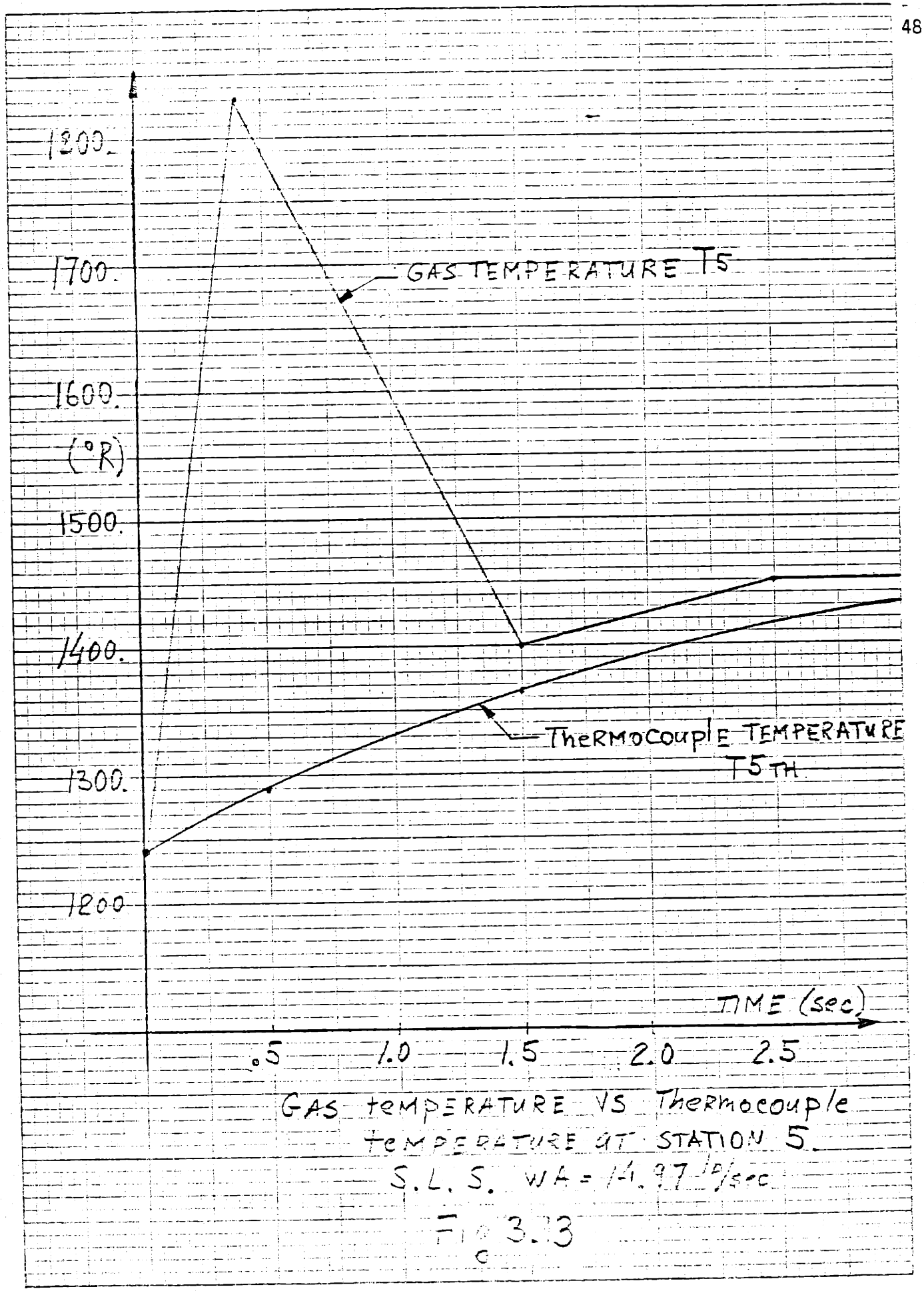

GAS TEMPERATURE VS THERMOCOUPLE TEMPERATURE AT STATION 5

S.L.S. WA = 14.97 lb/sec

Fig 3.13

4. GLOBAL CONTROL SYSTEM DESIGN

4.1 Introduction

In this chapter approach to the global control system design is developed. The global design consists of optimal control gains scheduling, target estimator, and trajectory control. Also, step response, crossover frequency band and Inverse Nyquist Arrays with Gershgorin band to evaluate control system stability at 36,000 ft altitude and .4 Mach number is presented. The global control system structure is given on Fig. 4.2.

4.2 Control System Optimal Gains Scheduling

The engine linear models were generated at sea level static standard day, and so the optimal control system was designed based on the engine dynamics as these specific conditions. Furthermore, engine dynamics were assumed to change linearly between design points, as a result, the optimal control gains are scheduled linearly from one design point to another.

To account for changes in engine dynamics due to the ambient temperature variations and altitude effects, the optimal control gains will be scheduled based on the engine corrected parameters. To develope expressions for these parameters we proceed as follows:

The dynamic equation for the fan rotor (see Fig. 2.5) in terms of of corrected parameters is:

$$\dot{N}_1' = a_{11}' \Delta N_1' + a_{12}' \Delta N_2' + b_{11}' \Delta W_F' \qquad (4.1)$$

Note that ΔVG term is not included because it is not an engine parameter.

The coefficient and variables of eq 4.1 can be expressed as follows:

$$a_{11}' = \frac{1}{J_1}\frac{\partial Q_1}{\partial N_1} = \frac{1}{J_1}\left(\frac{\partial Q_1}{\partial N_1}\right)_{SLS}\left(\frac{\sqrt{\theta_2}}{\delta_2}\right)$$

$$a_{12}' = \frac{1}{J_1}\frac{\partial Q_1}{\partial N_2} = \frac{1}{J_1}\left(\frac{\partial Q_1}{\partial N_2}\right)_{SLS}\left(\frac{\sqrt{\theta_2}}{\delta_2}\right) \qquad (4.2)$$

$$b_{11}' = \frac{1}{J_1}\frac{\partial Q_1}{\partial W_f} = \frac{1}{J_1}\left(\frac{\partial Q_1}{\partial W_f}\right)_{SLS}\left(\frac{\delta_2\sqrt{\theta_2}}{\delta_2}\right)$$

$$\dot{N}_1' = \frac{\dot{N}_1}{\sqrt{\theta_2}} \; ; \qquad \Delta N_1' = \frac{\Delta N_1}{\sqrt{\theta_2}} \; ;$$
$$\Delta N_2' = \frac{\Delta N_2}{\sqrt{\theta_2}} \; ; \qquad \Delta W f' = \frac{\Delta W f}{\delta_2 \sqrt{\theta_2}} \; ; \tag{4.3}$$

Substituting these expressions into eq (4.1) and multiplying both sides by $\sqrt{\theta_2}$ eq (4.1) can be rewritten:

$$\dot{N}_1 = \left(\frac{1}{J_1}\frac{\partial Q_1}{\partial N_1}\right)_{\substack{SLS \\ ST.DAY}} \cdot \left(\frac{\Delta N_1 \sqrt{\theta_2}}{\delta_2}\right) + \left(\frac{1}{J_1}\frac{\partial Q_1}{\partial N_1}\right)_{\substack{SLS \\ ST.DAY}} \cdot \left(\frac{\Delta N_2 \sqrt{\theta_2}}{\delta_2}\right) + \left(\frac{1}{J_1}\frac{\partial Q_1}{\partial W f}\right)_{\substack{SLS \\ ST.DAY}} \cdot \left(\frac{\Delta W f \sqrt{\theta_2}}{\delta_2}\right) ; \tag{4.4}$$

A similar equation can be developed for the compressor rotor dynamics:

$$N_2 = \left(\frac{1}{J_2}\frac{\partial Q_2}{\partial N_1}\right)_{\substack{SLS \\ ST.DAY}} \cdot \left(\frac{\Delta N_1 \sqrt{\theta_2}}{\delta_2}\right) + \left(\frac{1}{J_2}\frac{\partial Q_2}{\partial N_2}\right)_{\substack{SLS \\ ST.DAY}} \left(\frac{\Delta N_2 \sqrt{\theta_2}}{\delta_2}\right) + \left(\frac{1}{J_2}\frac{\partial Q_2}{\partial W f}\right)_{\substack{SLS \\ ST.DAY}} \left(\frac{\Delta W f \sqrt{\theta_2}}{\delta_2}\right) ; \tag{4.5}$$

The optimal control gains are scheduled based on N1COR, N2COR, and WFCOR, therefore there is no need to develope equations in terms of corrected paramters for PS3 and T5. The corrected parameters for optimal control gains schedules are defined as follows:

$$N_1 COR = \frac{N_1 \delta_2}{\sqrt{\theta_2}} \; ; \quad N_2 COR = \frac{N_2 \delta_2}{\sqrt{\theta_2}} \; ; \quad W f COR = \frac{W f \delta_2}{\sqrt{\theta_2}} \; ; \tag{4.6}$$

For optimal control gains schedules see Appendix H.

4.3 Target Estimator

At every design point along the engine operating line LQR desing was performed based on two neighboring steady state points; $\underline{X1}$ and $\underline{X1} + \Delta \underline{X}$. It is assumed that the engine linear model is invariant between $\underline{X1}$ and $\underline{X1} + \Delta \underline{X}$. For carefully chosen increment ΔX, this assumption is very close to reality.

The tradeoff (ρ) between weighting states (Q) and controls (R) matrices in performance index will define the location of the closed loop eigenvalues of the engine/control system. Furthermore, closed loop eigenvalues together with a state perturbation $\Delta \underline{X}$, will define the trajectory of the transient from $\underline{X1}$ to $\underline{X1} + \Delta \underline{X}$.

The tradeoff (ρ) was defined based on the following design criterion:

(I) { To accelerate engine from state $\underline{X1}$ to $\underline{X1} + \Delta \underline{X}$ in minimum time subject to engine constraints.

It is important to remember that tradeoff between states and controls in performance index and the trajectory of the acceleration between $\underline{X1}$ and $\underline{X1} + \Delta \underline{X}$ was defined with reference values (ΔXi) present in each state. Therefore, the total error signal to the actuators can be expressed as:

$$\Delta \underline{e}(t) = G \cdot \Delta \underline{X}(t) \qquad (4.7)$$

Where G is an optimal gain matrix and $X(t) = [X1(t)...X8(t)]^T$ is a reference value.

For control implementation, the requirements for referenced values in every state may seem to be redundant. In fact, the presence of integrators in two control loops will assure unique steady state convergence with only reference values on the integrator input states. However, engine control implemented in this fashion will perform less statisfactorily and will not have the transient trajectory predicted by LQR design.

To illustrate this fact consider the following:

$$\underline{e}_I(t) = G_I \cdot \Delta \underline{X}_I(t); \tag{4.8}$$

$$\underline{e}(t) = G \cdot \Delta X(t); \tag{4.9}$$

Where subscript "I" refers to the case where referenced values are introduced only on the integrator input states.

It will obviously take the same integrated error the engine to move between steady states $\underline{X1}$ and $\underline{X1} + \Delta \underline{X}$, or

$$\int_0^T e(t)dt = \int_0^{T_i} e_I(t)dt$$

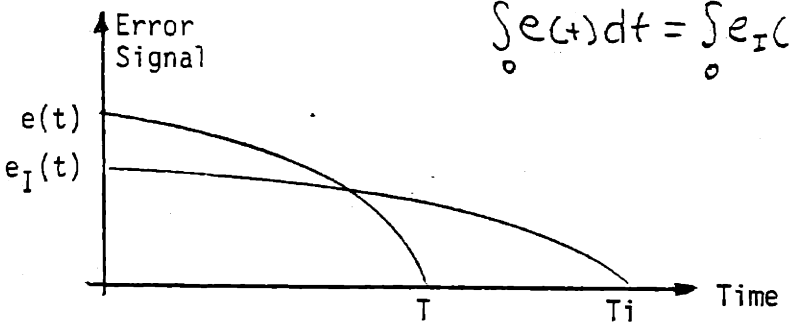

Fig. 4.1

So, the introduction of reference values only on the integrator input states will make acceleration slower than predicted by LQR design. The reasons being:

a) It takes time for integrators to have an effect

b) $e_I(0)$ is only part of $e(0)$

The introduction of reference values on all the states for a nonlinear system like a jet engine is a complicated task. The difficulties are in trying to estimate engine states as a function of the pilot input; power lever angle, ambient conditions; TT2, Po, Mn, external loads; bleed/power extraction, and engine deterioration. The accuracy required in state estimation can be relaxed by using "trajectory control" method. The development and reasons behind trajectory control will be discussed shortly. At this point let us note that introduction of reference values on nonintegrated states can be viewed as a basic feed-forward input which drives the engine towards the schedule steady state

before the integrated outputs start to have an effect.

The error contribution of reference value from each state $e_{ij} = g_{ij} \Delta x_j \quad \begin{matrix} i = 1,2 \\ j = 1 \ldots n \end{matrix}$; was compared to the maximum contribution in each actuator channel.

The following criterion was used to select states which will be introduced into the feed-forward:

1. $$\left| g_{ij} \Delta x_j \right| > \frac{1}{100} \left| (g_{ij} \Delta x_j)_{max} \right|$$

where g_{ij} - an optimal gain of i input from state j

Δx_j - reference value in state j

2. State estimation can be performed accurately and reliably.

Based on this criterion the following states are used in estimation and in feed-forward: N2, VG and WR. Note, that VG becomes a schedule based on instantaneous engine corrected core speed when fan speed is within 1% of the schedule value. T5 and P3 are not used in the feed-forward due to their small ($\approx$1%) relative error contribution. XN1 and XVG are not used because of the difficulties in their estimation, and relatively small ($\approx$ 2%) error contribution.

The estimation of N2, VG and WF can be done based on corrected dynamics so, altitude and ambient temperature effects are taken into account. Mach number and bleed/power extraction can be used as a bias for better estimation results.

4.4 Trajectory Control

The control system design about every design point ($\underline{X}1$ to $\underline{X}1 + \Delta \underline{X}$) was done based on LQR design criterion (I). This implies, in general, that engine constraints will be satisfield only for engine perturbation from the steady state $\underline{X}1$ to the neighboring steady state $\underline{X}1 + \Delta \underline{X}1$ were $\Delta \underline{X}1 \leq \Delta \underline{X}$. If the error signal is larger than the one defined by perturbation ΔX, or $e(t) > G \Delta x(t)$, the constraints may not be satisfied. To assure engine behavior within the constraints and at the same time to deliver performance close to LQR predictions. Trajectory control will be used in this design. Trajectory control will

provide variable limits on the error signal from each state which has a reference input. The limits are scheduled as a function of corrected dynamics (eq 4.4) and defined based on intervals used in LQR design ($\blacktriangle \underline{X}$). Note that limits are very tight at the region of rapidly changing engine dynamics (IDLE to INTER). On the other hand, limits can be relaxed at the region where engine dynamics are changing slower (INTER to MAX). At the same time, trajectory control will relax accuracy required in state estimation, because an error in state estimation will effect trajectory only slightly when engine approaches scheduled steady state point. Trajectory control limits schedules are presented in Appendix P.

4.5 Stability Analysis for the Global Design

To demonstrate stability and step response characteristics of the global design the engine linear model was generated at 36,000 ft. altitude and .4 Mach number flight conditions. This particularly extreme point in the engine flight envelope was selected based on the following considerations:

- o Largest fan and core rotos time constants
- o Largest thermodynamic gas temperature lag
- o High engine gains from fuel flow to fan and core speeds
- o Highest engine gain from fuel flow to T5

This kind of combination between engine time constants and its gains may result in oscillatory engine transient response when the control gains fail to provide required compensation. The optimal control gains scheduling is used to define the feedback gains, and the resultant loop transfer function is evaluated in the frequency domain by using singular value analysis and Inverse Nyquist Arrays with Gershgorin band. Figs. 4.4 and 4.5. In addition, transient response to step change in both fan speed and variable geometry references are present the Fig. 4.3.

The plot of the Inverse Nyquist arrays shows that the loop transfer function is a diagonally dominant. As a result stability margins can be estimated based on Gershgorin band.

The transient time response and Gershgorin band show that system is slightly underdamped, but has no excessive oscillations.

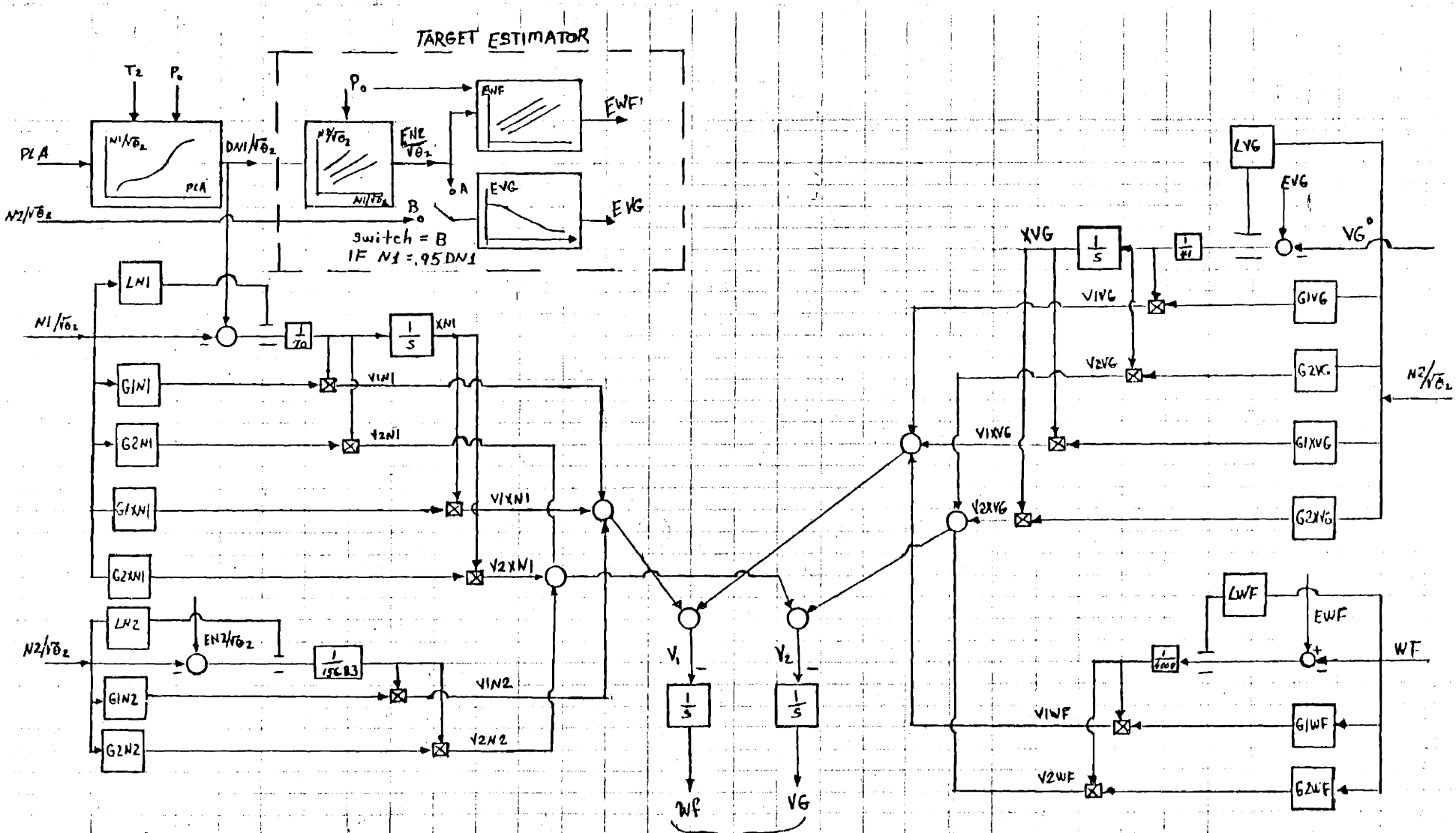

GLOBAL CONTROL STRUCTURE

Fig 4.2

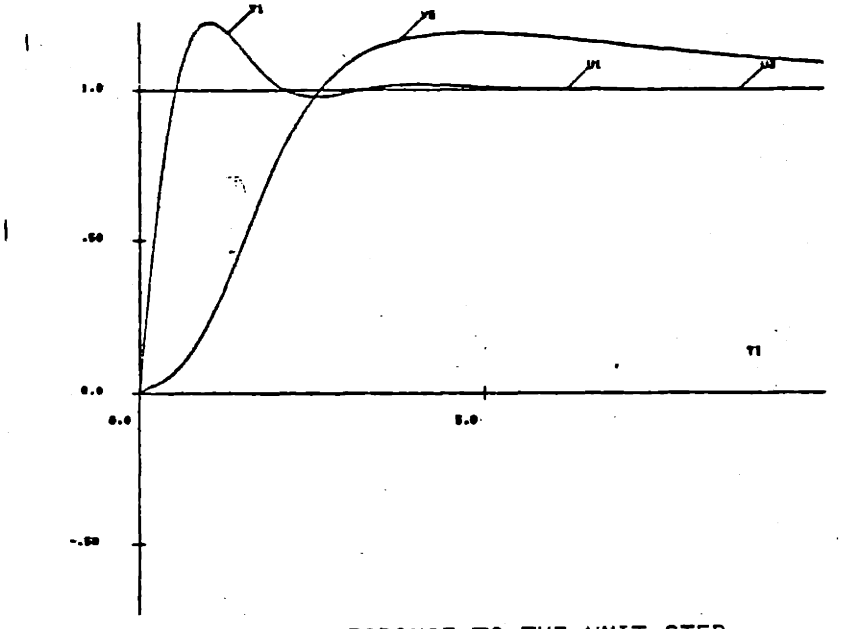

CLOSED LOOP TIME RESPONSE TO THE UNIT STEP
IN BOTH ACTUATORS AT 36,000 FT. ALTITUDE, .4 MACH NUMBER

FIG 4.3

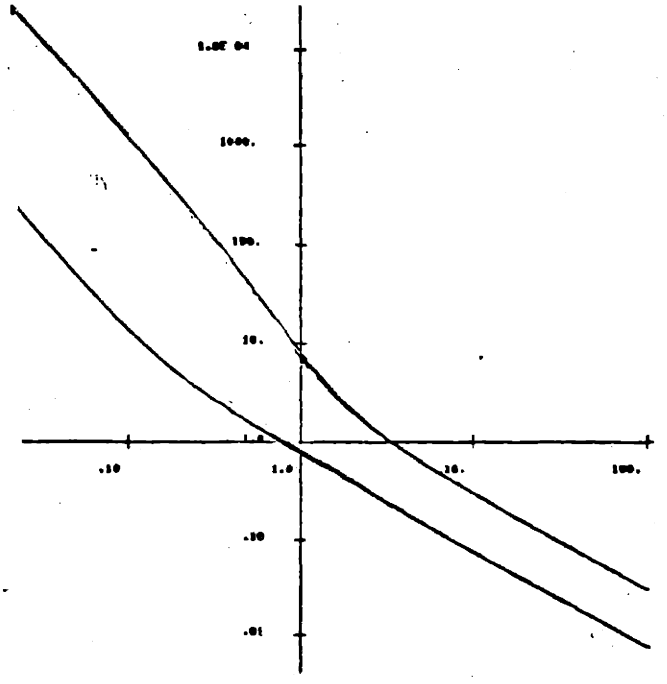

CROSSOVER FREQUENCY BAND AT
36,000 FT. ALTITUDE, .4 MACH NUMBER

FIG 4.4

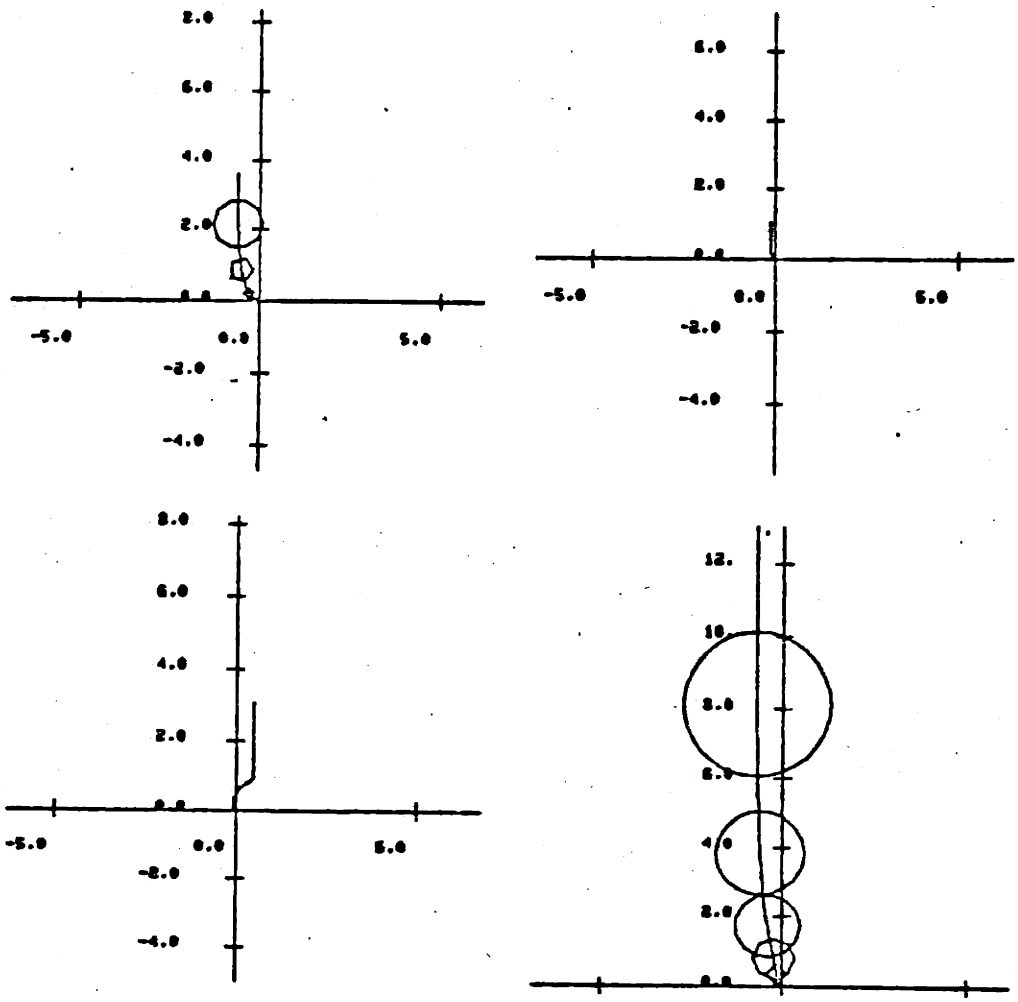

INVERSE NYQUIST ARRAYS WITH GERSHGORIN BAND FOR LOOP TRANSFER FUNCTION AT 36,000 FT. ALTIDUDE, .4 MACH NUMBER

FIG 4.5

5. CONCLUSIONS AND SUGGESTIONS FOR FUTURE RESEARCH

The multivariable control design procedure as developed in this report for TF34 engine control system design offers a systematic approach for designing a global control system for jet engines. The development of linearize engine model, which is a basic requirement for LQR design, is presented, and its validity is verified.

The procedure to integrate the linear controller into the global control system for jet engine is developed. The global control incorporates target estimator, optimal control gains scheduling, and trajectory control, all of which are scheduled as a function of corrected engine dynamics.

Better transient time and performance were achieved by formulating VG optimal transient trajectory within the stall margin constraints.

Due to the amount of time required to modify existing nonlinear TF34 transient deck to incorporate new control system, nonlinear simulation of the global control were not performed. However, it is concluded that new control system will perform better than existing one. The reasons behind this conclusion can be support by the fact, that optimal control gains scheduling adapts to the changing engine dynamics throughout the engine flight envelope.

More research is necessary to realize increased performance potential of multivariable design approach to advanced jet engine. In particular, more research is required to define a practical way to control engine transient trajectory while maintaining optimal gains scheduling and target estimator to utilize LQR predicted transient performances.

REFERENCES

1. Szuch, J.S., Soeder, J.F., Seldner, K., and Cynar, D.S., "F100 Multivariable Control Synthesis Program - Evaluation of a Multivariable Control using a Real-Time Engine Simulation" NASA final report. Proposed Technical Memo, June 1977.

2. DeHoff, R.L., Hall, W.E., Adams, R.J. and Gupta, N.K., "Design of a Multivariable Controller Utilizing Linear Quadratic Method", AFAPL-TR-77-35, June, 1977.

3. Barclay, B.A., and Richards, J.C., "FADEC Preliminary Design Overview for Variable Cycle Engine." AIAA/SAE 13th Propulsion Conference No. 77-837. July, 1977.

4. Merrill, W.C., "Design of Turbofan Engine Control using Output Feedback Regulator Theory", presented at the 1977 JACC, San Francisco, Cal., June, 1977.

5. Levine, W.S. and Athans, M. "On the Determination of the Optimal Constant Output Feedback Gains for Linear Multivariable System" IEEE Transactions on Automatic Control, Vol. AC-15, No. 1, p. 44, February, 1970.

6. DeHoff, R.L. and Hall, W.E., "System Identification Pricinples Applied to Multivariable Control Synthesis of the F100 Turbofan Engine". Presented at 1977 JACC, San Fransisco, Cal., June, 1977.

7. Kwakernaak, H. Sivan, R., "Linear Optimal Control Systems".

8. Lehtomaki, N.A., Sandell, N.R. Jr., and Athans, M. "Robustness Results in LQG based on Multivariable Control Designs", IEEE Transactions on Automatic Control. February, 1981.

9. Beattie, E.C., Spock, W.C., "Application of Multivariable Control Techniques to a Variable Area Turbine Engine", JACC August, 1976.

10. McFarlane, A.G.J., "Multivariable Control System Design and Applications", IEEE, September, 1971.

11. Michael, G.J., Farrar, F.A., "Development of Optimal Control Modes for Advanced Technology Propulsion Systems". UARL Rpt. N911620-1, August, 1973.

12. Athans, M., "On the Design of P-I-D Controllers using Optimal Linear Regulator Theory". Automatica Vol. 7, 1971.

13. Bryson, A.E., Ho, Y.C., "Applied Optimal Control", Waltham, MA, 1969.

APPENDIX A

TF34 LINEAR MODEL GENERATION

TF34 Linear Model Generation

The engine linear dynamics in the state space form can be expressed as:

$$\Delta\dot{X} = A\,\Delta X + B\,\Delta u \tag{1A}$$

as identified for the TF34 engine

$$\begin{bmatrix} \Delta\dot{N}_1 \\ \Delta\dot{N}_2 \\ \Delta\dot{T}_5 \\ \Delta\dot{P}_{S3} \end{bmatrix} = \begin{bmatrix} a_{11} & a_{12} & a_{13} & a_{14} \\ a_{21} & a_{22} & a_{23} & a_{24} \\ a_{31} & a_{32} & a_{33} & a_{34} \\ a_{41} & a_{42} & a_{43} & a_{44} \end{bmatrix} \begin{bmatrix} \Delta N_1 \\ \Delta N_2 \\ \Delta T_5 \\ \Delta P_{S3} \end{bmatrix} + \begin{bmatrix} b_{11} & b_{12} \\ b_{21} & b_{22} \\ b_{31} & b_{32} \\ b_{41} & b_{42} \end{bmatrix} \begin{bmatrix} \Delta WF \\ \Delta VG \end{bmatrix} \tag{2A}$$

As an example, we develop expressions for the first column of matrices A and B.

a) Elements of Matrix A

Perturbing one state at a time while keeping all other states and controls constant solution for elements of A matrix can be obtained as follows:

Let $\Delta N2 = \Delta T5 = \Delta PS3 = \Delta WF = \Delta VG = 0$ then $a_{11} = \dfrac{\Delta\dot{N}_1}{\Delta N_1}$;

but from the fan rotor dynamics:

$$\Delta\dot{N}_1 = \frac{\Delta Q_1}{J_1} \text{ ; and } \Delta Q_1 = \frac{\partial Q_1}{\partial N_1}\Delta N_1 \text{ ;}$$

Substituting expressions (4A) into eq 3A yeilds:

$$a_{11} = \frac{1}{J_1}\frac{\partial Q_1}{\partial N_1} \text{ ;} \tag{3A}$$

In a similar way:

$$a_{12} = \frac{\Delta\dot{N}_2}{\Delta N_1} \text{ , but } \Delta N_2 = \frac{\Delta Q_2}{J_2} \text{ ; and } \Delta Q_2 = \frac{\partial Q_2}{\partial N_1}\Delta N_1 \text{ ;}$$

substituting back into eq for a21 :

$$a_{21} = \frac{1}{J_2} \frac{\partial Q_2}{\partial N_1}; \tag{4A}$$

Equations for a31 and a41 are developed from engine linear model block diagram Fig. 2.7. The development of the expression is fairly straight forward:

$$a_{31} = \frac{1}{J_2} \frac{\partial T_5}{\partial N_2} \frac{\partial Q_2}{\partial N_1};$$

$$a_{41} = \frac{1}{J_1} \frac{\partial P_{S3}}{\partial N_1} \frac{\partial Q_1}{\partial N_1} + \frac{1}{\tau_1} \frac{\partial P_{S3}}{\partial N_1} + \frac{1}{J_2} \frac{\partial P_{S3}}{\partial N_2} \frac{\partial Q_2}{\partial N_1}; \tag{5A}$$

Following the procedure described above, the rest of elements of Matrix A are defined as follows:

$$a_{12} = \frac{1}{J_1} \frac{\partial Q_1}{\partial N_2};$$

$$a_{22} = \frac{1}{J_2} \frac{\partial Q_2}{\partial N_2};$$

$$a_{32} = \frac{1}{\tau} \frac{\partial T_5}{\partial N_2} + \frac{1}{J_2} \frac{\partial T_5}{\partial N_2} \frac{\partial Q_2}{\partial N_2};$$

$$a_{42} = \frac{1}{J_1} \frac{\partial P_{S3}}{\partial N_1} \frac{\partial Q_1}{\partial N_2} + \frac{1}{\tau_1} \frac{\partial P_{S3}}{\partial N_1} + \frac{1}{J_2} \frac{\partial P_{S3}}{\partial N_2} \frac{\partial Q_2}{\partial N_2};$$

$$a_{13} = 0; \tag{6A}$$

$$a_{23} = 0;$$

$$a_{33} = -\frac{1}{\tau};$$

$$a_{43} = 0;$$

$$a_{14} = 0;$$

$a_{24} = 0$;

$a_{34} = 0$;

$a_{44} = -\frac{1}{\tau_1}$;

(6A Cont.)

τ and τ_1 are defined in section 2.3

B. Elements of Matrix B

To define B matrix forced match technique is used. The principle of this technique is as follows:

At steady state $\Delta \dot{X} = 0$, eq (A) reduces to:

$$-A \Delta X = B \Delta U \; ; \tag{7A}$$

Now perturbing one control variable at a time, while keeping another constant we can solve for elements of B matrix.

Let $\Delta VG = 0$, then expanding eq (7A) we get four linear equations:

$$\begin{aligned}
b_{11} \Delta W_f &= -(a_{11}\Delta N_1 + a_{12}\Delta N_2 + a_{13}\Delta T_5 + a_{14}\Delta P_{S3}) \\
b_{12} \Delta W_f &= -(a_{21}\Delta N_1 + a_{22}\Delta N_2 + a_{23}\Delta T_5 + a_{24}\Delta P_{S3}) \\
b_{13} \Delta W_f &= -(a_{31}\Delta N_1 + a_{32}\Delta N_2 + a_{33}\Delta T_5 + a_{34}\Delta P_{S3}) \\
b_{141} \Delta W_f &= -(a_{41}\Delta N_1 + a_{42}\Delta N_2 + a_{43}\Delta T_5 + a_{44}\Delta P_{S3})
\end{aligned} \tag{8A}$$

In a similar way, letting WR = 0, and perturbing VG, b12 through b42 can be calculated

APPENDIX B

A AND B MATRICES OF THE LINEAR MODEL

Engine Linear Model

1) TAKEOFF POWER

A Matrix

ROW \ COL	1	2	3	4
1	-5.3682D+00	4.7028D+00	0.0	0.0
2	-1.5670D-01	-4.8523D+00	0.0	0.0
3	8.0000D-04	-1.5830D-01	-3.5714D+01	0.0
4	1.1190D-01	1.7012D+00	0.0	-1.0000D+02

B Matrix

1.1880D+02	-1.6306D+02
1.1920D+02	1.4883D+02
1.8274D+01	7.1586D+00
2.7621D+01	-5.7194D+01

2) 90% N2

A Matrix

ROW \ COL	1	2	3	4
1	-1.6510D+00	1.9796D+00	0.0	0.0
2	-1.1540D-01	-1.1740D+00	0.0	0.0
3	2.0000D-03	-1.2300D-01	-1.4285D+01	0.0
4	1.7600D-01	8.1800D-01	0.0	-1.0000D+02

B Matrix

1.7100D+02	-3.9692D+01
9.3800D+01	2.0625D+01
1.7110D+01	3.2500D+00
6.3250D+01	-1.6562D+01

3) 80% N2

A Matrix

ROW \ COL	1	2	3	4
1	-1.1940D+00	1.5120D+00	0.0	0.0
2	6.0000D-03	-6.4900D-01	0.0	0.0
3	-1.0000D-04	-2.2100D-01	-1.3333D+01	0.0
4	1.5000D-03	7.7700D-01	0.0	-1.0000D+02

B Matrix

1.0059D+02	-6.0540D+01
1.0351D+02	1.2500D+01
3.4967D+01	9.3200D+00
4.9241D+01	-3.0544D+01

4) Idle

A Matrix

ROW \ COL	1	2	3	4
1	-9.5910D-01	7.4500D-01	0.0	0.0
2	-1.7100D-02	-2.2750D-01	0.0	0.0
3	2.4000D-04	-1.8430D-01	-1.3333D+01	0.0
4	8.3000D-03	4.3100D-01	0.0	-1.0000D+02

B Matrix

6.0620D+01	-1.2840D+01
9.4659D+01	-1.5500D+00
5.3734D+01	2.8810D+00
3.0420D+01	-7.0680D+00

APPENDIX C

COMPARISON: LINEAR AND NON-LINEAR MODELS

_____ - Non-linear Model

0 - Linear Model

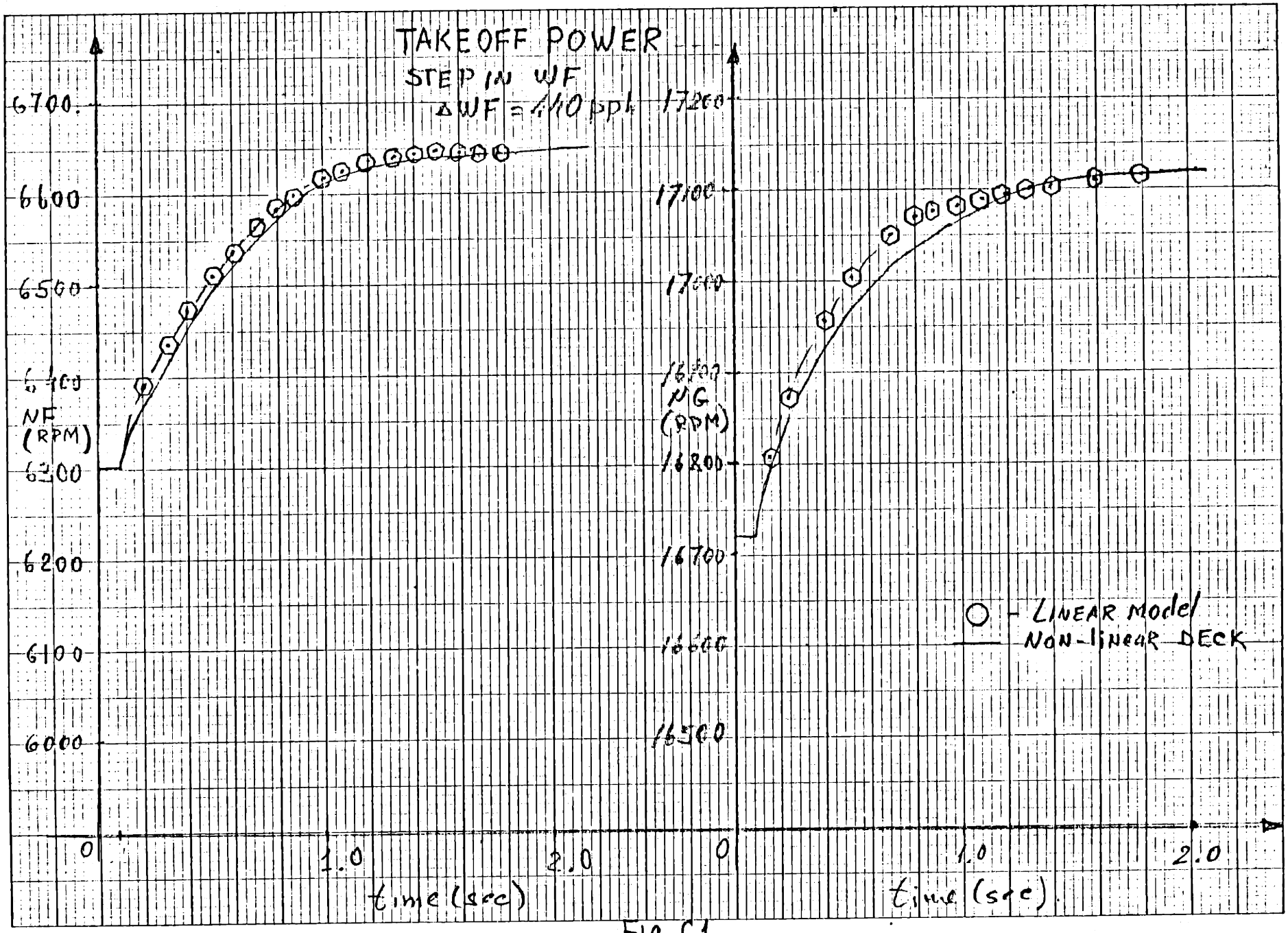
TAKEOFF POWER
STEP IN WF
ΔWF = 440 pph
6700
6600
6500
6400
NF (RPM)
6300
6200
6100
6000
0
1.0
2.0
time (sec)
17200
17100
17000
16900
NG (RPM)
16800
16700
16600
16500
0
1.0
2.0
time (sec)
○ - LINEAR Model
— NON-LINEAR DECK

Fig C1

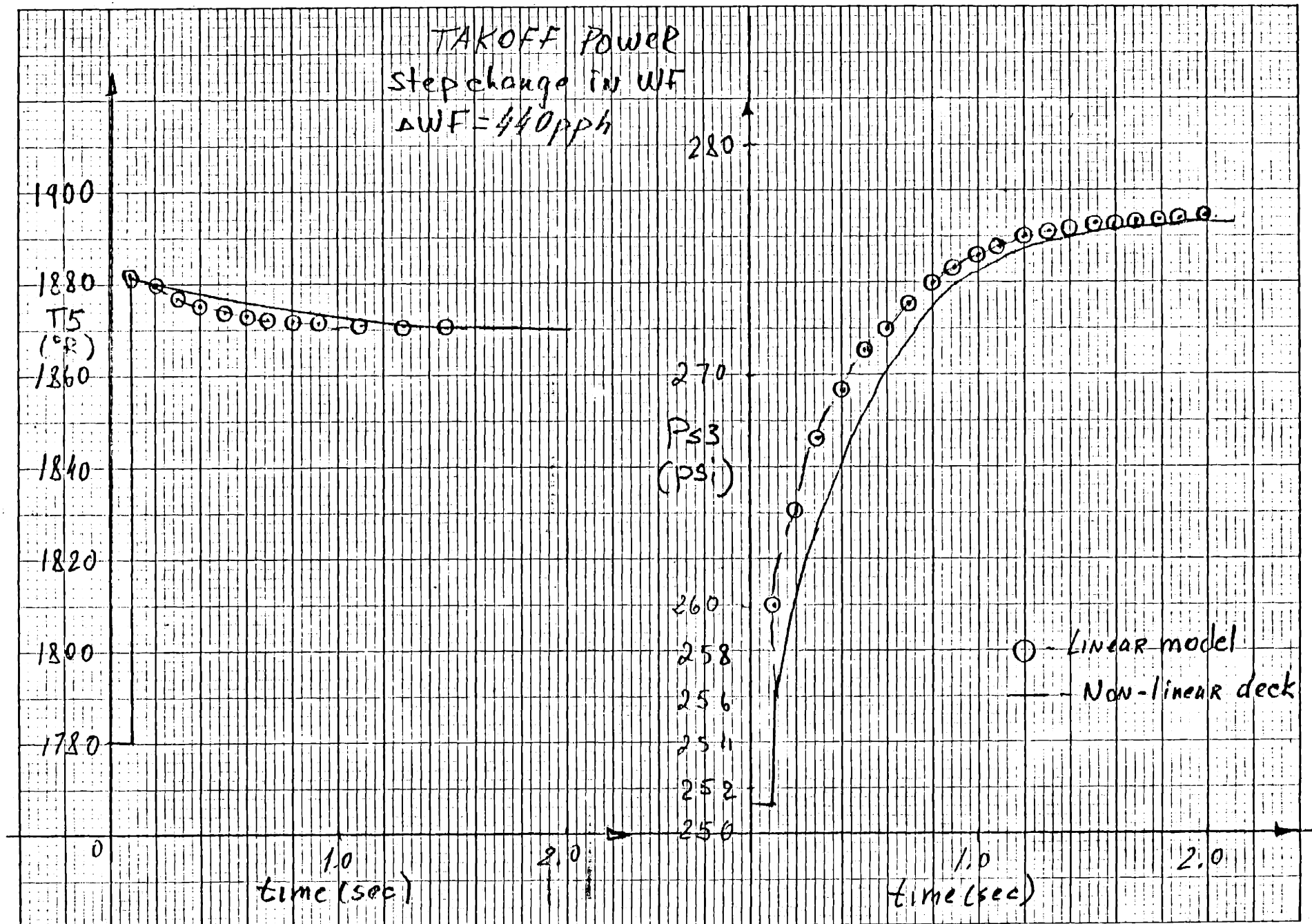
TAKOFF POWER
step change in WF
ΔWF = 440 pph
1900
1880
T5 (°R)
1860
1840
1820
1800
1780
0
1.0
2.0
time (sec)
280
270
Ps3 (psi)
260
258
256
254
252
250
1.0
2.0
time (sec)
Linear model
Non-linear deck

Fig C2

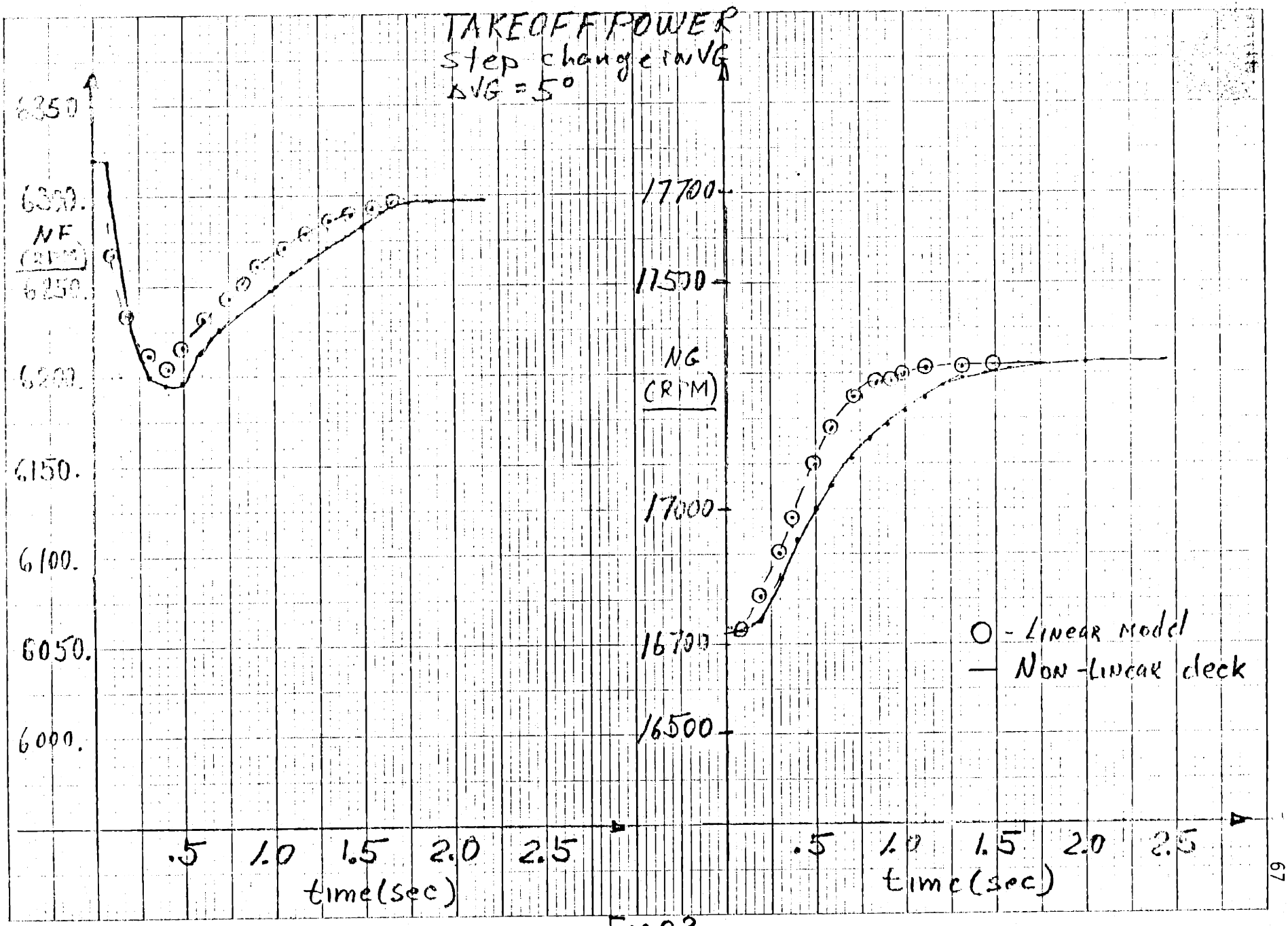
TAKEOFF POWER
Step change in VG
ΔVG = 5°
6350
6300.
NF (RPM)
6250.
6200.
6150.
6100.
6050.
6000.
17700
17500
NG (RPM)
17000
16700
16500
.5
1.0
1.5
2.0
2.5
time (sec)
O - Linear model
— Non-Linear deck

Fig C3

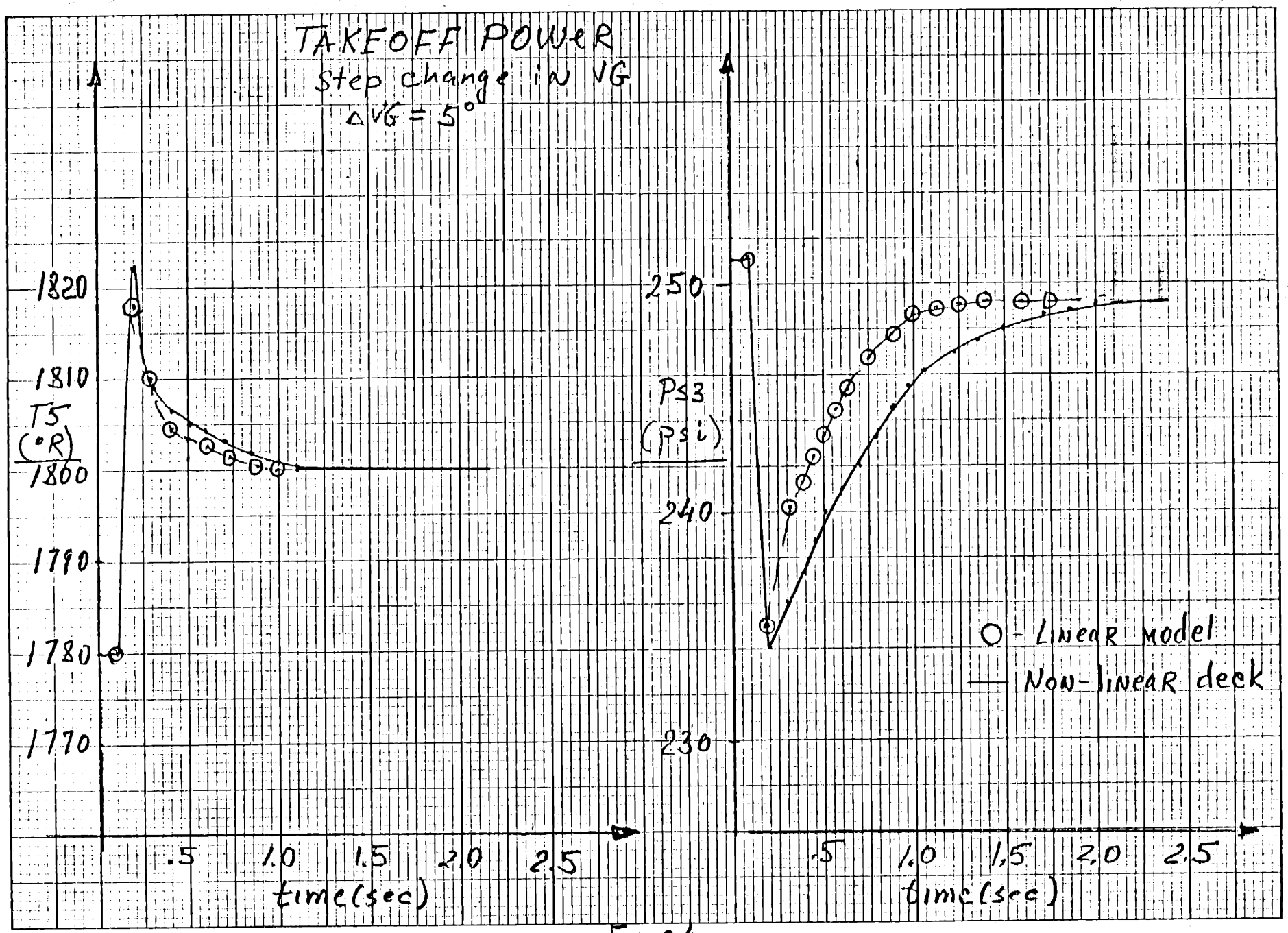

Fig C4

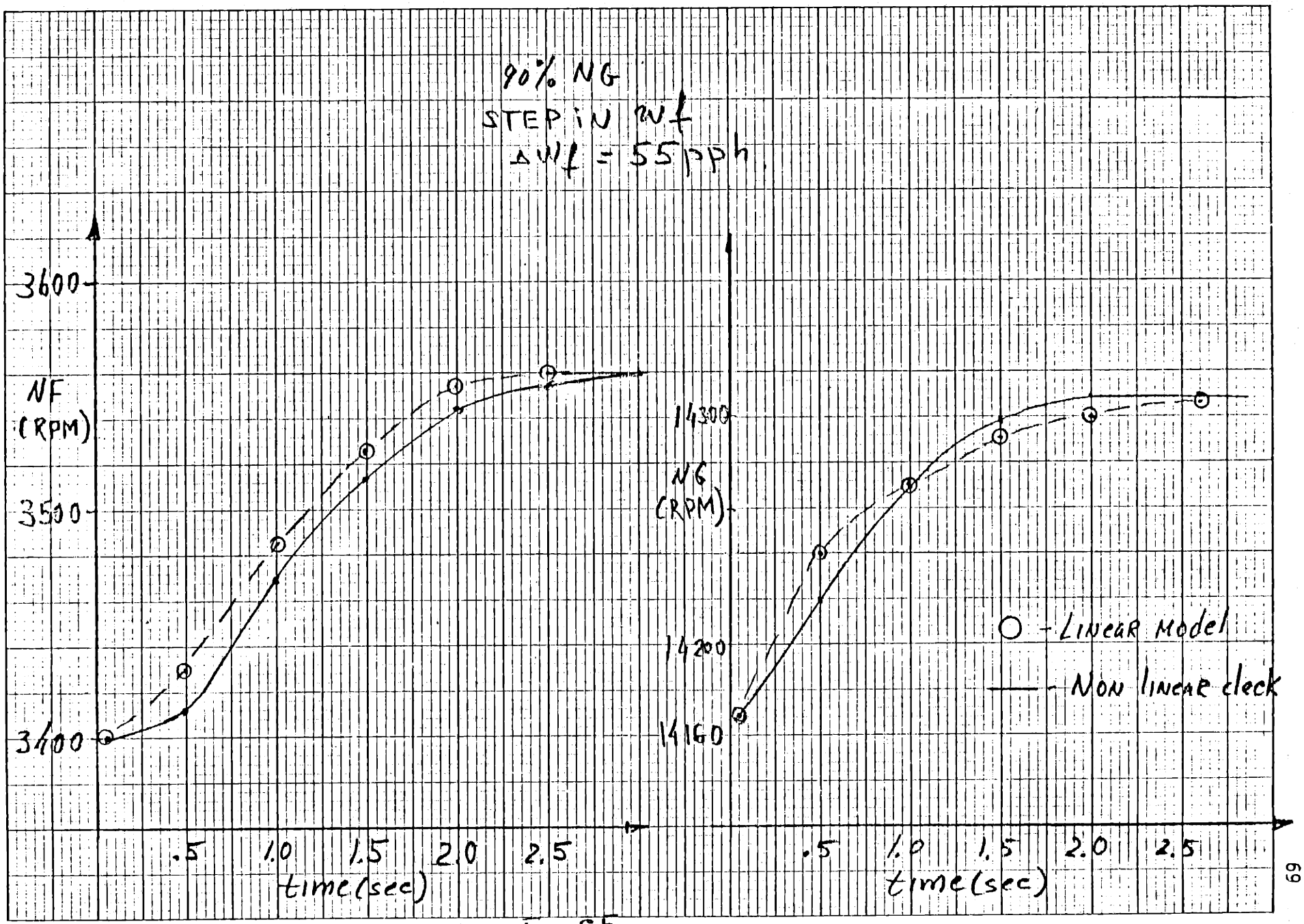
90% NG
STEP IN Wf
ΔWf = 55 pph
3600
NF (RPM)
3500
3400
14300
NG (RPM)
14200
14160
○ - Linear Model
—— - Non linear clock
.5
1.0
1.5
2.0
2.5
time (sec)
.5
1.0
1.5
2.0
2.5
time (sec)

Fig C5

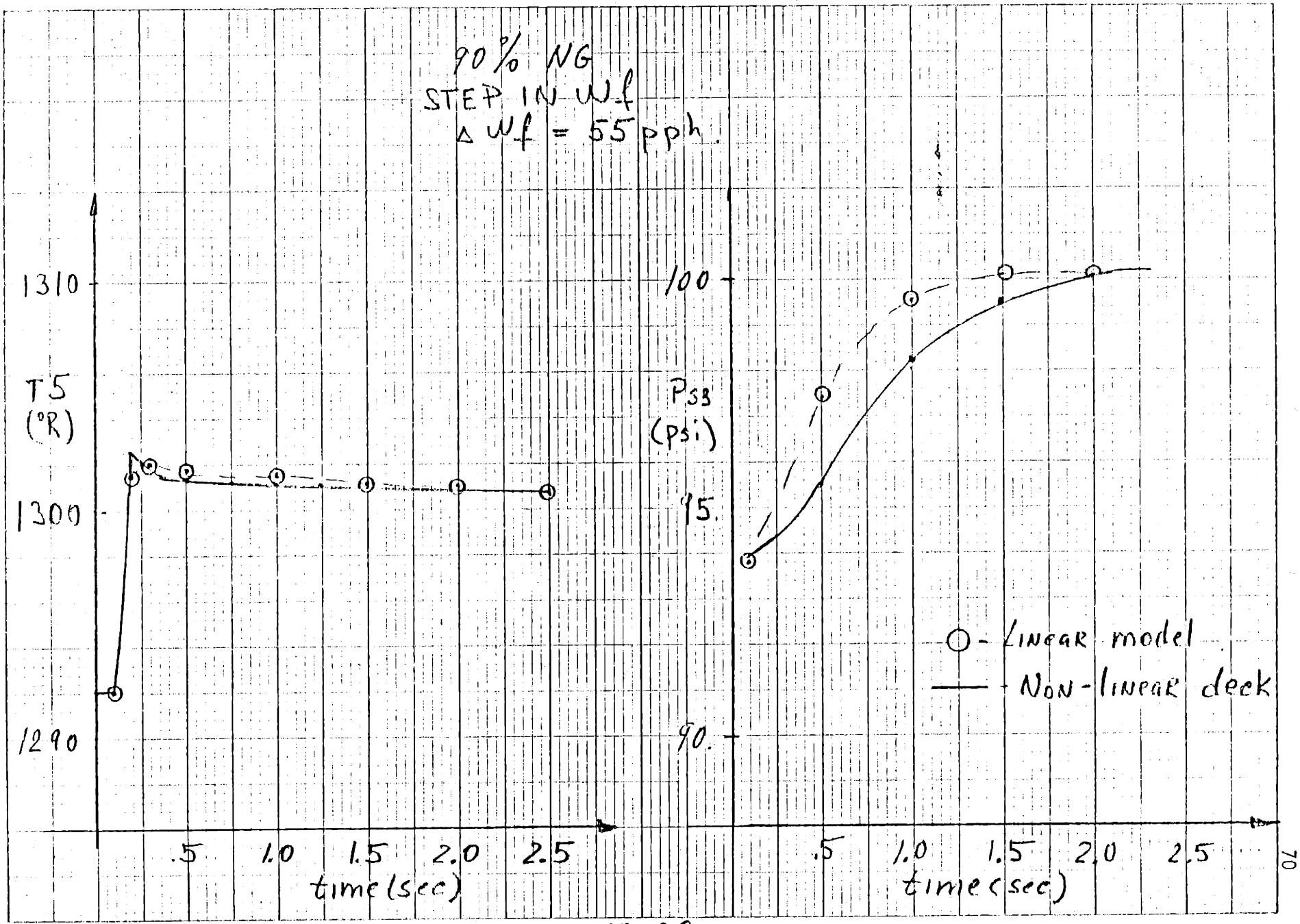
90% NG
STEP IN Wf
Δ Wf = 55 pph
1310
T5 (°R)
1300
1290
100
Ps3 (psi)
95.
90.
○ - Linear model
— - Non-linear deck
.5
1.0
1.5
2.0
2.5
time (sec)
.5
1.0
1.5
2.0
2.5
time (sec)

Fig C6

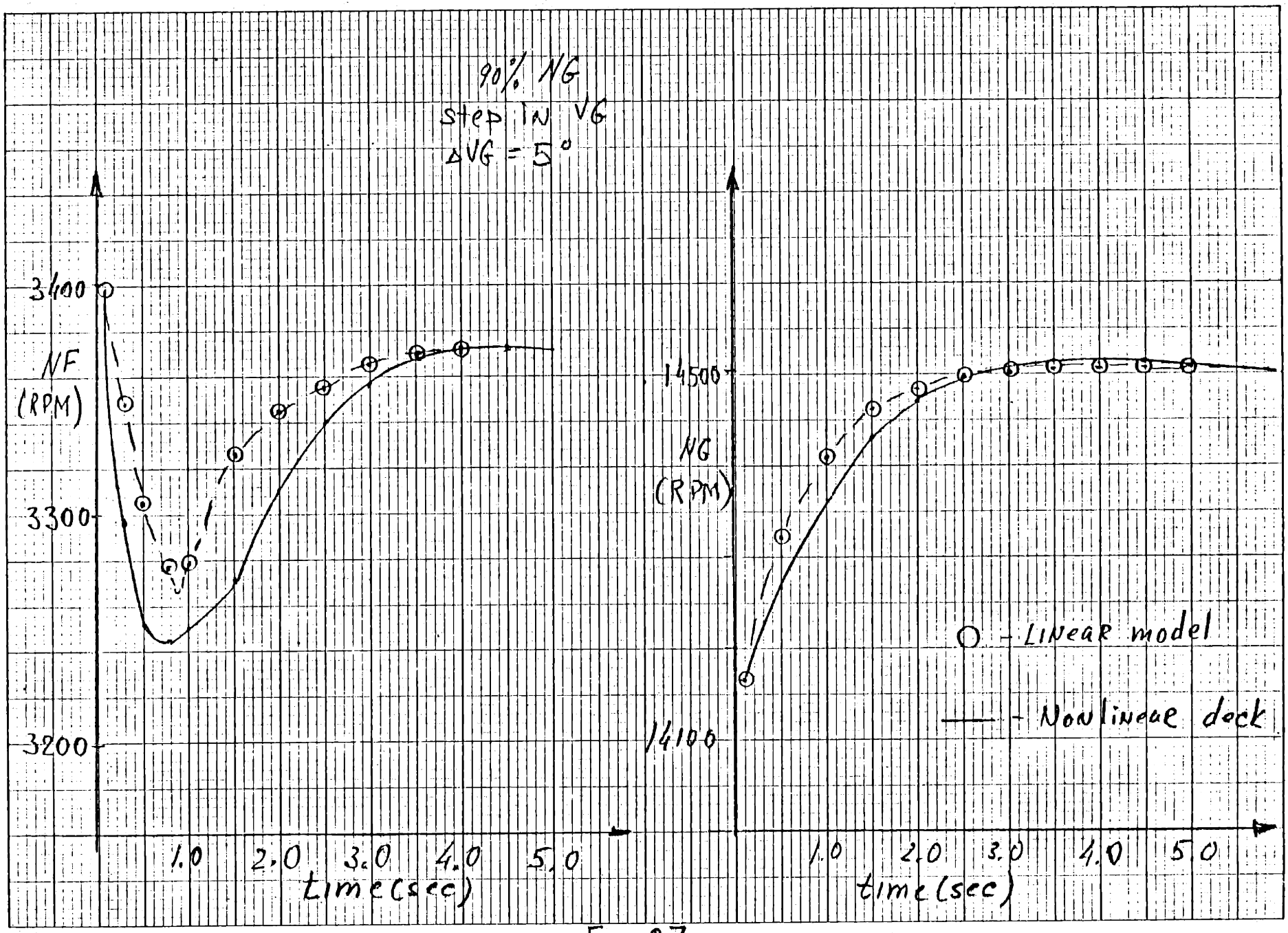
90% NG
step in VG
ΔVG = 5°
3400
NF
(RPM)
3300
3200
1.0
2.0
3.0
4.0
5.0
time(sec)
14500
NG
(RPM)
14100
1.0
2.0
3.0
4.0
5.0
time(sec)
O - Linear model
—— - Nonlinear deck

Fig C7

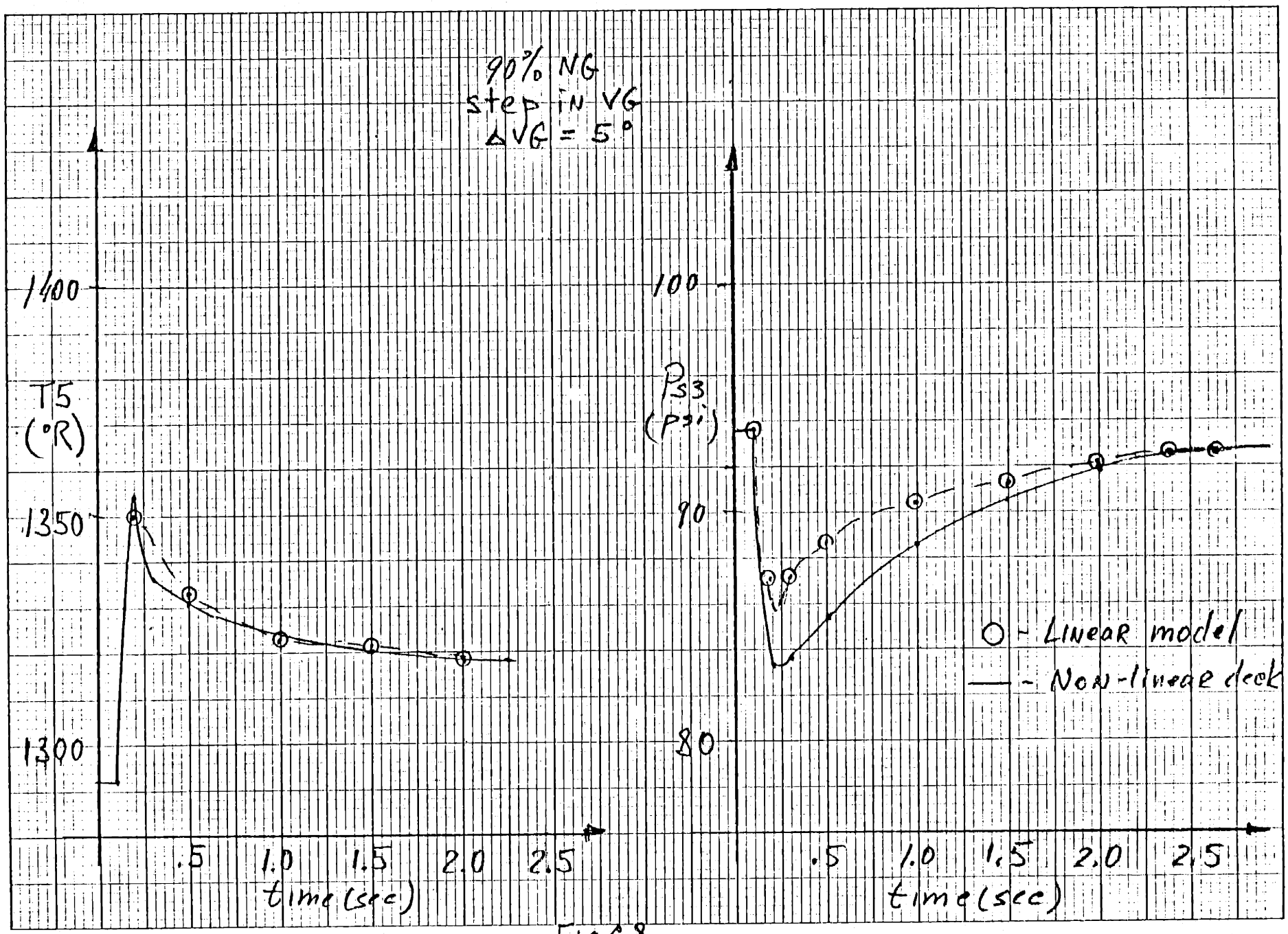
90% NG
step in VG
ΔVG = 5°
1400
1350
1300
T5
(°R)
.5
1.0
1.5
2.0
2.5
time (sec)
100
90
80
Ps3
(psi)
.5
1.0
1.5
2.0
2.5
time (sec)
○ - Linear model
— - Non-linear deck

Fig C 8

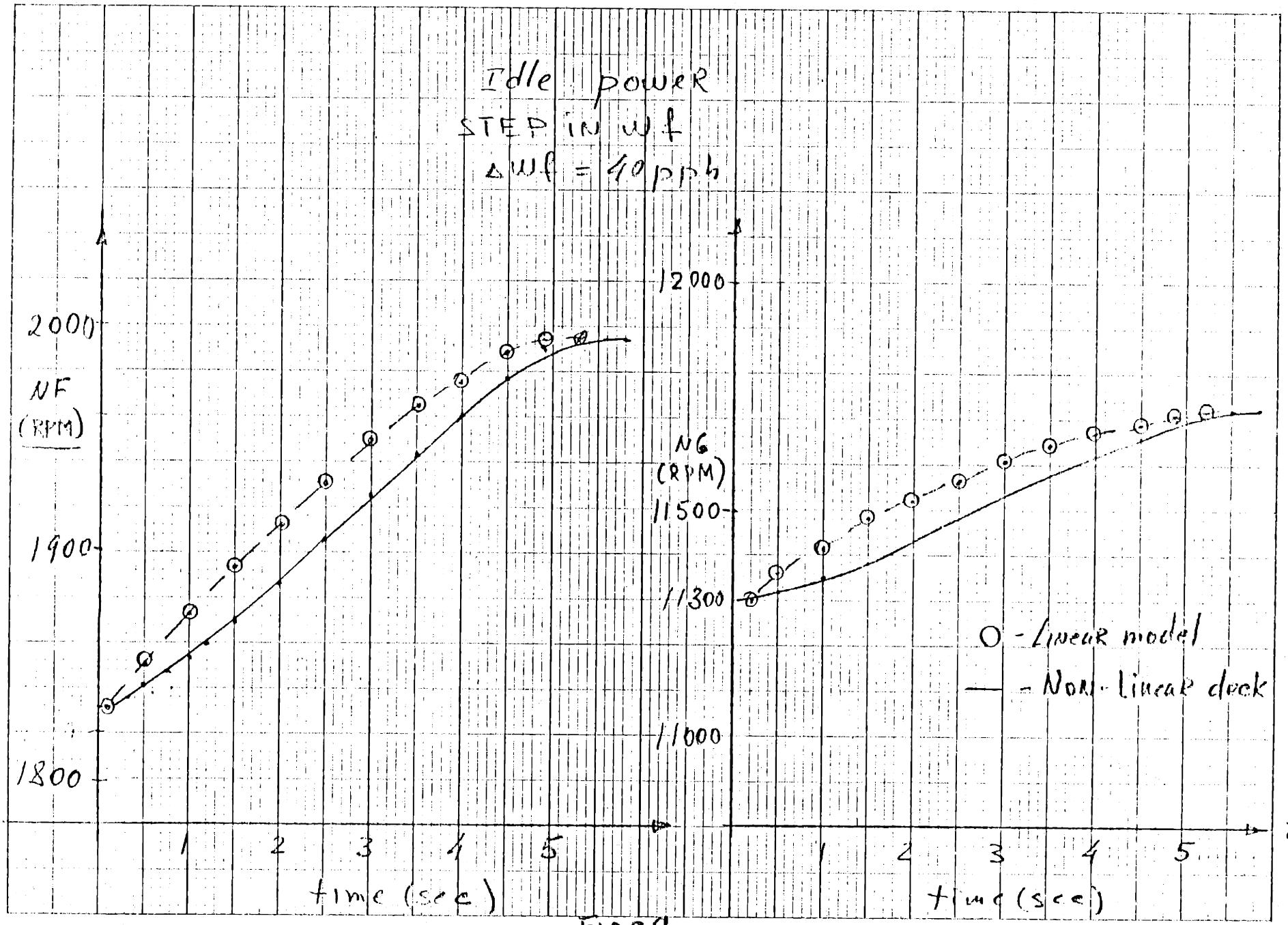
Idle power
STEP IN Wf
ΔWf = 40 pph
2000
NF
(RPM)
1900
1800
12000
NG
(RPM)
11500
11300
11000
O - Linear model
— - Non-linear deck
1
2
3
4
5
time (sec)
1
2
3
4
5
time (sec)

Fig 9

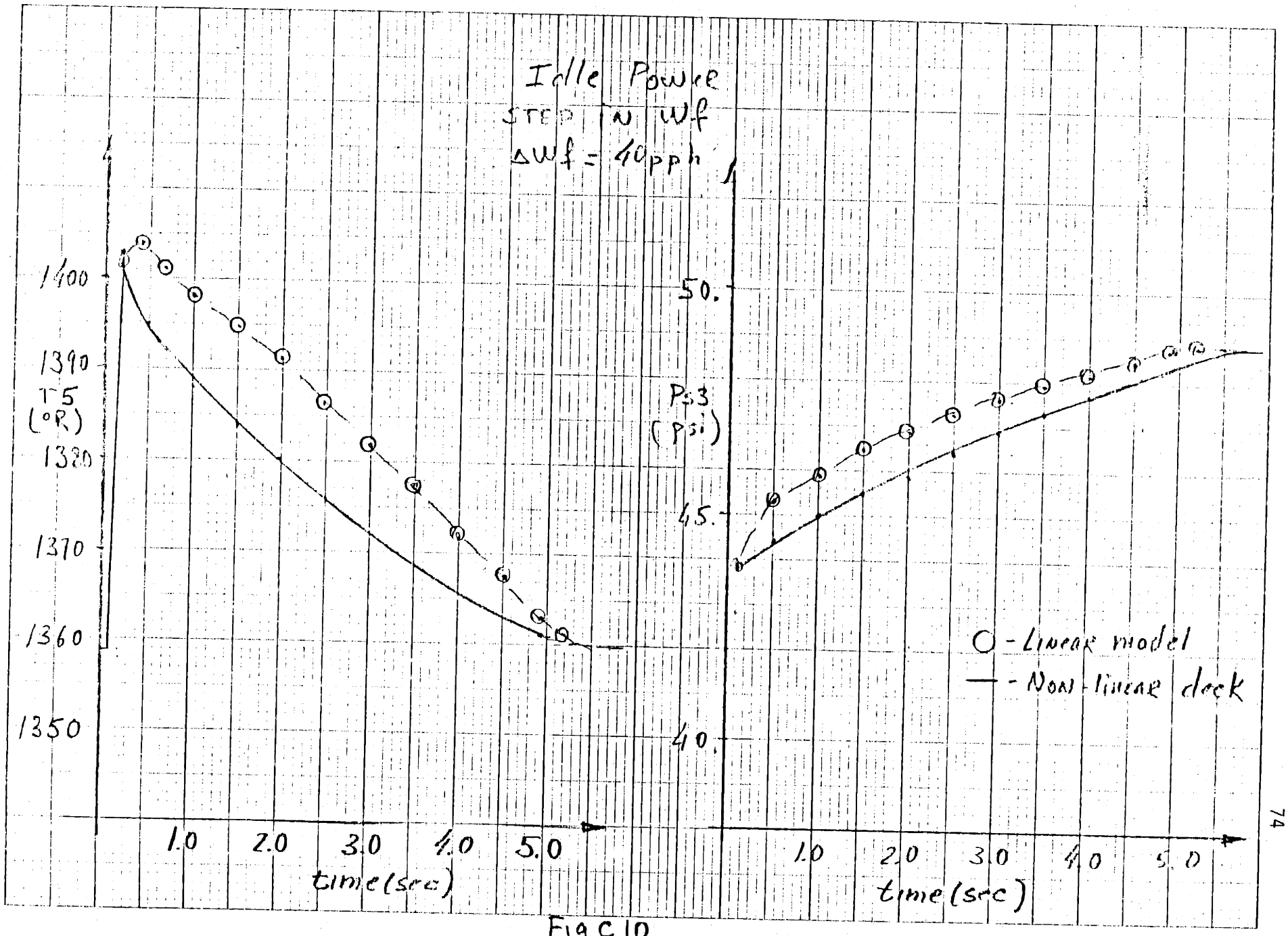
Idle Power
STEP IN Wf
ΔWf = 40 pph
T5 (°R)
1400
1390
1380
1370
1360
1350
1.0
2.0
3.0
4.0
5.0
time (sec)
50.
45.
40.
Ps3 (psi)
1.0
2.0
3.0
4.0
5.0
time (sec)
O - Linear model
— - Non-linear deck

Fig C 10

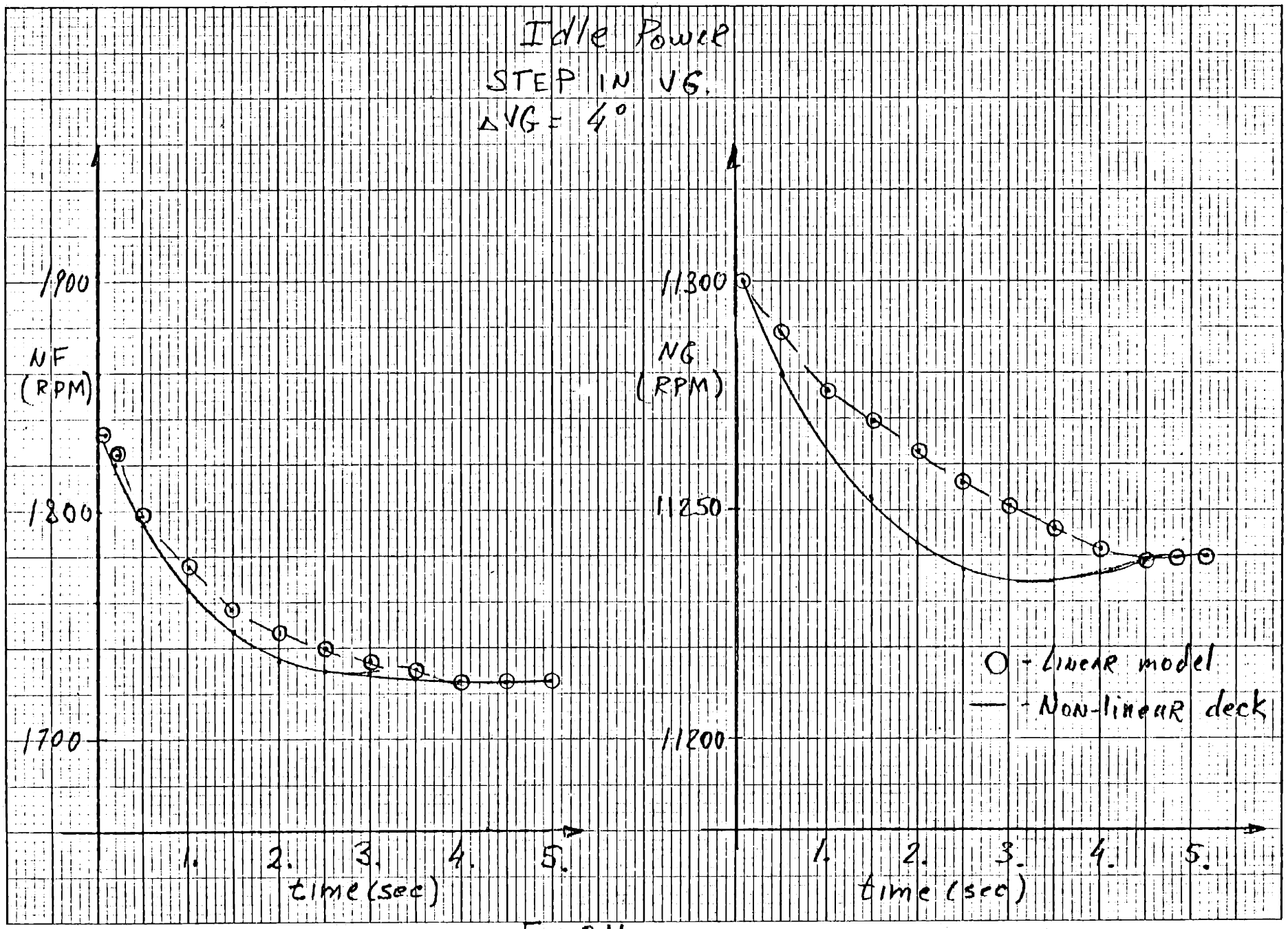
Idle Power
STEP IN VG.
ΔVG = 4°
1900
NF (RPM)
1800
1700
1. 2. 3. 4. 5.
time (sec)
11300
NG (RPM)
11250
11200
1. 2. 3. 4. 5.
time (sec)
O - Linear model
— - Non-linear deck

Fig C11

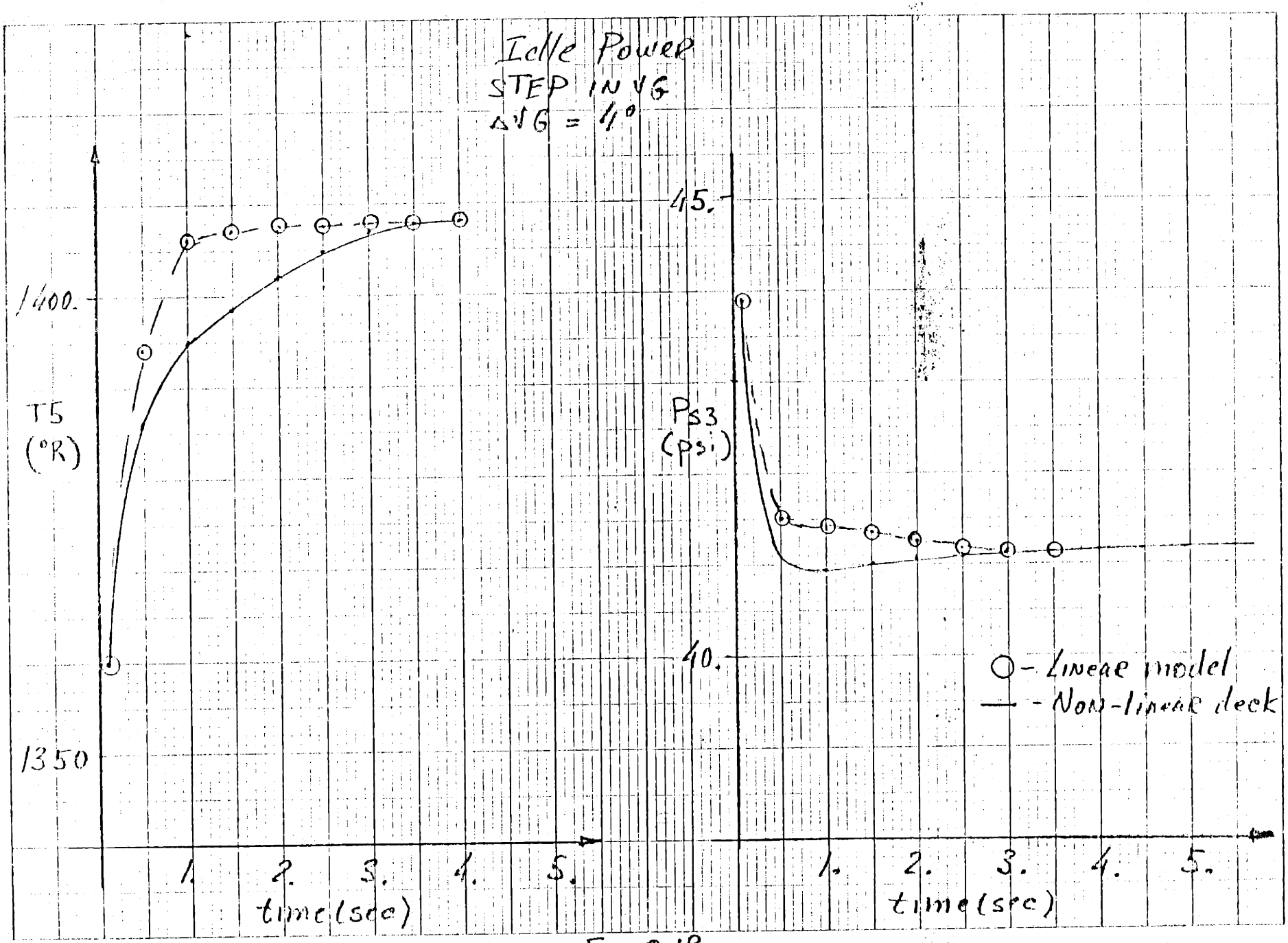
Idle Power
STEP INVG
ΔVG = 1°
1400.
1350
T5
(°R)
45.
40.
Ps3
(psi)
○ - Linear model
— - Non-linear deck
1.
2.
3.
4.
5.
time (sec)
1.
2.
3.
4.
5.
time (sec)

Fig C 12

APPENDIX D

TRANSMISSION ZEROS

Transmission Zeros

The transmission zeros for single input, single output are known to the Engineering community under a somewhat different name: the roots of the numerator polynominal of the transfer function. This definition is translated for multivarialbe system, with number of inputs equal to the number of outputs as follows:

The transmission zeros are those values of S, including multiplicities, but not including uncontrollable or unobservable modes, that reduce the rank of P(s), where P(s) is defined as:

$$P(s) = \begin{bmatrix} A - SI & B \\ -C & 0 \end{bmatrix} \tag{1D}$$

For square case, the determinant of P(s) is equal to:

$$\det (A - SI) \det [C (A - SI)^{-1} B] \tag{2D}$$

and other equivalent definition of transmission zeros is the roots of (2D). This definition is used by Kwakernaak and Sivan [7].

APPENDIX E

Q AND R MATRICES

1) Takeoff

Q Matrix

COL	1	2	3	4	5	6	7	8
1	1.00000D+00	0.0	0.0	0.0	0.0	0.0	0.0	0.0
2	0.0	1.00000D+00	0.0	0.0	0.0	0.0	0.0	0.0
3	0.0	0.0	0.0	0.0	0.0	0.0	0.0	0.0
4	0.0	0.0	0.0	0.0	0.0	0.0	0.0	0.0
5	0.0	0.0	0.0	0.0	1.00000D+00	0.0	0.0	0.0
6	0.0	0.0	0.0	0.0	0.0	1.00000D+00	0.0	0.0
7	0.0	0.0	0.0	0.0	0.0	0.0	1.00000D+01	0.0
8	0.0	0.0	0.0	0.0	0.0	0.0	0.0	1.00000D+02

R Matrix

ROW \ COL	1	2
1	1.00000D+02	0.0
2	0.0	5.00000D+01

2) 90% M2

Q Matrix

ROW \ COL	1	2	3	4	5	6	7	8
1	1.00000D+00	0.0	0.0	0.0	0.0	0.0	0.0	0.0
2	0.0	1.00000D+00	0.0	0.0	0.0	0.0	0.0	0.0
3	0.0	0.0	0.0	0.0	0.0	0.0	0.0	0.0
4	0.0	0.0	0.0	0.0	0.0	0.0	0.0	0.0
5	0.0	0.0	0.0	0.0	1.00000D+00	0.0	0.0	0.0
6	0.0	0.0	0.0	0.0	0.0	1.00000D+00	0.0	0.0
7	0.0	0.0	0.0	0.0	0.0	0.0	5.00000D+00	0.0
8	0.0	0.0	0.0	0.0	0.0	0.0	0.0	5.00000D+01

R Matrix

ROW \ COL	1	2
1	1.50000D+02	0.0
2	0.0	1.00000D+02

3) 80% N2

Q Matrix

ROW	COL 1	2	3	4	5	6	7	8
1	1.00000D+00	0.0	0.0	0.0	0.0	0.0	0.0	0.0
2	0.0	1.00000D+00	0.0	0.0	0.0	0.0	0.0	0.0
3	0.0	0.0	0.0	0.0	0.0	0.0	0.0	0.0
4	0.0	0.0	0.0	0.0	0.0	0.0	0.0	0.0
5	0.0	0.0	0.0	0.0	1.00000D+03	0.0	0.0	0.0
6	0.0	0.0	0.0	0.0	0.0	1.00000D+00	0.0	0.0
7	0.0	0.0	0.0	0.0	0.0	0.0	1.00000D+00	0.0
8	0.0	0.0	0.0	0.0	0.0	0.0	0.0	5.00000D+01

R Matrix

ROW	COL 1	2
1	6.50000D+02	0.0
2	0.0	5.50000D+02

4) Idle

Q Matrix

ROW	COL 1	2	3	4	5	6	7	8
1	1.00000D+00	0.0	0.0	0.0	0.0	0.0	0.0	0.0
2	0.0	1.00000D+00	0.0	0.0	0.0	0.0	0.0	0.0
3	0.0	0.0	1.00000D+00	0.0	0.0	0.0	0.0	0.0
4	0.0	0.0	0.0	1.00000D+00	0.0	0.0	0.0	0.0
5	0.0	0.0	0.0	0.0	1.00000D+03	0.0	0.0	0.0
6	0.0	0.0	0.0	0.0	0.0	5.00000D+01	0.0	0.0
7	0.0	0.0	0.0	0.0	0.0	0.0	1.00000D+00	0.0
8	0.0	0.0	0.0	0.0	0.0	0.0	0.0	1.00000D+01

R Matrix

	COL 1	2
1	1.50000D+03	0.0
2	0.0	5.50000D+02

APPENDIX F

OPTIMAL GAIN MATRIX G AND OPEN/CLOSED LOOP EIGENVALUES

1) Takeoff

G Matrix

ROW \ COL	1	2	3	4	5	6	7	8
1	5.6730D-02	5.7873D-02	0.0	0.0	5.1985D+00	-3.6143D-01	2.7295D-01	5.0497D-01
2	-5.2605D-02	-2.9488D-03	0.0	0.0	-7.2287D-01	4.2985D+00	-2.2583D-01	1.2207D+00

OPEN LOOP
---EIGENVALUES---

	REAL PART	IMAG PART	NAT FREQ(HZ)	ZETA	FREQ(HZ)
1	-1.000D+02	0.0	1.592D+01	1.000000	0.0
2	-3.571D+01	0.0	5.684D+00	1.000000	0.0
3	-5.110D+00	8.188D-01	8.237D-01	0.987406	1.303D-01
4	-5.110D+00	-8.188D-01	8.237D-01	0.987406	1.303D-01
5	0.0	0.0	0.0	0.0	0.0
6	0.0	0.0	0.0	0.0	0.0
7	0.0	0.0	0.0	0.0	0.0
8	0.0	0.0	0.0	0.0	0.0

CLOSED-LOOP EIGENVALUES

	REAL PART	IMAG PART	NAT FREQ(HZ)	ZETA	FREQ(HZ)
1	-1.000D+02	0.0	1.592D+01	1.000000	0.0
2	-3.571D+01	0.0	5.684D+00	1.000000	0.0
3	-4.670D+00	3.101D+00	8.922D-01	0.833086	4.935D-01
4	-4.670D+00	-3.101D+00	8.922D-01	0.833086	4.935D-01
5	-3.997D+00	0.0	6.362D-01	1.000000	0.0
6	-3.037D+00	1.999D+00	5.786D-01	0.835314	3.181D-01
7	-3.037D+00	-1.999D+00	5.786D-01	0.835314	3.181D-01
8	-3.063D-01	0.0	4.875D-02	1.000000	0.0

2) 90% N2

G Matrix

ROW \ COL	1	2	3	4	5	6	7	8
1	8.8126D-02	6.4385D-02	0.0	0.0	6.9407D+00	-6.8830D-01	1.7271D-01	1.8716D-01
2	-3.8912D-02	4.4820D-03	0.0	0.0	-1.0324D+00	1.9776D+00	-7.2487D-02	6.6892D-01

OPEN LOOP
---EIGENVALUES---

	REAL PART	IMAG PART	NAT FREQ(HZ)	ZETA	FREQ(HZ)
1	-1.000D+02	0.0	1.592D+01	1.000000	0.0
2	-1.428D+01	0.0	2.274D+00	1.000000	0.0
3	-1.412D+00	4.142D-01	2.343D-01	0.959593	6.592D-02
4	-1.412D+00	-4.142D-01	2.343D-01	0.959593	6.592D-02
5	0.0	0.0	0.0	0.0	0.0
6	0.0	0.0	0.0	0.0	0.0
7	0.0	0.0	0.0	0.0	0.0
8	0.0	0.0	0.0	0.0	0.0

CLOSED-LOOP EIGENVALUES

	REAL PART	IMAG PART	NAT FREQ(HZ)	ZETA	FREQ(HZ)
1	-1.000D+02	0.0	1.592D+01	1.000000	0.0
2	-1.428D+01	0.0	2.274D+00	1.000000	0.0
3	-2.889D+00	2.753D+00	6.352D-01	0.723921	4.382D-01
4	-2.889D+00	-2.753D+00	6.352D-01	0.723921	4.382D-01
5	-2.059D+00	0.0	3.277D-01	1.000000	0.0
6	-1.764D+00	9.523D-01	3.190D-01	0.879938	1.516D-01
7	-1.764D+00	-9.523D-01	3.190D-01	0.879938	1.516D-01
8	-3.786D-01	0.0	6.026D-02	1.000000	0.0

3) 80% N2

G Matrix

ROW \ COL	1	2	3	4	5	6	7	8
1	2.9702D-02	3.6887D-02	0.0	0.0	3.8245D+00	-6.6508D-01	3.2383D-02	1.5649D-01
2	-2.1982D-02	-5.1700D-03	0.0	0.0	-7.8600D-01	1.5761D+00	-2.4059D-02	2.4893D-01

OPEN LOOP
---EIGENVALUES---

	REAL PART	IMAG PART	NAT FREQ(HZ)	ZETA	FREQ(HZ)
1	-1.000D+02	0.0	1.592D+01	1.000000	0.0
2	-1.333D+01	0.0	2.122D+00	1.000000	0.0
3	-1.210D+00	0.0	1.926D-01	1.000000	0.0
4	-6.328D-01	0.0	1.007D-01	1.000000	0.0
5	0.0	0.0	0.0	0.0	0.0
6	0.0	0.0	0.0	0.0	0.0
7	0.0	0.0	0.0	0.0	0.0
8	0.0	0.0	0.0	0.0	0.0

CLOSED-LOOP EIGENVALUES

	REAL PART	IMAG PART	NAT FREQ(HZ)	ZETA	FREQ(HZ)
1	-1.000D+02	0.0	1.592D+01	1.000000	0.0
2	-1.333D+01	0.0	2.122D+00	1.000000	0.0
3	-1.722D+00	1.752D+00	3.909D-01	0.701018	2.788D-01
4	-1.722D+00	-1.752D+00	3.909D-01	0.701018	2.788D-01
5	-1.276D+00	6.201D-01	2.258D-01	0.899371	9.870D-02
6	-1.276D+00	-6.201D-01	2.258D-01	0.899371	9.870D-02
7	-1.041D+00	0.0	1.656D-01	1.000000	0.0
8	-2.076D-01	0.0	3.304D-02	1.000000	0.0

4) Idle

G Matrix

ROW \ COL	1	2	3	4	5	6	7	8
1	2.3851D-02	2.5829D-02	7.9730D-05	9.9706D-07	2.8804D+00	-2.4228D-01	2.3407D-02	3.4464D-02
2	-1.8543D-02	-4.8935D-03	1.8040D-05	-6.3143D-07	-6.6076D-01	8.1716D-01	-1.7998D-02	1.2224D-01

OPEN LOOP

---EIGENVALUES---

	REAL PART	IMAG PART	NAT FREQ(HZ)	ZETA	FREQ(HZ)
1	-1.000D+02	0.0	1.592D+01	1.000000	0.0
2	-1.333D+01	0.0	2.122D+00	1.000000	0.0
3	-9.413D-01	0.0	1.498D-01	1.000000	0.0
4	-2.453D-01	0.0	3.905D-02	1.000000	0.0
5	0.0	0.0	0.0	0.0	0.0
6	0.0	0.0	0.0	0.0	0.0
7	0.0	0.0	0.0	0.0	0.0
8	0.0	0.0	0.0	0.0	0.0

CLOSED-LOOP EIGENVALUES

	REAL PART	IMAG PART	NAT FREQ(HZ)	ZETA	FREQ(HZ)
1	-1.000D+02	0.0	1.592D+01	1.000000	0.0
2	-1.333D+01	0.0	2.122D+00	1.000000	0.0
3	-1.219D+00	1.196D+00	2.717D-01	0.713718	1.903D-01
4	-1.219D+00	-1.196D+00	2.717D-01	0.713718	1.903D-01
5	-9.405D-01	0.0	1.497D-01	1.000000	0.0
6	-6.458D-01	2.826D-01	1.122D-01	0.916117	4.498D-02
7	-6.458D-01	-2.826D-01	1.122D-01	0.916117	4.498D-02
8	-2.155D-01	0.0	3.430D-02	1.000000	0.0

APPENDIX G

COMPARISON: LQR DESIGN VS. CURRENT TF34 DESIGN TRANSIENT RESPONSES

_____ - CURRENT TF34 DESIGN

0 - LQR DESIGN

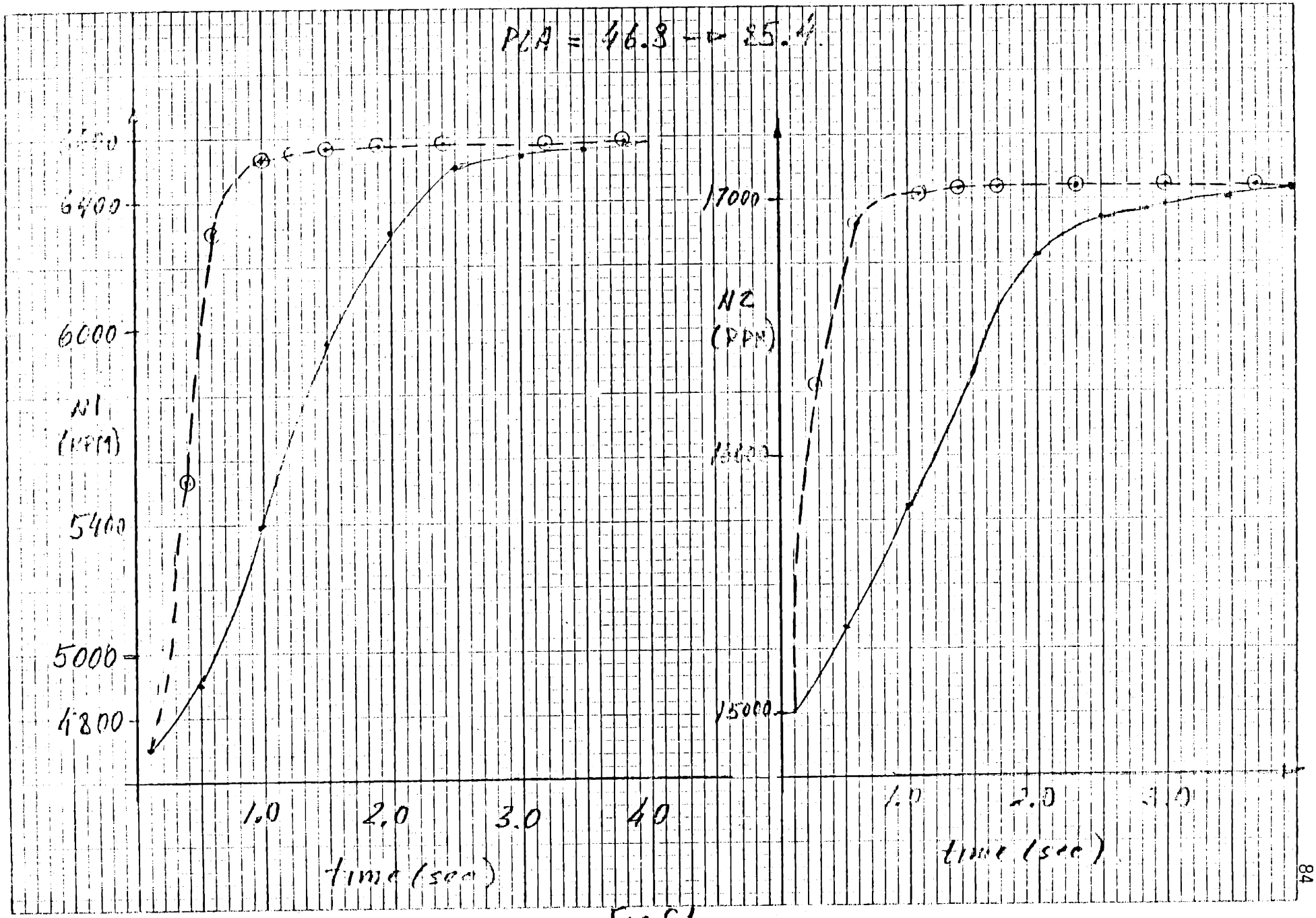
PLA = 46.8 → 85.4
6400
6000
N1 (RPM)
5400
5000
4800
1.0
2.0
3.0
4.0
time (sec)
17000
N2 (PPM)
15000
time (sec)

Fig G1

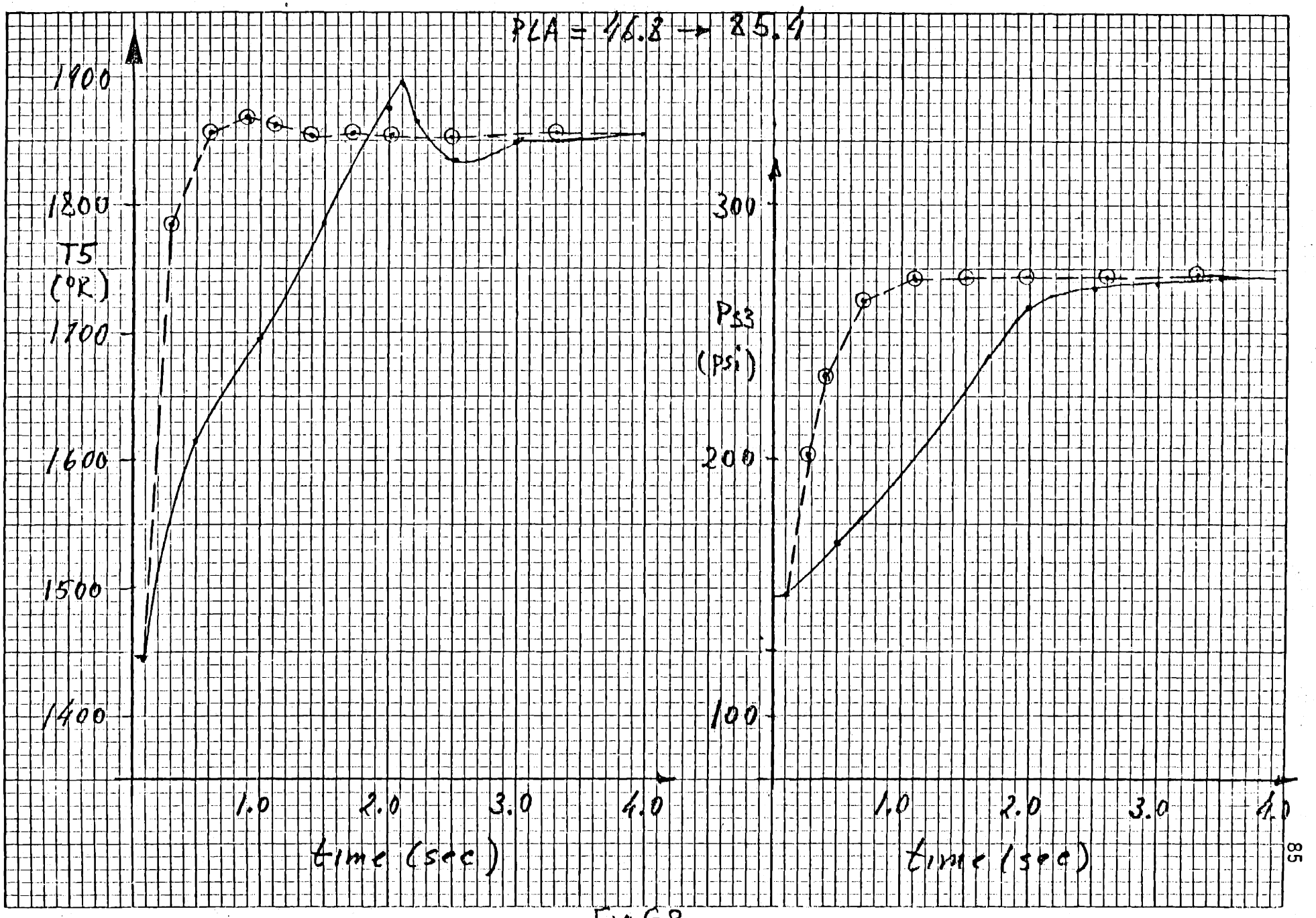
PLA = 16.8 → 85.4
1900
1800
T5
(°R)
1700
1600
1500
1400
1.0
2.0
3.0
4.0
time (sec)
300
P53
(psi)
200
100
1.0
2.0
3.0
4.0
time (sec)

Fig G2

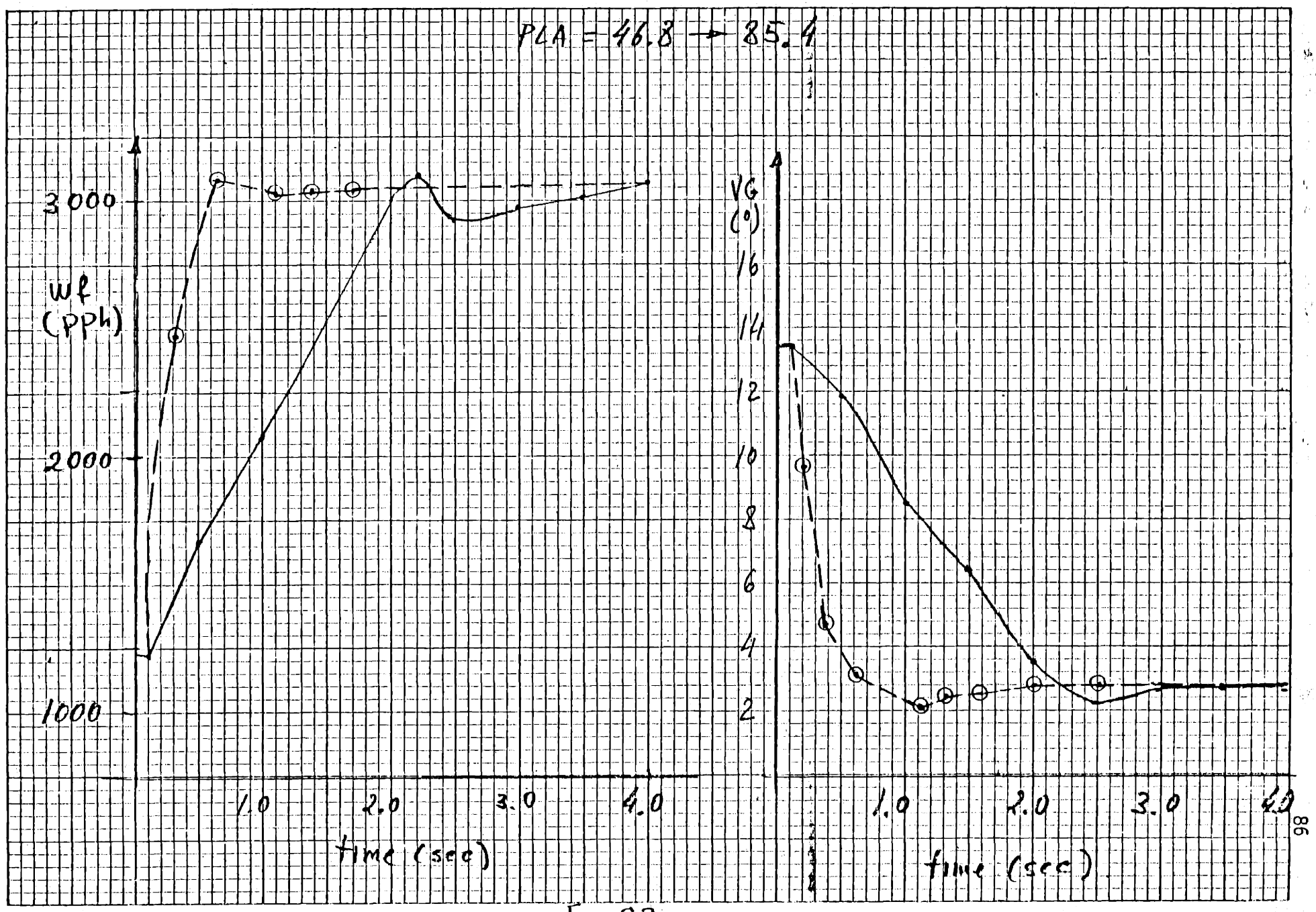
PLA = 46.8 → 85.4
3000
Wf (PPH)
2000
1000
1.0
2.0
3.0
4.0
time (sec)
VG (°)
16
14
12
10
8
6
4
2
1.0
2.0
3.0
4.0
time (sec)

Fig G3

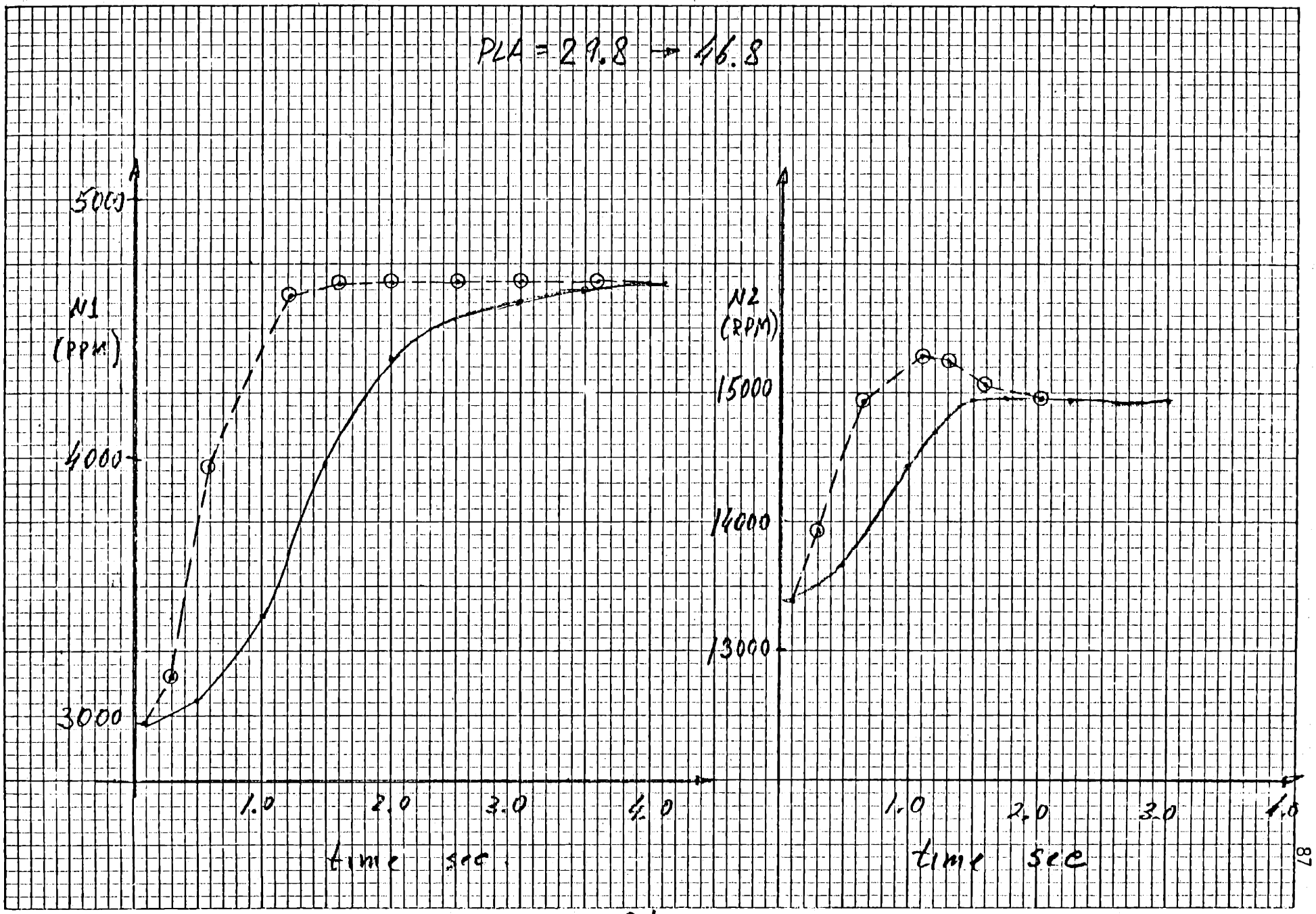
PLA = 29.8 → 46.8
N1 (RPM)
5000
4000
3000
1.0
2.0
3.0
4.0
time sec.
N2 (RPM)
15000
14000
13000
1.0
2.0
3.0
4.0
time sec

Fig G4

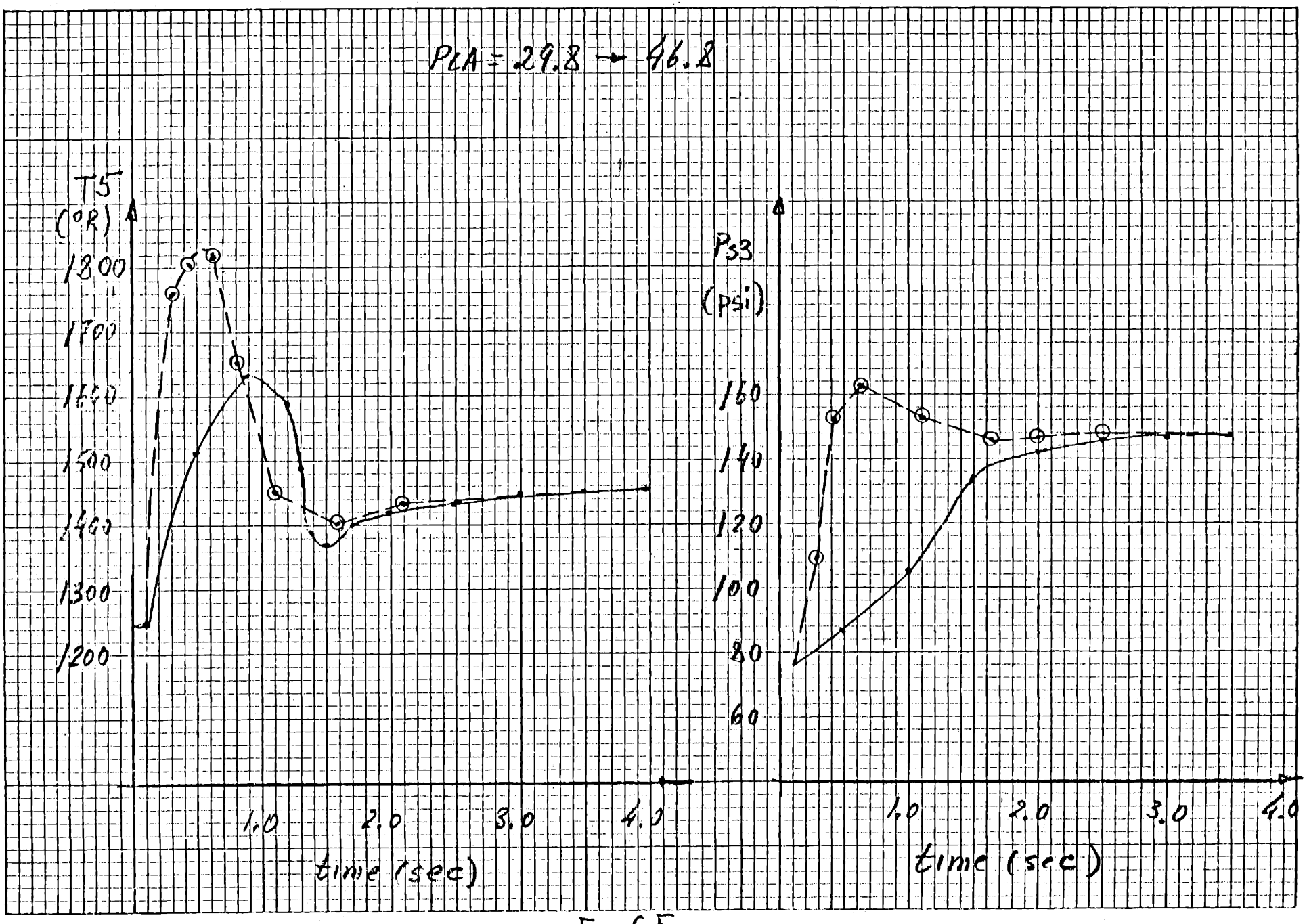
PLA = 29.8 → 86.8
T5 (°R)
1800
1700
1600
1500
1400
1300
1200
1.0
2.0
3.0
4.0
time (sec)
P53 (Psi)
160
140
120
100
80
60
1.0
2.0
3.0
4.0
time (sec)

Fig G5


PLA = 29.8 → 46.8
1500
1400
1200
1000
ωf (rpm)
500
VG (°)
22
26
24
22
20
18
16
14
12
1.0
2.0
3.0
4.0
time (sec)
1.0
2.0
3.0
4.0
time (sec)

Fig G6

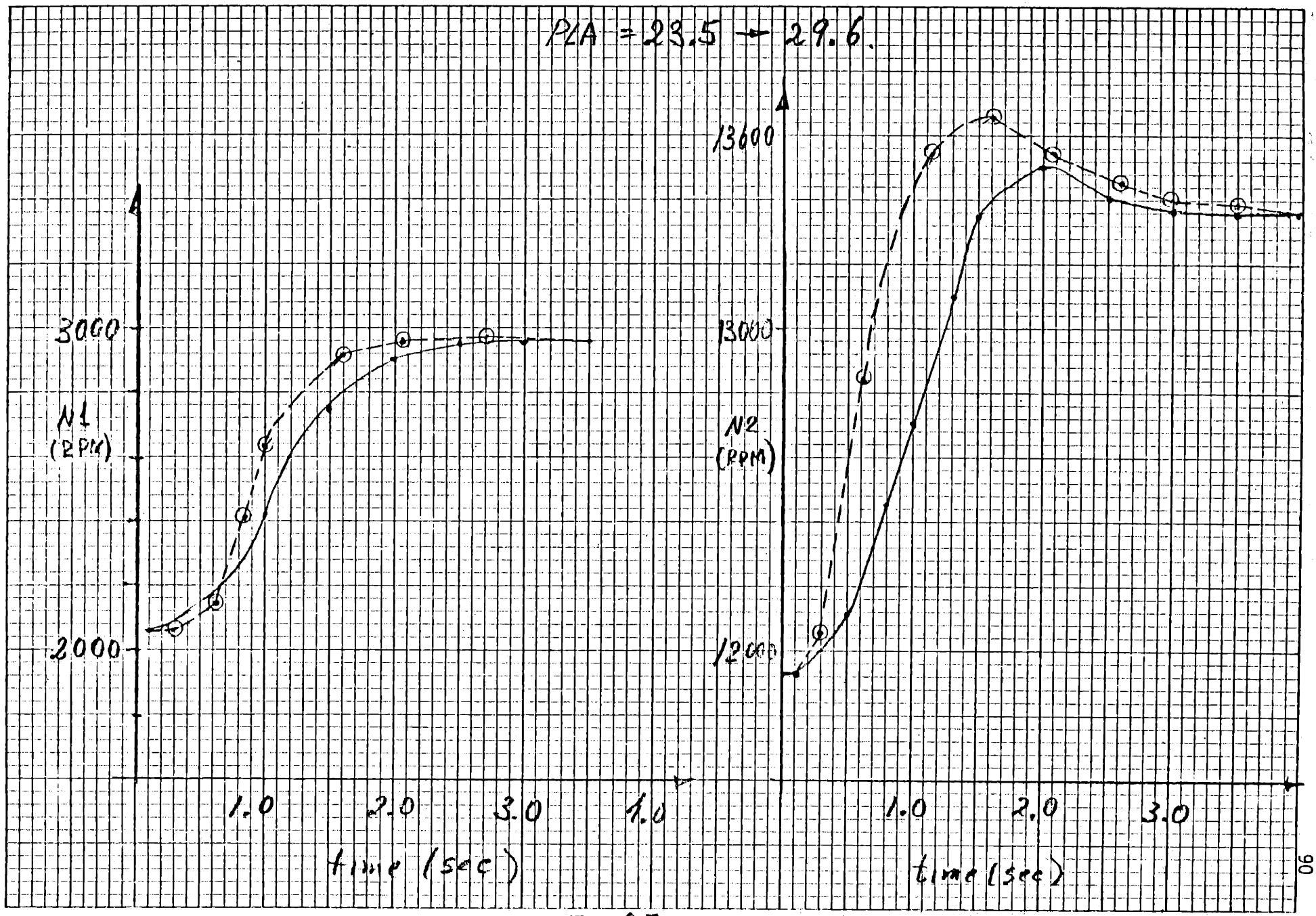
PLA = 23.5 → 29.6.
3000
2000
N1
(RPM)
1.0
2.0
3.0
time (sec)
13600
13000
12000
N2
(RPM)
1.0
2.0
3.0
time (sec)

Fig G7

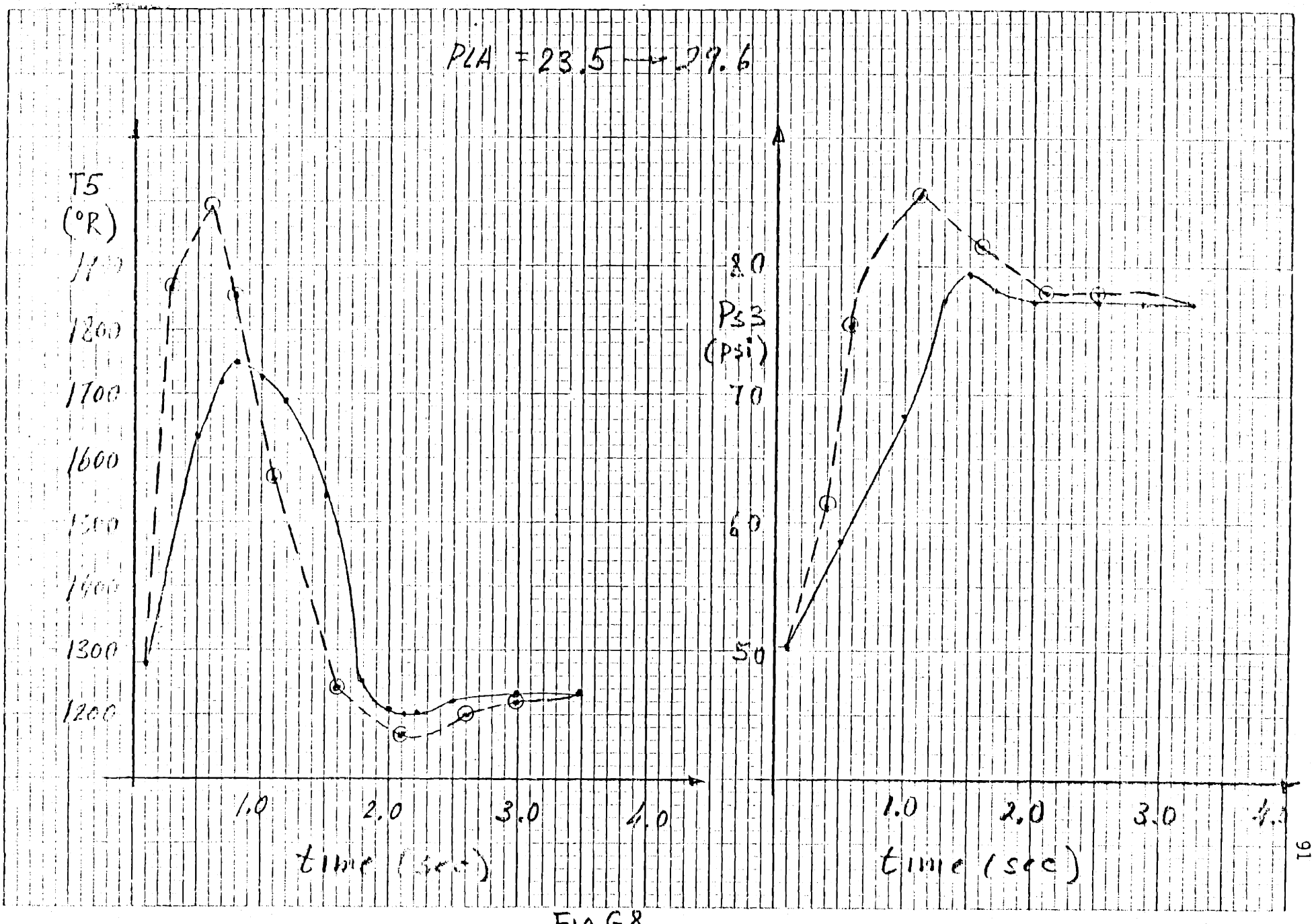
PLA = 23.5 → 29.6
T5
(°R)
1700
1600
1300
1200
1.0
2.0
3.0
time (sec)
80
P33
(psi)
70
60
50
1.0
2.0
3.0
time (sec)

Fig G8

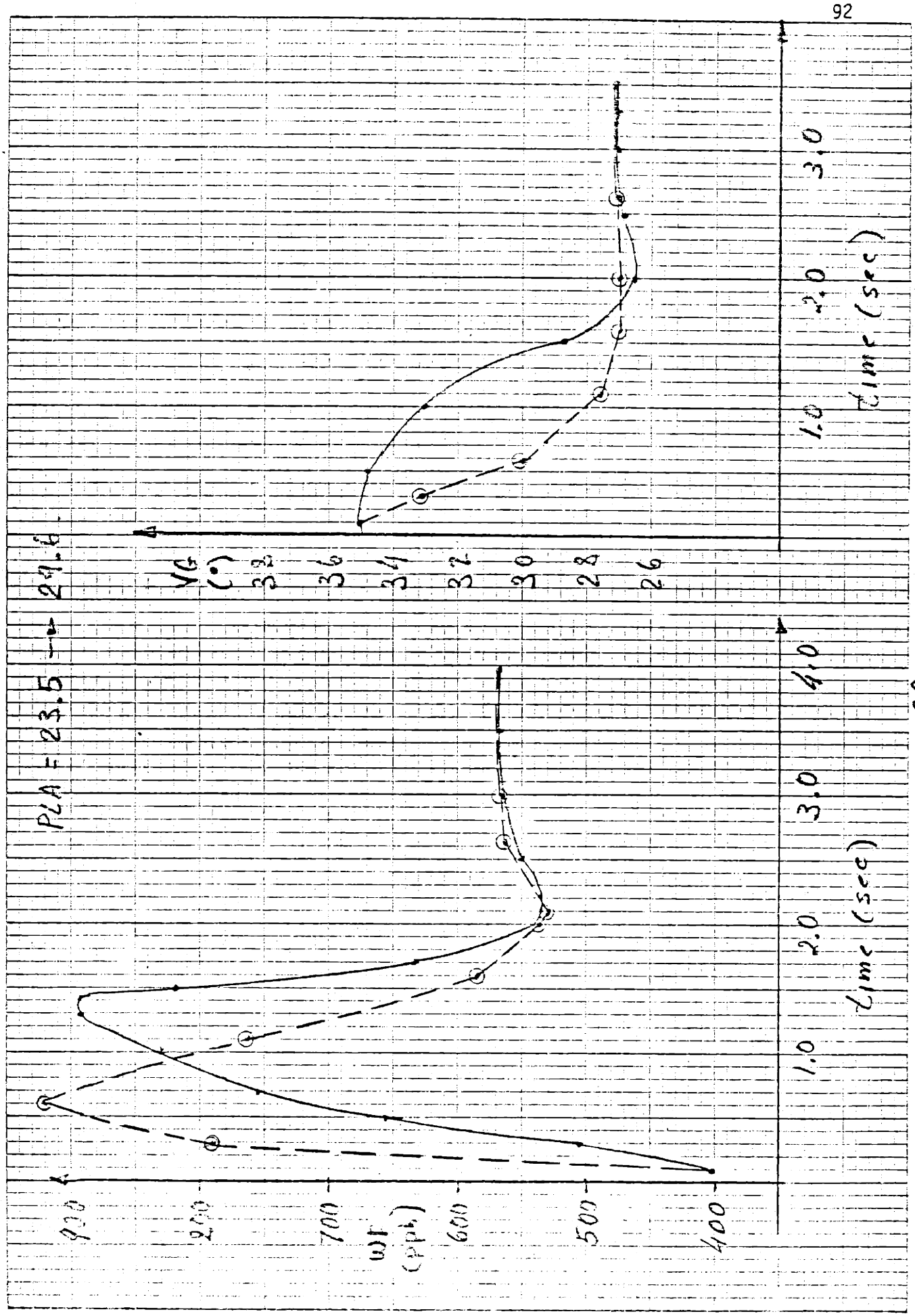
PLA = 23.5
24.4
VG (°)
32
30
28
26
1.0
2.0
3.0
Time (sec)
WF (PPH)
900
800
700
600
500
400
4.0

Fig 69

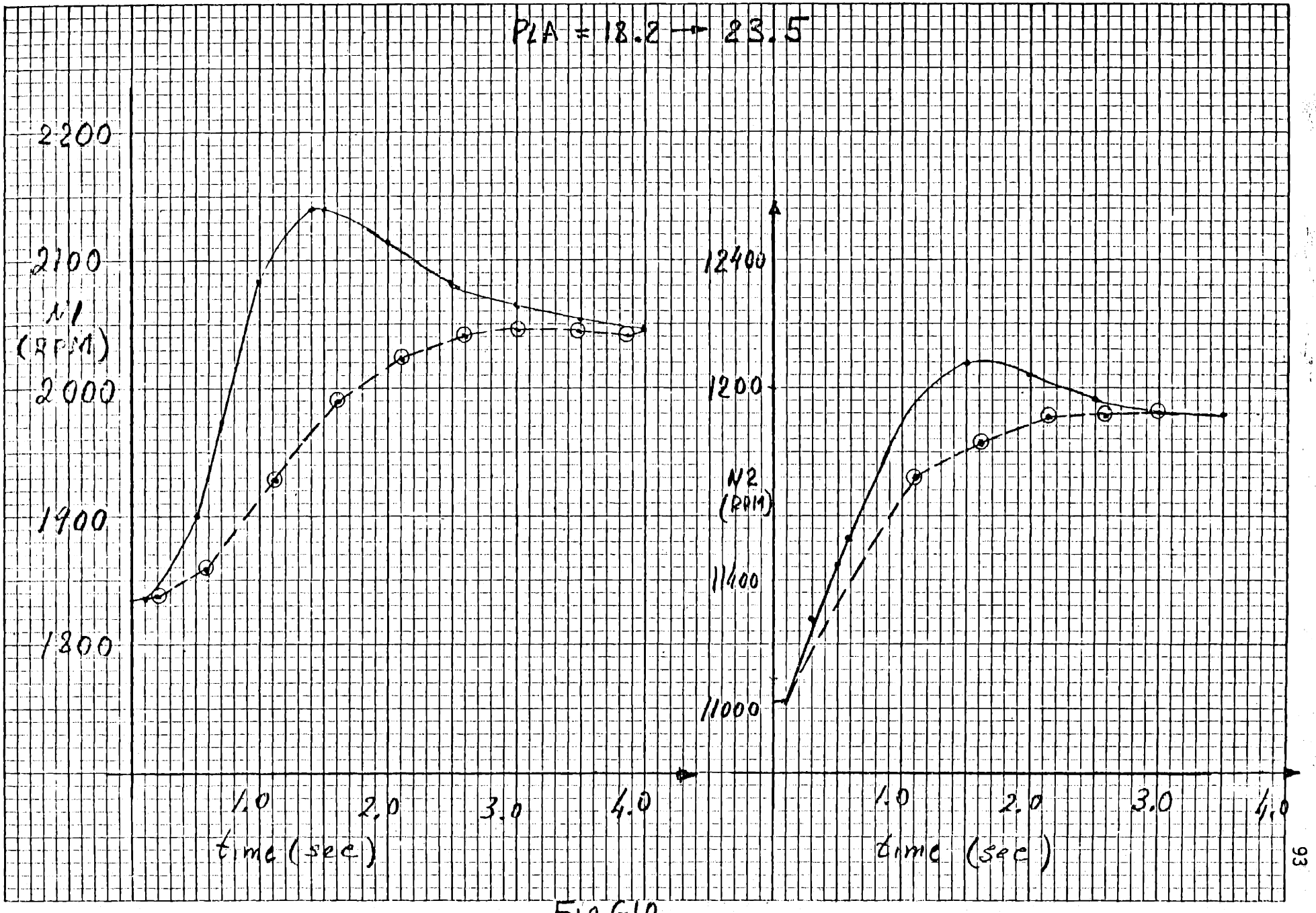
PLA = 18.2 → 23.5
2200
2100
N1
(RPM)
2000
1900
1800
12400
12000
N2
(RPM)
11400
11000
1.0
2.0
3.0
4.0
time (sec)
1.0
2.0
3.0
4.0
time (sec)

Fig G10

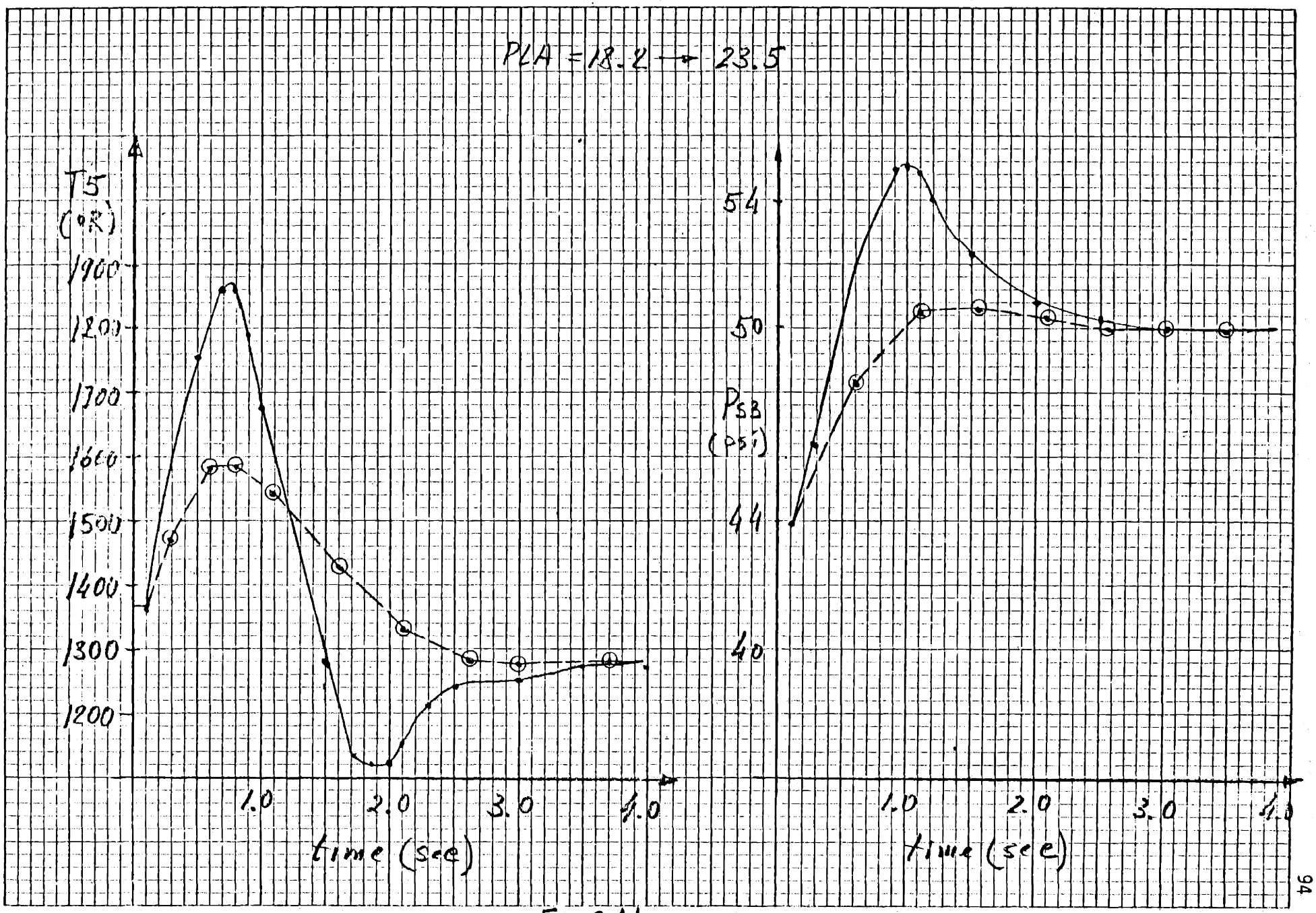
PLA = 18.2 → 23.5
T5 (°R)
1900
1800
1700
1600
1500
1400
1300
1200
1.0
2.0
3.0
4.0
time (sec)
54
50
PSB (psi)
44
40
1.0
2.0
3.0
time (sec)

Fig G11

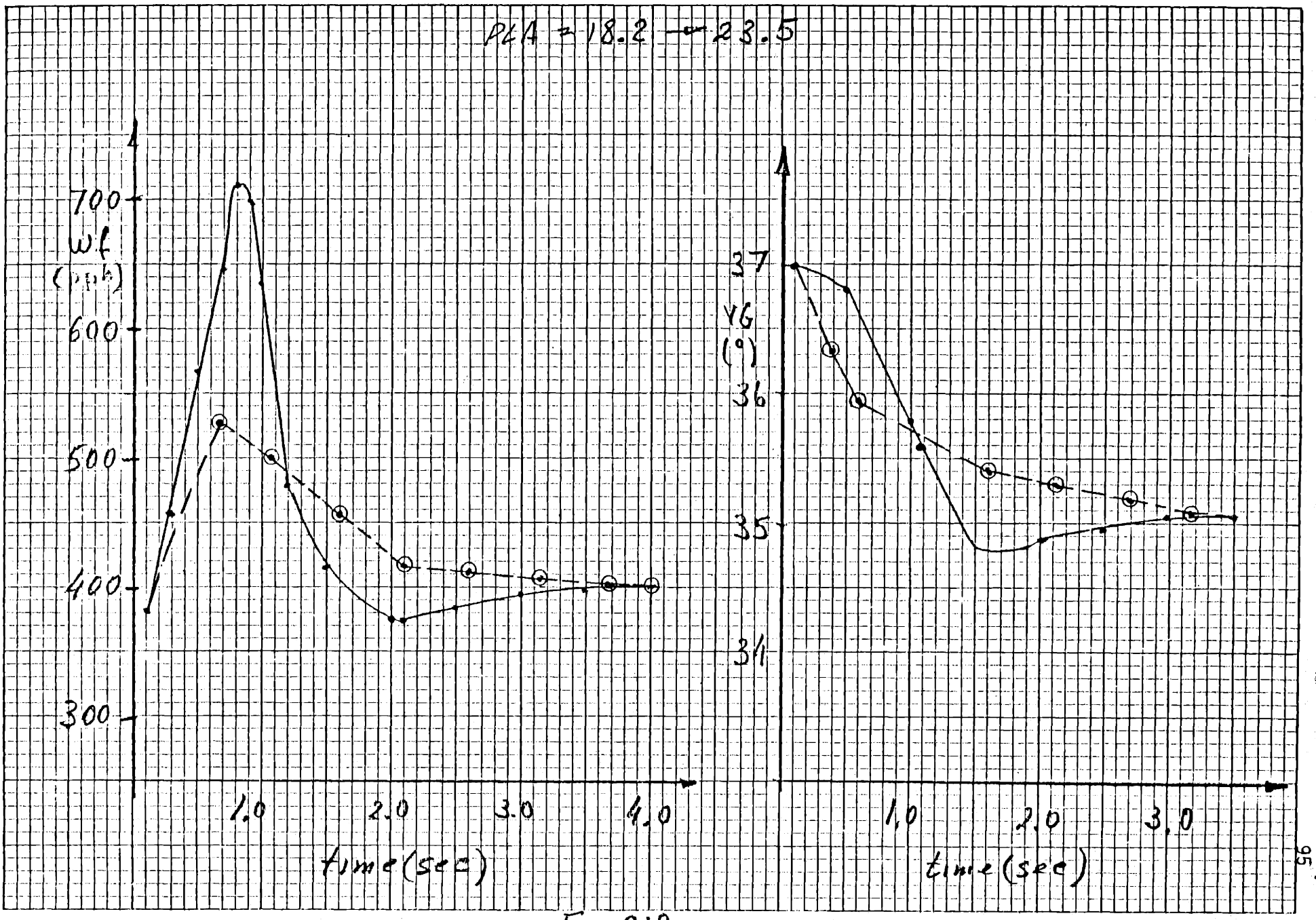
PLA = 18.2 — 23.5
700
wf
(lb)
600
500
400
300
1.0
2.0
3.0
4.0
time (sec)
37
γG
(°)
36
35
34
1.0
2.0
3.0
time (sec)

Fig G12

APPENDIX H

OPTIMAL CONTROL GAINS SCHEDULES

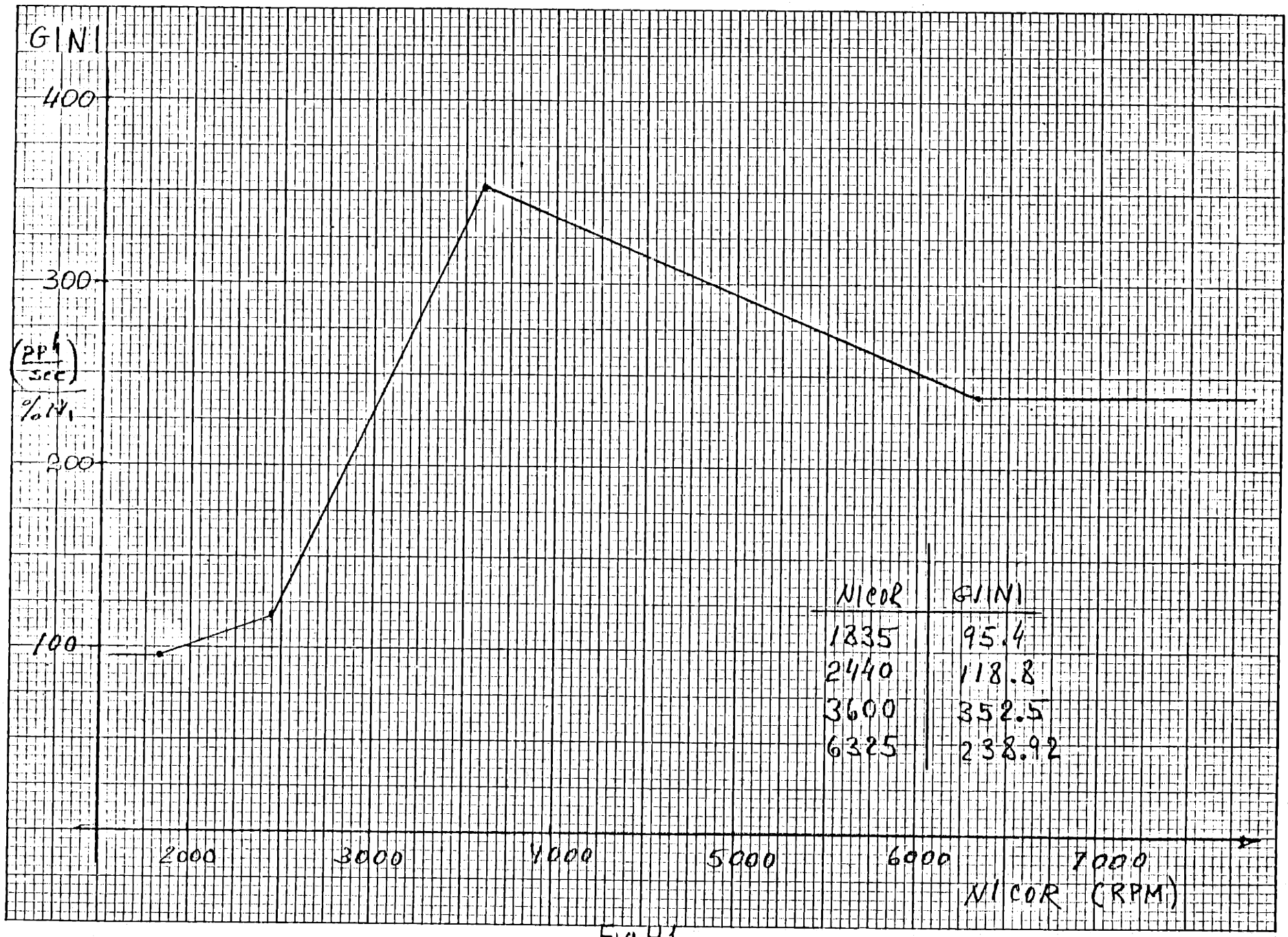

NICOR	GINI
1835	95.4
2440	118.8
3600	352.5
6325	238.92

Fig H1

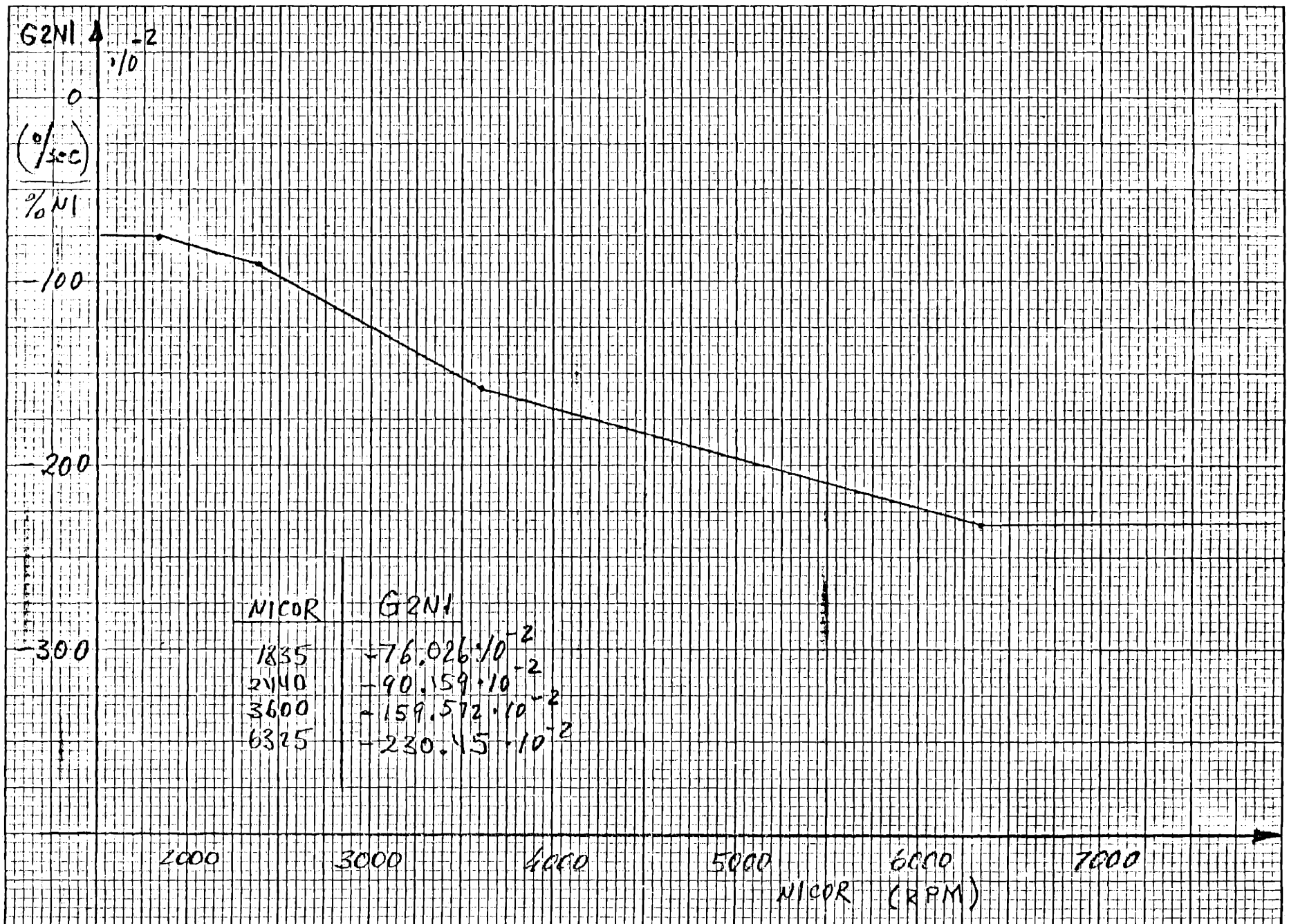
G2N1
$\cdot 10^{-2}$
0
(%/sec)
%N1
-100
-200
-300
NICOR
G2N1
1835
2140
3600
6325
$+76.026 \cdot 10^{-2}$
$-90.159 \cdot 10^{-2}$
$-159.572 \cdot 10^{-2}$
$-230.15 \cdot 10^{-2}$
2000
3000
4000
5000
6000
7000
NICOR (RPM)

Fig H2

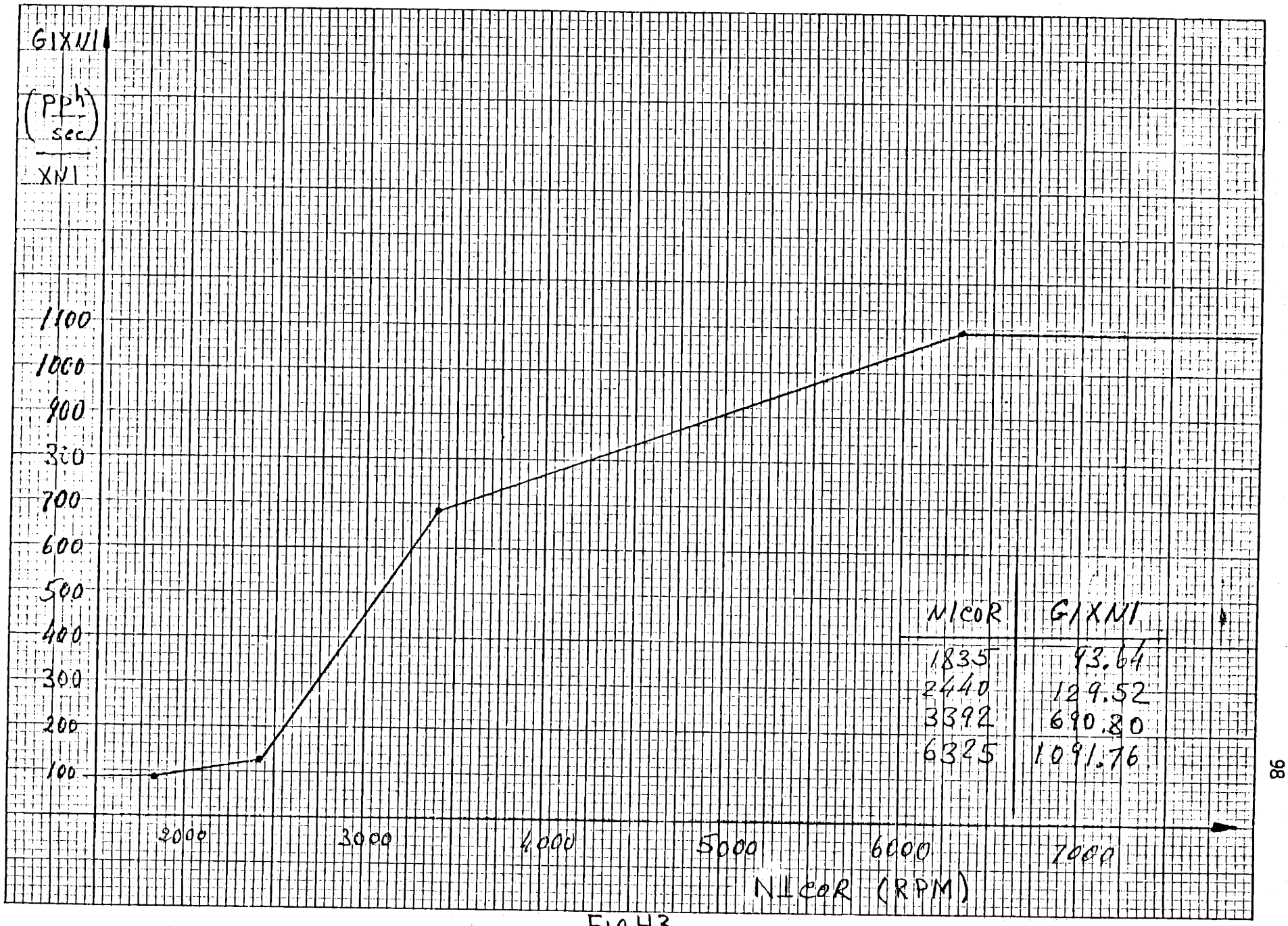
GIXNI
(Pph/sec)
XNI
1100
1000
900
800
700
600
500
400
300
200
100
2000
3000
4000
5000
6000
7000
NIcoR (RPM)
NIcoR | GIXNI
1835 | 93.64
2440 | 129.52
3392 | 690.80
6325 | 1091.76

Fig H3

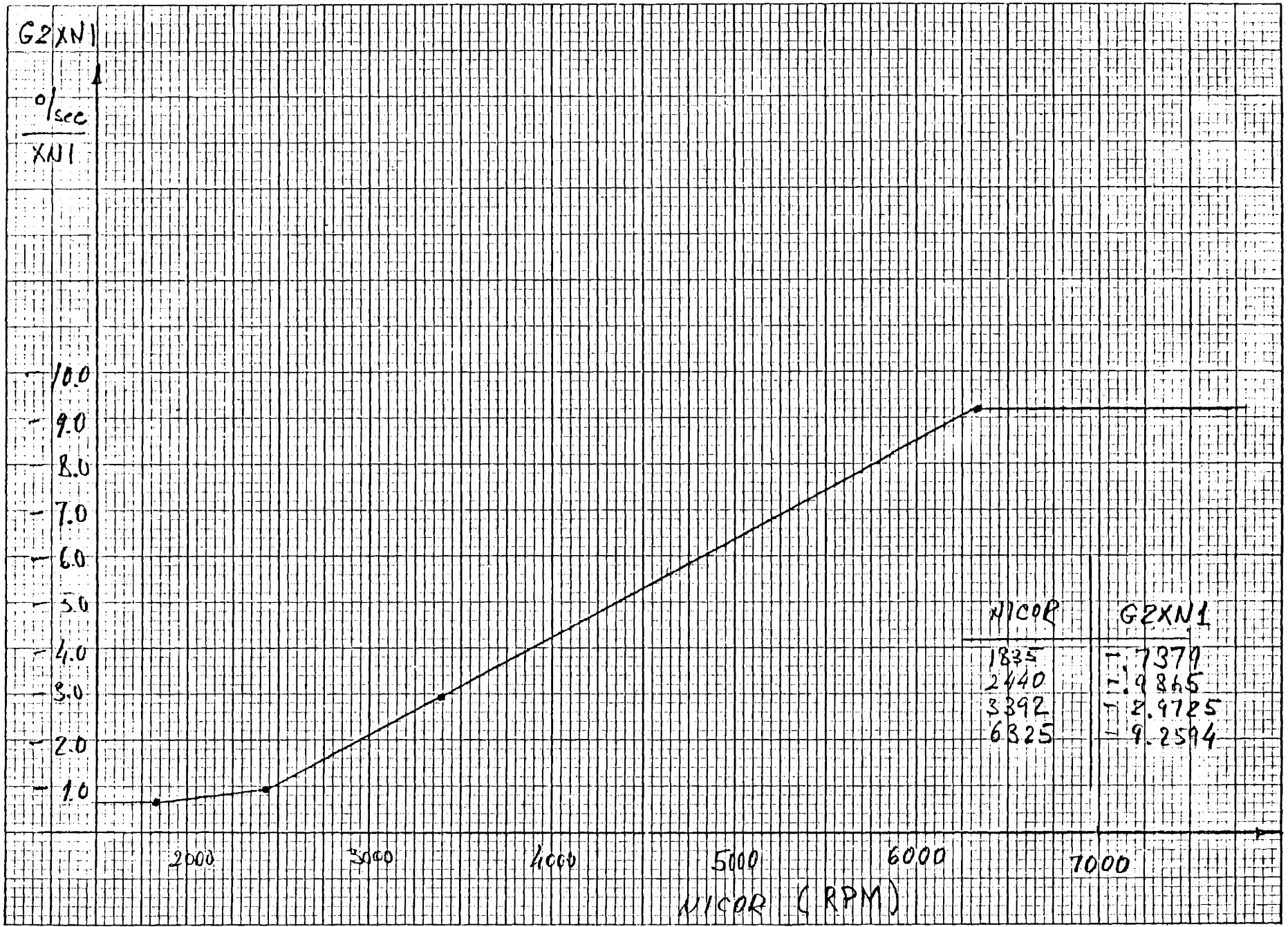
G2XN1
θ/sec
XN1
10.0
9.0
8.0
7.0
6.0
5.0
4.0
3.0
2.0
1.0
2000
3000
4000
5000
6000
7000
NICOR (RPM)
NICOR
G2XN1
1835
2440
3392
6325
7.7379
8.9865
8.9725
9.2594

Fig H4

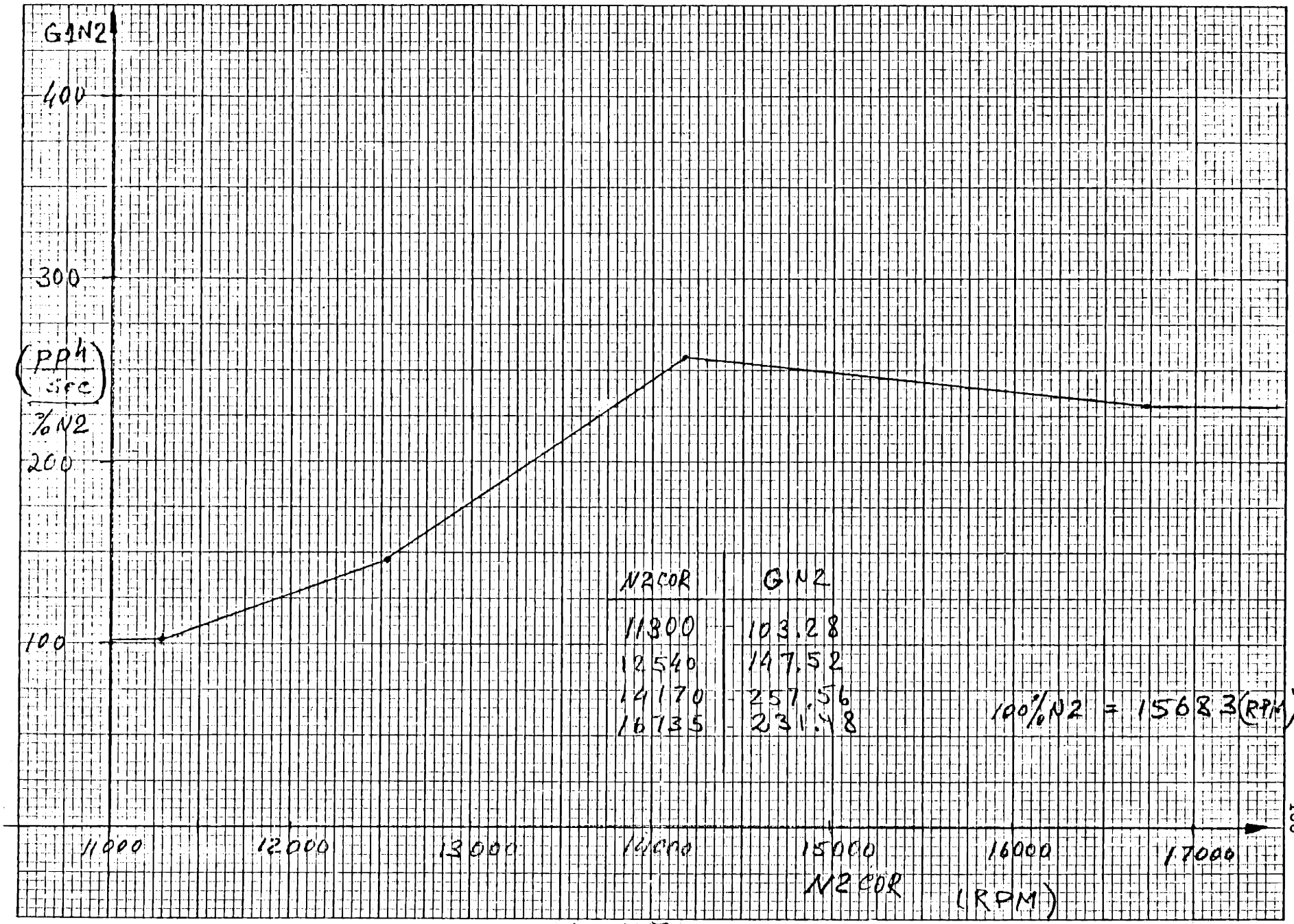
GIN2
400
300
(PPH/sec)
%N2
200
100
N2COR
GIN2
11800
12540
14170
16735
103.28
147.52
257.56
231.48
100%N2 = 15683 (RPM)
100
11000
12000
13000
14000
15000
16000
17000
N2COR (RPM)

Fig H5

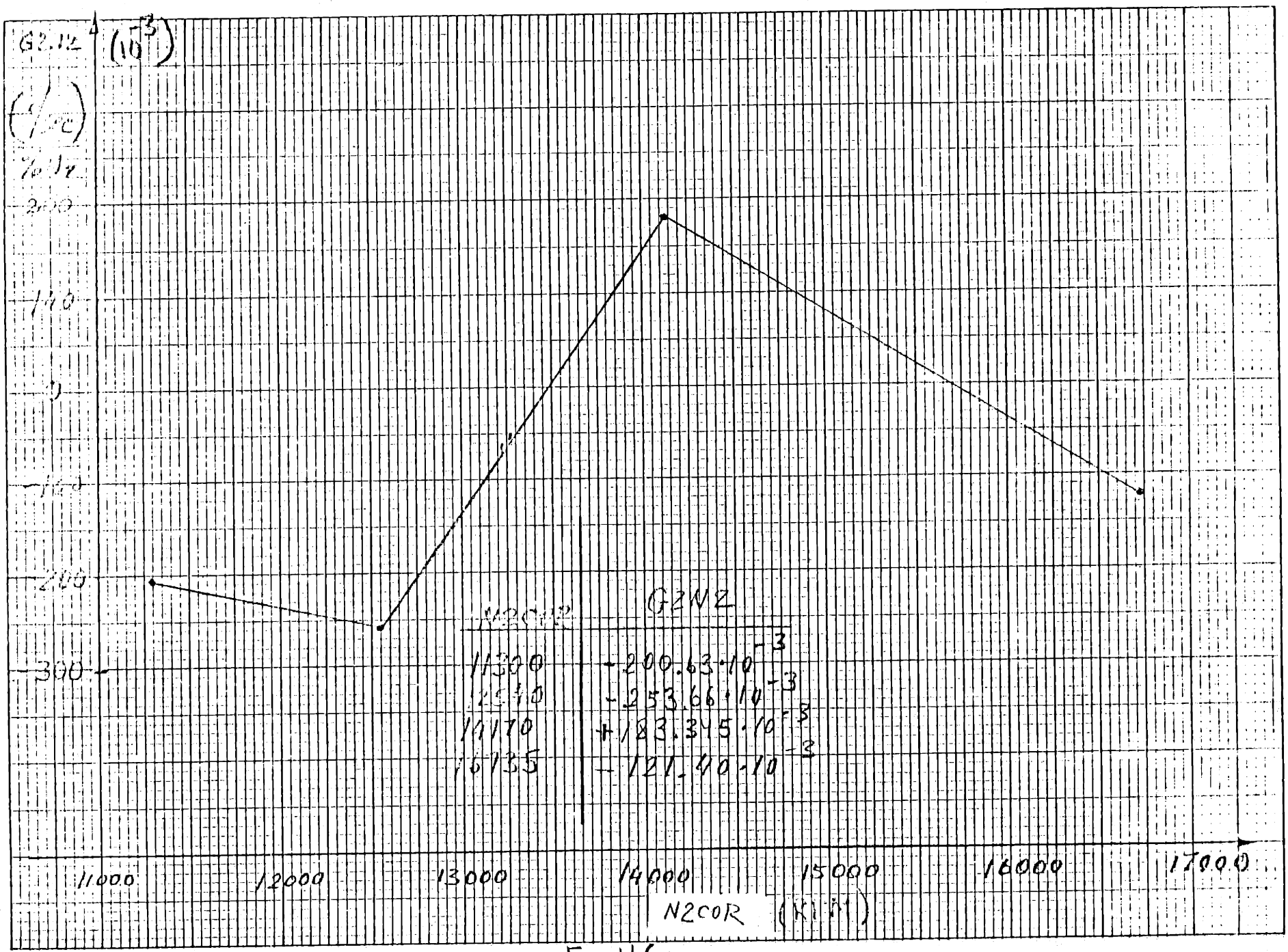
G2.N2
(10^3)
(1/sec)
-200
-300
11000
12000
13000
14000
15000
16000
17000
N2COR (K)
G2N2
+200.63·10^-3
+253.66·10^-3
+183.345·10^-3
-121.40·10^-3

Fig H6

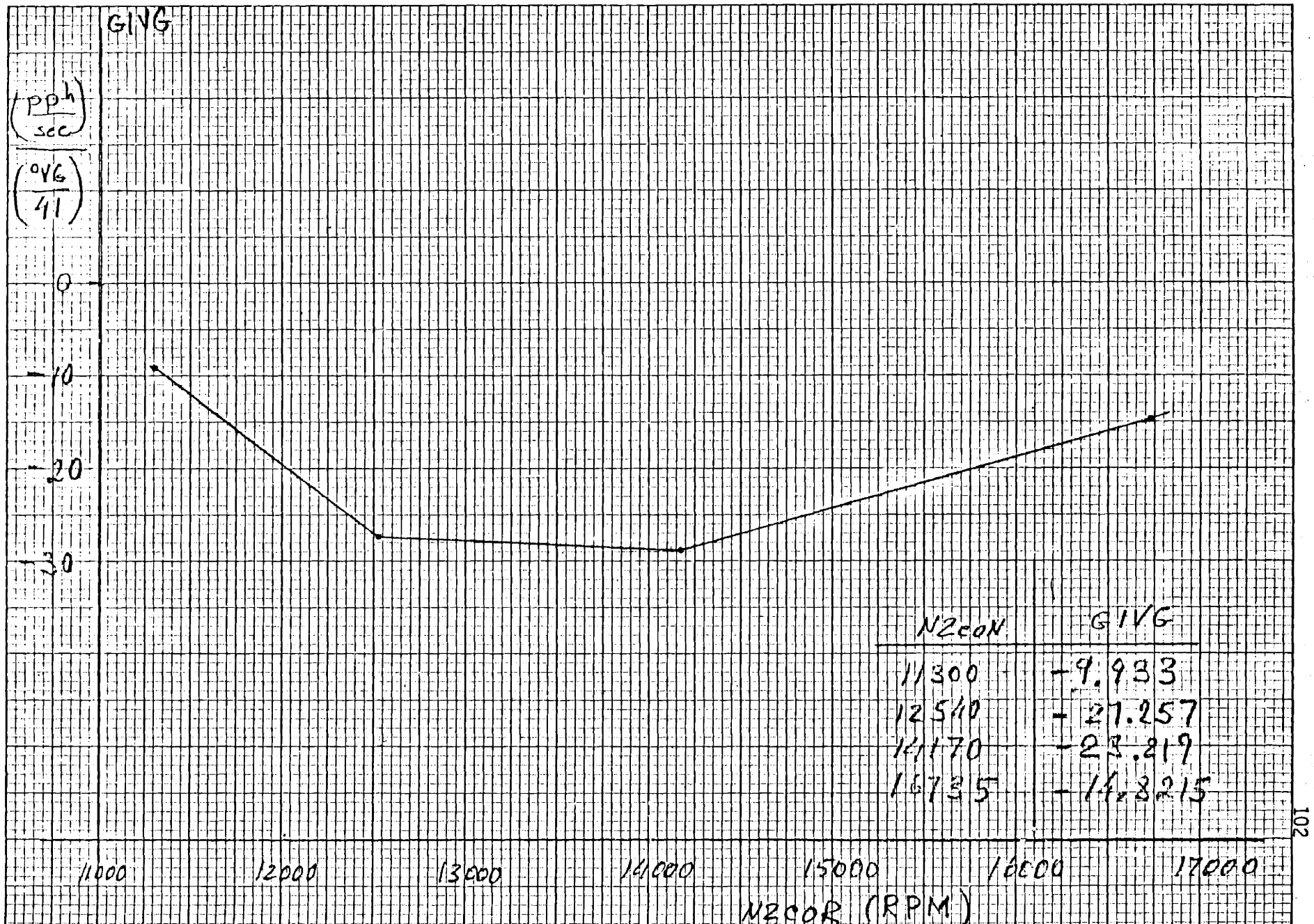
G1VG
(pph/sec)/(°VG/41)
0
-10
-20
-30
11000
12000
13000
14000
15000
16000
17000
N2COR (RPM)
N2COR G1VG
11300 -9.933
12510 -21.257
14170 -23.219
16735 -14.8215

Fig H7

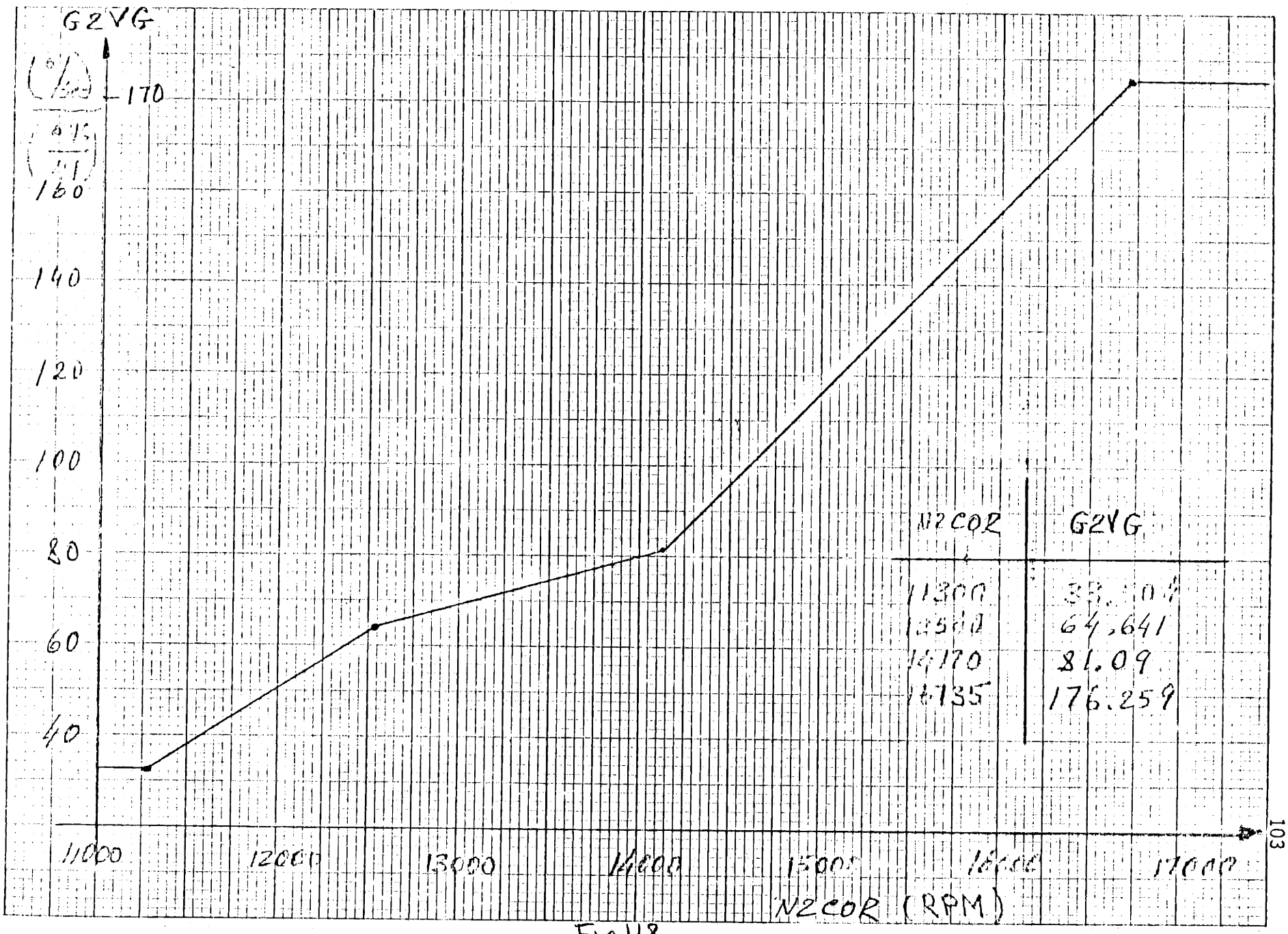
G2VG
(°/sec)
(°/sec)
170
160
140
120
100
80
60
40
11000
12000
13000
14000
15000
16000
17000
N2COR (RPM)
N2COR
G2VG
11300
12500
14170
14735
35.104
64.641
81.09
176.259

Fig H8

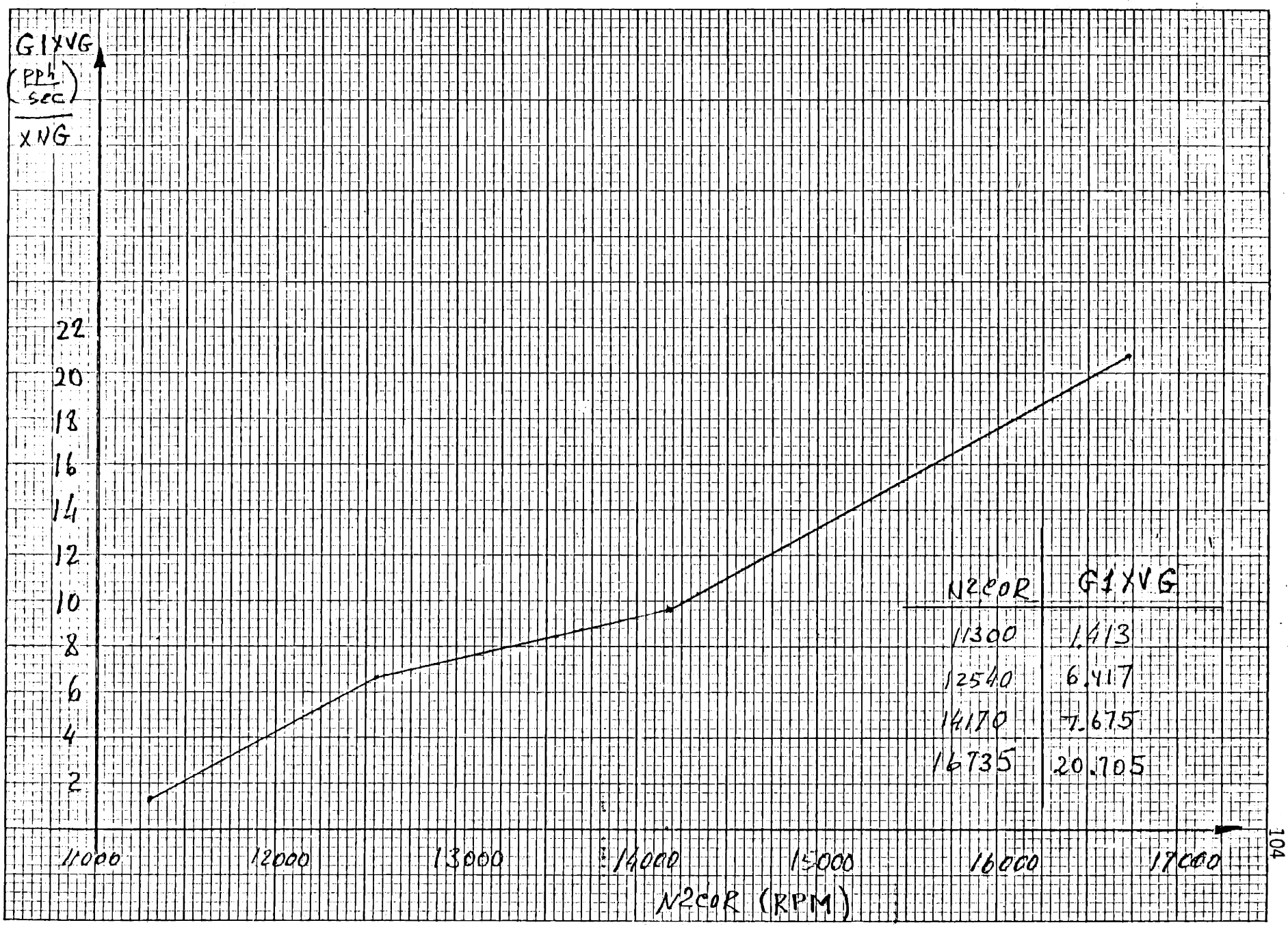
G1XVG
(PPH/sec)
XNG
22
20
18
16
14
12
10
8
6
4
2
11000
12000
13000
14000
15000
16000
17000
N2COR (RPM)
N2COR G1XVG
11300 1.413
12540 6.417
14170 7.675
16735 20.705

Fig H9

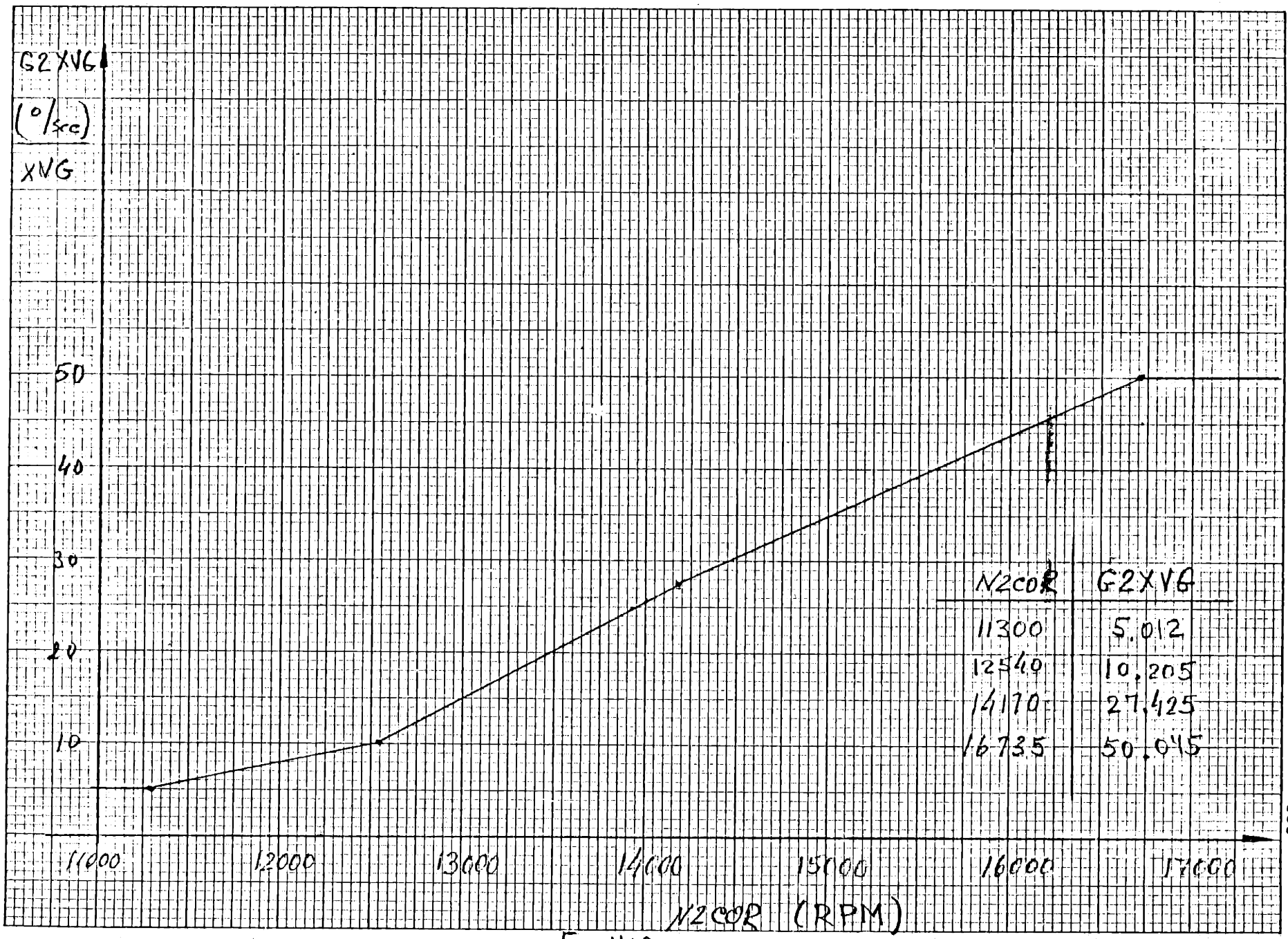
G2XVG
(°/sec)
XVG
50
40
30
20
10
11000
12000
13000
14000
15000
16000
17000
N2COR (RPM)
N2COR | G2XVG
11300 | 5.012
12540 | 10.205
14170 | 27.425
16735 | 50.045

Fig H10

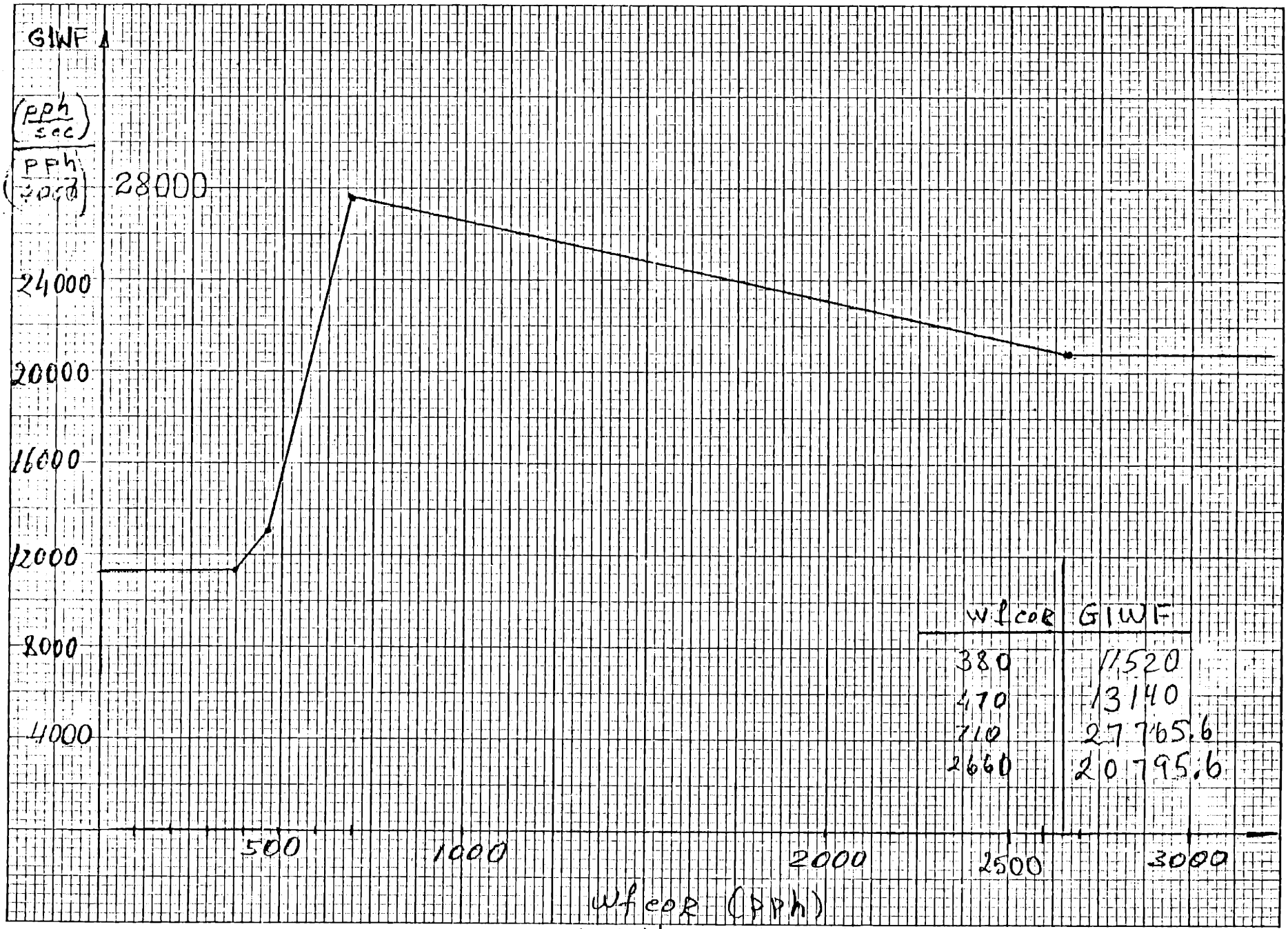
GIWF
(PPH/sec)
(PPH/hour)
28000
24000
20000
16000
12000
8000
4000
500
1000
2000
2500
3000
Wf cor (PPH)
Wf cor | GIWF
380 | 11520
470 | 13140
710 | 27765.6
2660 | 20795.6

Fig H11

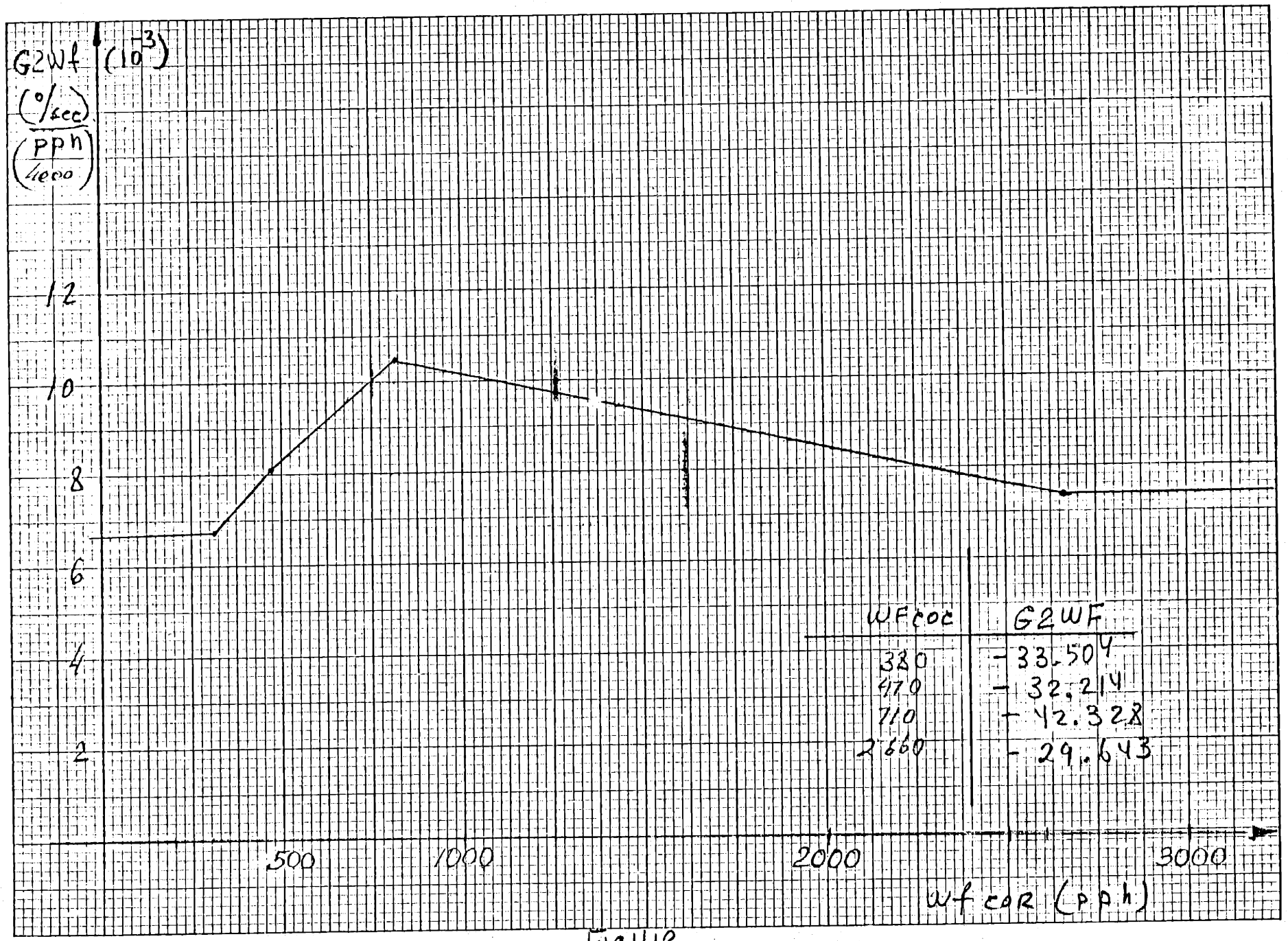
G2Wf (10^-3)
(°/sec)/(pph/1000)
12
10
8
6
4
2
500
1000
2000
3000
Wf cor (pph)
WFcor
G2WF
330
470
710
2660
- 33.504
- 32.214
+ 12.328
- 29.643

Fig H12

APPENDIX P

TRAJECTORY CONTROL LIMITS SCHEDULES

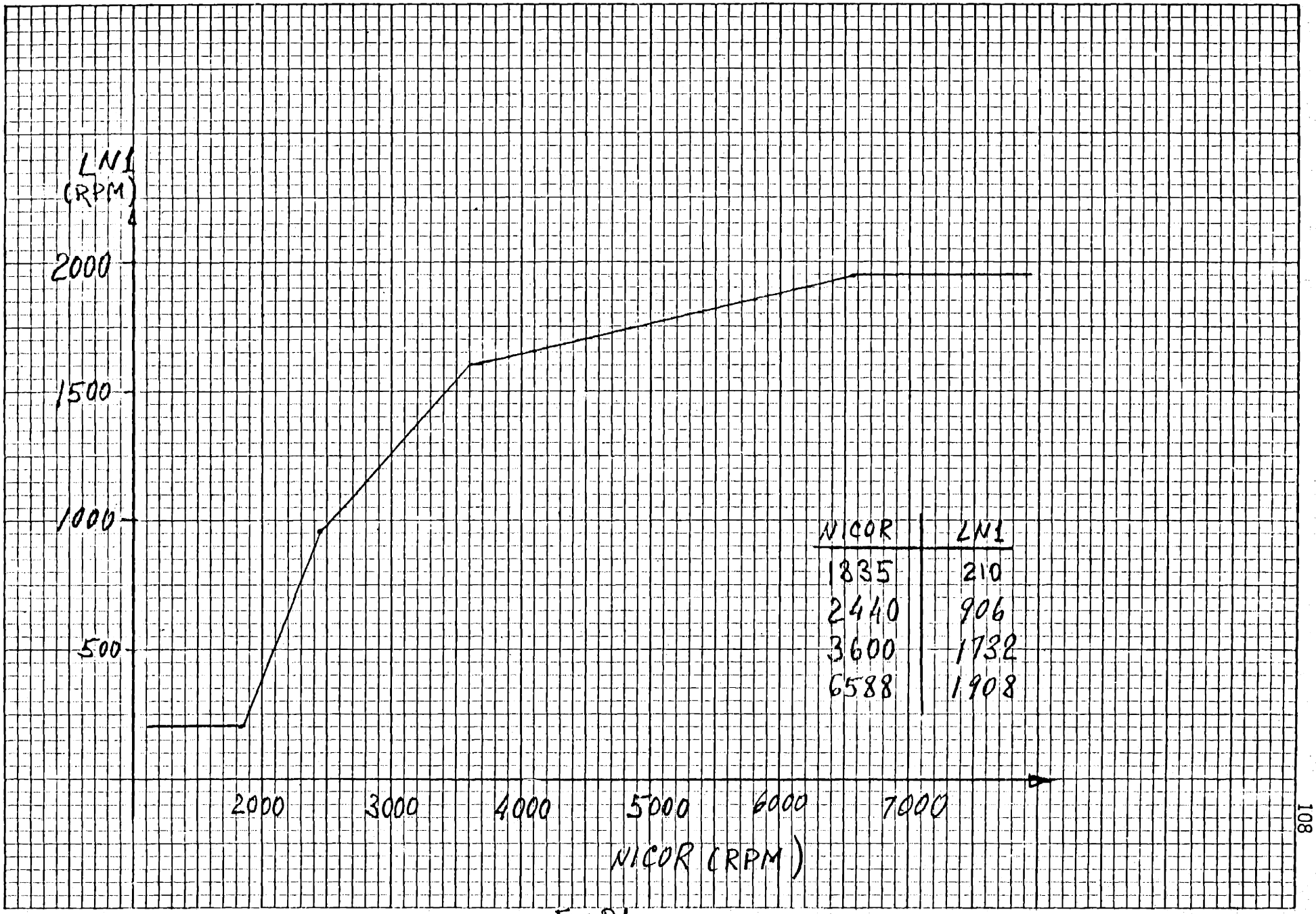
LN1 (RPM)
2000
1500
1000
500
2000
3000
4000
5000
6000
7000
NICOR (RPM)
NICOR | LN1
1835 | 210
2440 | 906
3600 | 1732
6588 | 1908

Fig P1

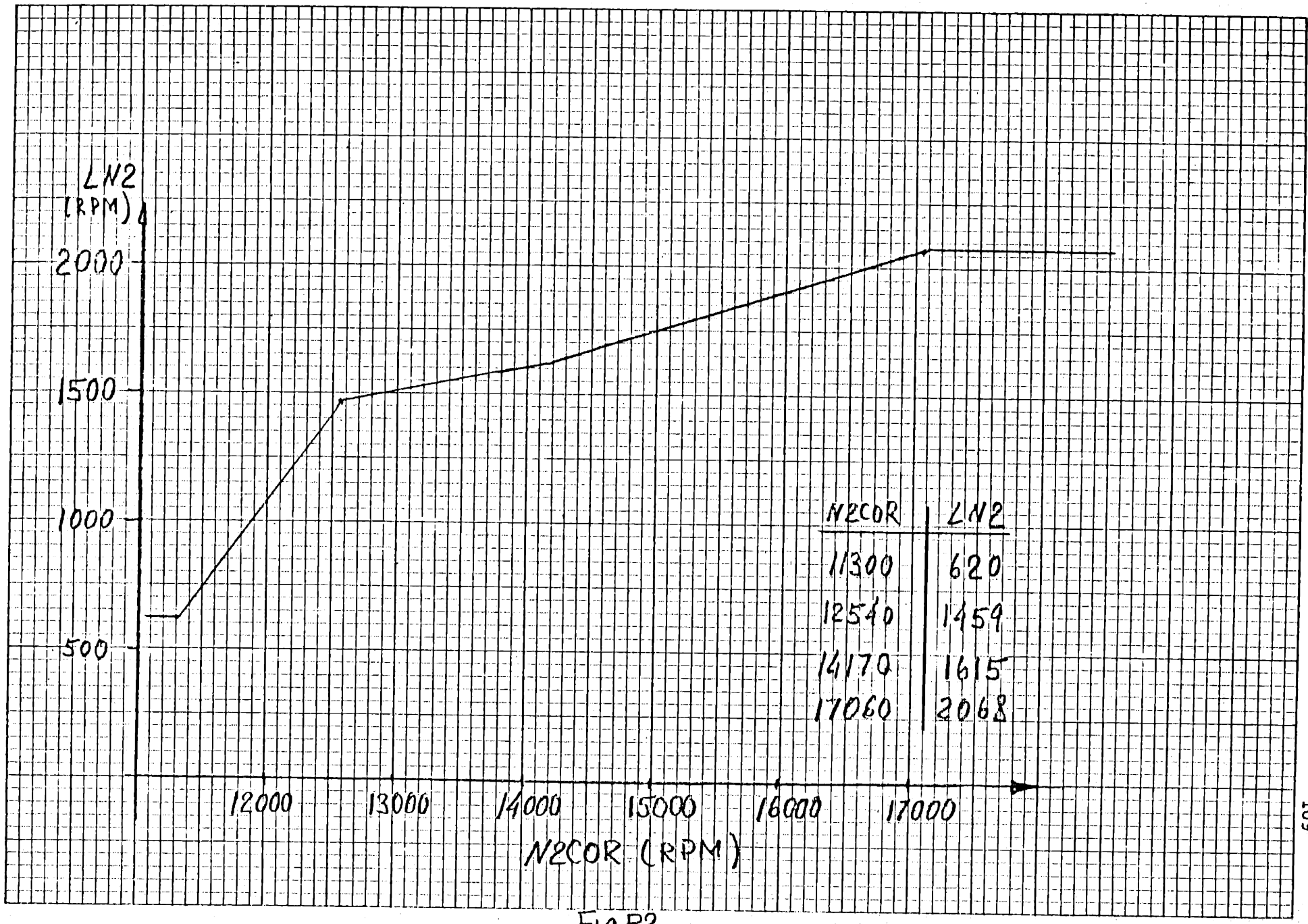
LN2 (RPM)
2000
1500
1000
500
12000
13000
14000
15000
16000
17000
N2COR (RPM)
N2COR | LN2
11300 | 620
12540 | 1459
14170 | 1615
17060 | 2068

Fig P2

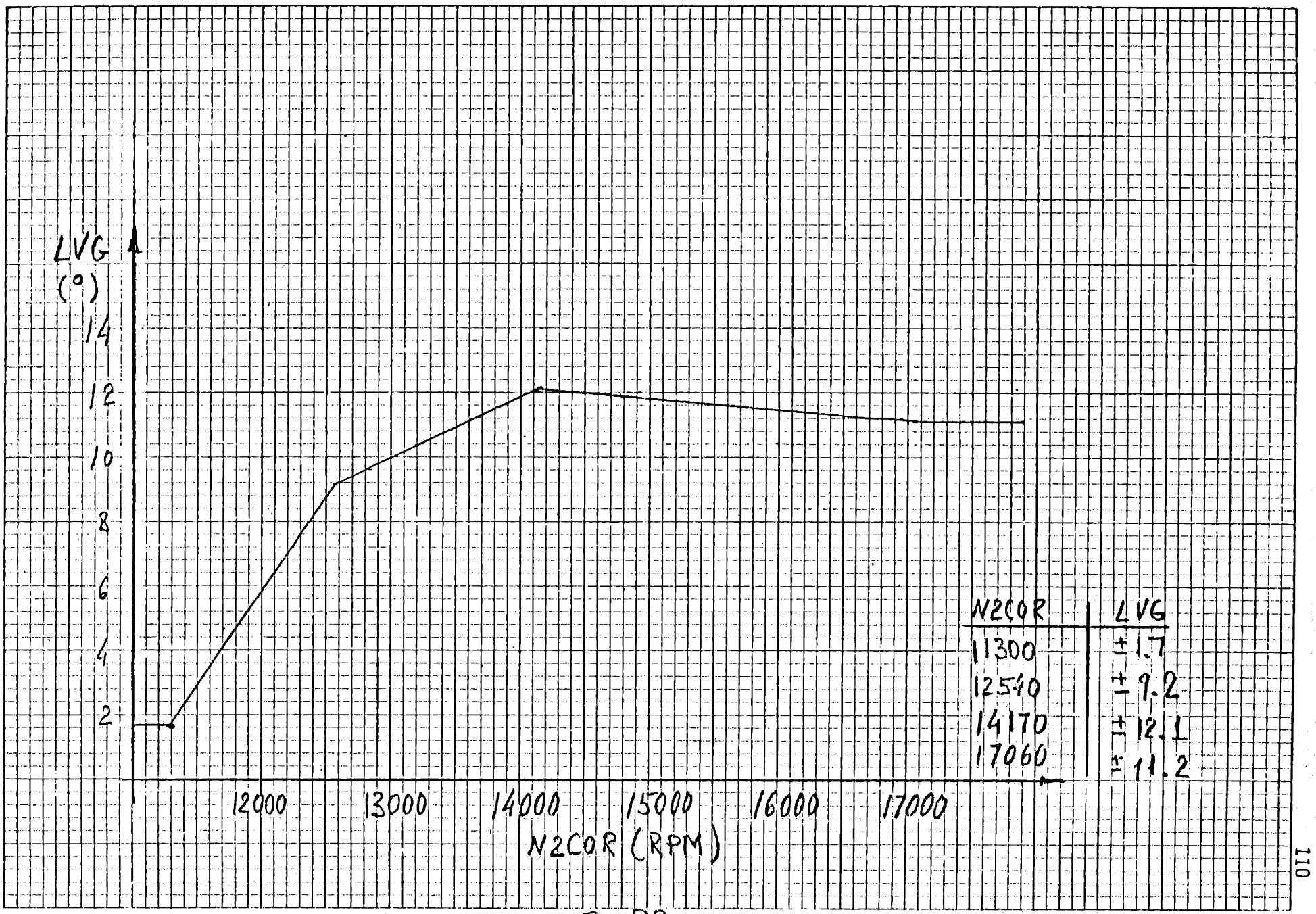
LVG
(°)
14
12
10
8
6
4
2
12000
13000
14000
15000
16000
17000
N2COR (RPM)
N2COR | LVG
11300 | ±1.7
12540 | ±9.2
14170 | ±12.1
17060 | ±11.2

Fig P3

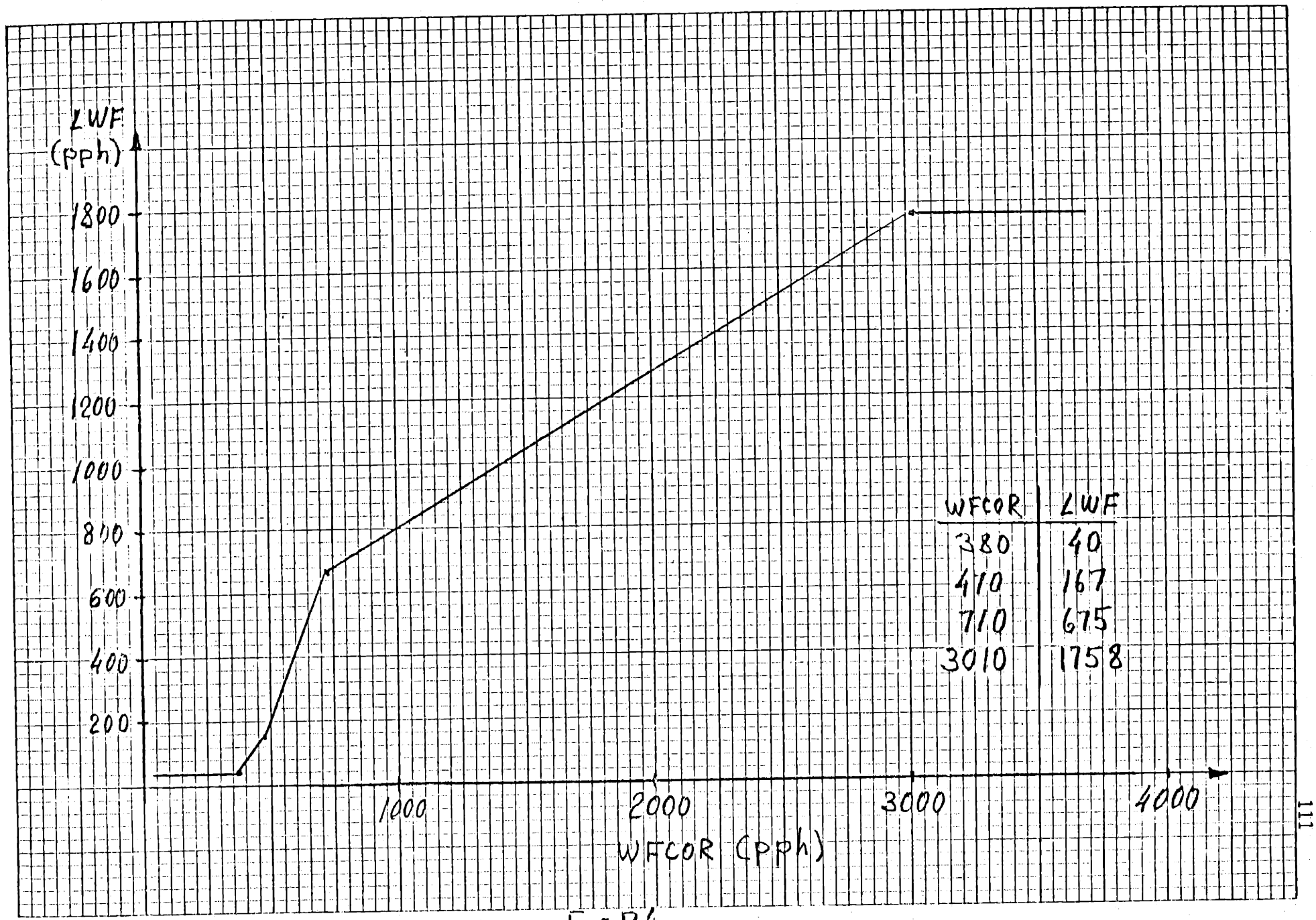

WFCOR	LWF
380	40
410	167
710	675
3010	1758

Fig P4